THE PROCEEDINGS OF
THE PHYSICAL SOCIETY

Section A

VOL. 65, PART 6 1 June 1952 No. 390A

The Thermal Conductivity of Metals at Low Temperatures I: The Elements of Groups 1, 2 and 3

BY K. MENDELSSOHN AND H. M. ROSENBERG
The Clarendon Laboratory, Oxford

Communicated by F. E. Simon; MS. received 28th January 1952

ABSTRACT. The thermal conductivity of Cu, Ag, Au, Mg, Cd, Al, In and one polycrystalline and two single crystal specimens of Zn have been measured in the range 2–40° K. Each specimen shows a maximum in the conductivity in this range. The values of the coefficients α and β in the equation for the thermal resistance $R=\alpha T^2+\beta/T$ have been calculated for each specimen.

§1. INTRODUCTION

VERY few data are available regarding the heat conductivity of metals at low temperatures. Most of the experimental work has been done on superconductors and on the change in heat conductivity during the superconducting–normal transition (e.g. Mendelssohn and Olsen 1950, Hulm 1950). Except for one or two isolated metals and alloys we have little information on the non-superconductors. In order to be able to test current theories and also to provide information for their improvement, it was decided to study systematically the thermal conductivities of the metallic elements. Since even minute amounts of impurity can cause an appreciable change in the heat conductivity, only specimens which were in a high state of purity were used. In the main these were Johnson Matthey spectrographically standardized substances.

The specimens were in rod form about 5 cm long and, as a rule, between 1 and 2 mm in diameter. A small electric heater was wound around one end and the other end was connected to the expansion chamber of a Simon helium liquefier. Helium gas thermometers were attached to the specimen by copper contacts 3 cm apart. The pressure difference in the thermometers corresponding to their temperature difference was read on a differential oil manometer. As a rule measurements were taken between 2 and 40° K. The relative accuracy for the results for one specimen was about 2% except for very good conductors, where the temperature difference obtainable was very small. The absolute accuracy was usually limited by the determination of the form factor of the specimen and was of the order of 2 to 3%. A more detailed description of the experimental arrangement and procedure will be published later.

This first paper gives the results so far obtained for the metals of groups 1, 2 and 3. A further paper will deal with those transition elements that have been

investigated so far. Since these communications are both in the nature of preliminary reports, no detailed analysis of the results is presented.

The metals used are shown in table 1. The annealing was done in evacuated quartz tubes for several hours at two-thirds the melting temperature.

Table 1

	Origin	Purity %	Heat treatment and crystal structure
Copper 1	JM 4234	99·999	Annealed polycrystalline
Silver 1	JM 1722	99·99	Polycrystalline wire
Gold 1	JM 1916a	99·999	Polycrystalline wire
Magnesium 1	JM 1703	99·95	Polycrystalline
Zinc 1	HS 8392	99·9995	Polycrystalline
Zinc 2	I.S.C.	99·997	Single crystal; hex. axis 80° to rod axis
Zinc 3	I.S.C.	99·997	Single crystal; hex. axis 13° to rod axis
Cadmium 1	HS 10547	99·9999	Cast in glass
Aluminium 1	JM 4899	99·994	Annealed polycrystalline
Indium 1	JM 4398	99·993	Polycrystalline wire

JM=Johnson Matthey.
HS=Hilger H.S. brand.
I.S.C.=Imperial Smelting Corp., Avonmouth.

§ 2. RESULTS

The results are shown in figs. 1–4. In all cases the conductivity has a maximum in the region investigated, and the value of the conductivity at this maximum is of the order of 10 watts/cm/deg, except in the case of copper. Electrical resistance measurements on all the specimens have not yet been made, but it seems unlikely that there is any appreciable lattice heat conduction. Hence we assume that the thermal resistance R can be written in the form $R=\alpha T^2+\beta/T$, where α is a term depending on the scattering of the electrons by the lattice vibrations and β is an impurity scattering term. In each case graphs of RT against T^3 have been plotted and the coefficients α and β have been determined for the low-temperature part of the curves, since in no case are they linear over their whole extent. These values are shown in table 2.

Table 2

Specimen	Cu 1	Ag 1	Au 1	Mg 1	Zn 1	Zn 2	Zn 3	Cd 1	Al 1	In 1
$\alpha\times10^5$	3·2	9·0	18	10·6	21	34	31	140	2·2	190
β	0·35	1·60	1·15	1·25	0·4	0·7	0·6	0·25	2·3	0·4

Copper, Silver and Gold

The values of the thermal conductivity are shown in fig. 1. The copper specimen was rather too thick to measure the extremely high conductivity, and this accounts for the scatter in the points. Berman and MacDonald (1952) have obtained a thinner specimen from the same batch of copper, and their conductivity curve has a much higher and sharper maximum at approximately the same temperature as ours. The curves agree at the higher temperatures. The higher maximum is presumably due to the difference in the annealing and preparation of the specimens. The conductivity of the gold and silver is much less than that of the copper. The broad maximum of the silver seems to indicate a large impurity scattering term, and it is hoped to repeat the determination with a purer sample of the metal.

Zinc, Cadmium and Magnesium

The results for the three specimens of zinc are shown in fig. 2. Zn 1 is a polycrystalline specimen. Zn 2 and Zn 3 are single crystals from the same batch of metal, but differing from Zn 1. They have their hexagonal axes at 80° and 13° to the rod axis respectively. These directions were the nearest that could be obtained easily to axes parallel and perpendicular to the rod. It will be seen that the curves for Zn 2 and Zn 3 coincide at high and low temperatures but

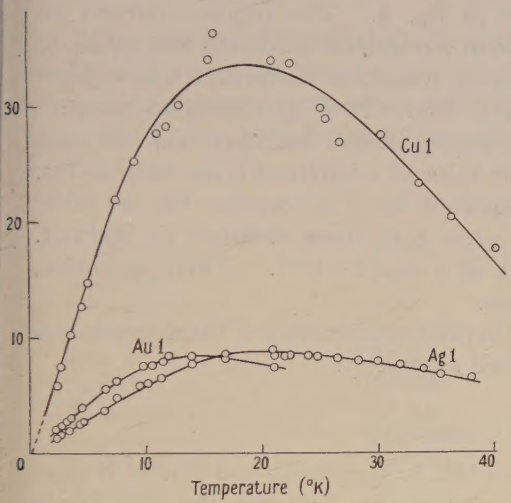

Fig. 1. The thermal conductivity of copper, silver and gold.

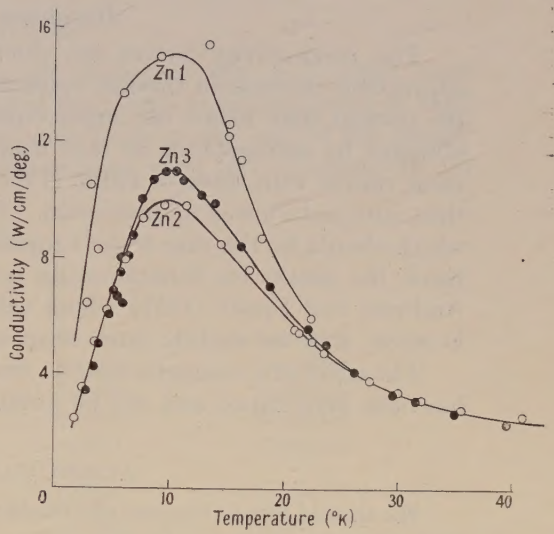

Fig. 2. The thermal conductivity of polycrystalline zinc, Zn 1 and single crystals of zinc, Zn 2 and Zn 3.

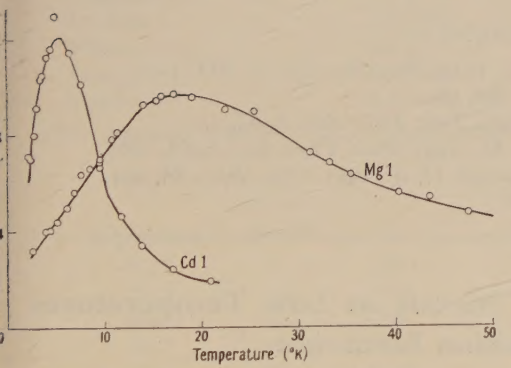

Fig. 3. The thermal conductivity of cadmium and magnesium.

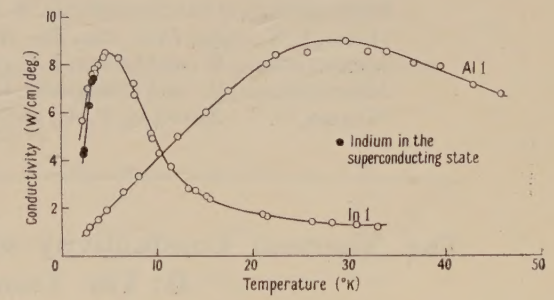

Fig. 4. The thermal conductivity of aluminium and indium.

that Zn 3 has a maximum about 10% greater than that of Zn 2. This probably has some connection with the fact that the atomic spacing in zinc is different perpendicular and parallel to the hexagonal planes, but experiments on more single crystals need to be done in order to clarify this point.

Figure 3 gives the conductivity curves for magnesium and cadmium. The cadmium specimen is the one which showed a large increase in thermal resistance in a magnetic field, as has been reported previously (Mendelssohn and Rosenberg 1951).

In metals such as gold and magnesium, where a minimum often occurs in the electrical resistivity, no such corresponding effect was found in the thermal resistance. The electrical minimum is usually very shallow, and in the thermal case this would be reflected as only a very slight change in the slope of a curve, and not, as in the electrical case, by a change from a constant value. It is not surprising, therefore, that no analogous results to the electrical minimum have been found in these experiments.

Aluminium and Indium

The conductivity curves are shown in fig. 4. The indium showed an appreciable increase in thermal resistance in a magnetic field, and the values in the normal state below the superconducting transition temperature have been obtained by extrapolating to zero magnetic field. It is interesting to compare these results with those of Hulm (1950), whose indium specimen was less pure than ours and showed no maximum. The value of α obtained is the same as his, which should be the case if the simple equation for R is correct. On the other hand, the results for aluminium do not agree with those obtained by Webber, Andrews and Spohr (1951) whose value of α is $2{\cdot}7\times10^{-5}$. Their specimen, however, may be slightly purer than ours.

The effect of a magnetic field on the thermal conductivity of these specimens has been determined and will be published separately.

ACKNOWLEDGMENTS

We should like to express our thanks to Mr. S. Weintroub and Mr. A. J. Goss of University College, Southampton, for presenting us with the zinc single crystals. One of us (H. M. R.) is in receipt of a maintenance award from the Ministry of Education.

REFERENCES

Berman, R., and MacDonald, D. K. C., 1952, *Proc. Roy. Soc.* A, **211**, 122.
Hulm, J. K., 1950, *Proc. Roy. Soc.* A, **204**, 98.
Mendelssohn, K., and Olsen, J. L., 1950, *Proc. Phys. Soc.* A, **63**, 2.
Mendelssohn, K., and Rosenberg, H. M., 1951, *Proc. Phys. Soc.* A, **64**, 1067.
Webber, R. T., Andrews, F. A., and Spohr, D. A., 1951, *Phys. Rev.*, **84**, 994.

The Thermal Conductivity of Metals at Low Temperatures II: The Transition Elements

By K. Mendelssohn and H. M. Rosenberg
The Clarendon Laboratory, Oxford

Communicated by F. E. Simon ; MS. received 28th January 1952

ABSTRACT. The thermal conductivity in the range 2–40°K has been measured for Ti, Mn, Fe, Ni, Zr, Cb, Mo, Rh, Pd, Ta, W, Ir, Pt, U, and for a Pb single crystal. As a rule, the metals of group 8 have a much higher conductivity than have the metals of the earlier groups. The values of α and β in the equation for the thermal resistance $R=\alpha T^2+\beta/T$ have been calculated for each specimen. The experiments on Cb indicate that the normal state was not reached in a field of 3300 gauss at temperatures below 5°K.

§ 1. INTRODUCTION

In a previous paper (Mendelssohn and Rosenberg 1952) we have dealt with the thermal conductivity of some metals of groups 1, 2 and 3. This paper presents the results of the rest of our work so far completed. In addition to some transition elements, it also gives the results of experiments on a lead single crystal and on uranium. The specimens used are described in table 1.

Experimental procedure is similar to that outlined in the paper referred to above.

§ 2. RESULTS

The graphs of thermal conductivity are shown in figs. 1–7. The most outstanding result is that the conductivity of the metals at the beginning of each transition group is very small compared with those at the end of the group, i.e. the group 8 elements. For those elements with low conductivity no

Table 1

Specimen	Origin	Purity (%)	Notes
Titanium 1	A.E.I.	99·9	
Titanium 2	A.E.I.	99·99	Annealed
Manganese 1	JM 2472	99·99	Annealed
Iron 1	JM 4975	99·99	Annealed
Nickel 1	JM 4884	99·997	Annealed
Zirconium 1	JM 3062	~98	Annealed
Columbium 1	JM 4526	99·99	
Molybdenum 1	JM 2331	99·95	
Rhodium 1	JM 2357	99·995	Wire
Palladium 1	JM 2134	99·995	Annealed wire
Tantalum 1	JM 3804	99·98	
Tungsten 1	JM 2260	99·99	Annealed
Iridium 1	JM 3441	99·995	Annealed wire
Platinum 1	JM 2157 b	99·999	Annealed wire
Lead 1	Tadenac	99·998	Single crystal
Uranium 1	A.E.R.E.		

JM = Johnson Matthey, A.E.I. = Associated Electrical Industries Research Laboratories.

Table 2

Specimen	$\alpha \times 10^5$	β	Specimen	$\alpha \times 10^5$	β
Ti 1	—	290	Rh 1	22	1·4
Ti 2	—	170	Pd 1	64	11
Mn 1	—	1200	Ta 1	—	27
Fe 1	18	9·5	W 1	10·2	5·9
Ni 1	22	4·4	Ir 1	3·6	0·77
Zr 1	130	76	Pt 1	43	0·40
Cb 1	—	—	Pb 1	325	0·10
Mo 1	7·5	6·7	U 1	750	95

maximum was found in the experimental range covered. In some cases the curves were linear within the limits of experimental error, and values of the coefficient α in the equation for the thermal resistance $R = \alpha T^2 + \beta/T$ could not be evaluated. In all other cases graphs were drawn of RT against T^3 and the values of α and β for low temperatures were calculated. These values are shown in table 2.

Titanium, Manganese, Iron and Nickel

The results for these metals are shown in figs. 1 and 2. The manganese and titanium both have very small conductivities of the form dictated by impurity scattering. On the other hand, the low conductivity of manganese may have

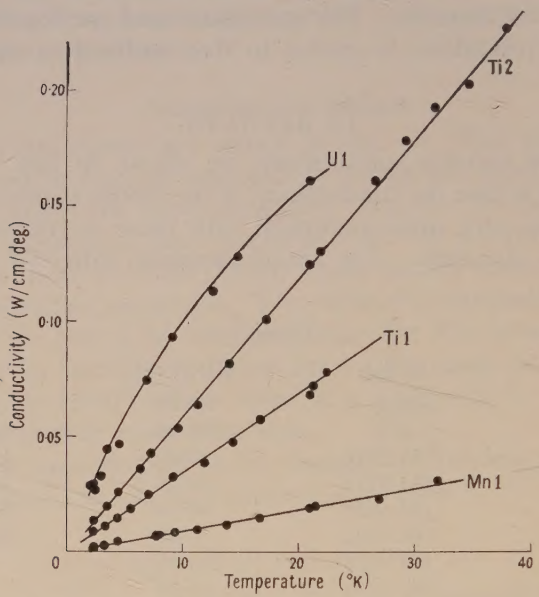

Fig. 1. The thermal conductivity of uranium, titanium and manganese.

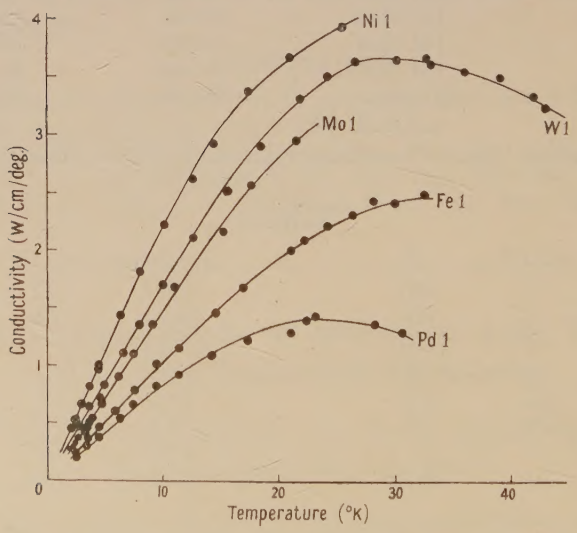

Fig. 2. The thermal conductivity of nickel, iron, molybdenum, palladium and tungsten.

some connection with its extremely complicated crystal structure. Ti2 has been annealed and may be slightly purer than Ti1. Nickel and iron show the large increase in the conductivity for the group 8 elements.

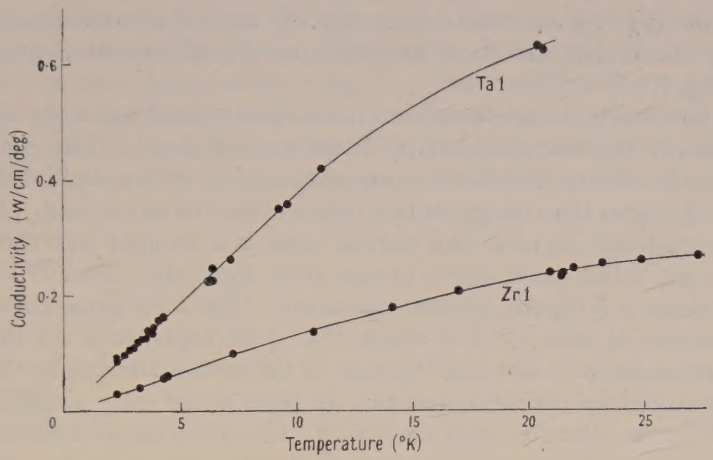

Fig. 3. The thermal conductivity of zirconium and tantalum.

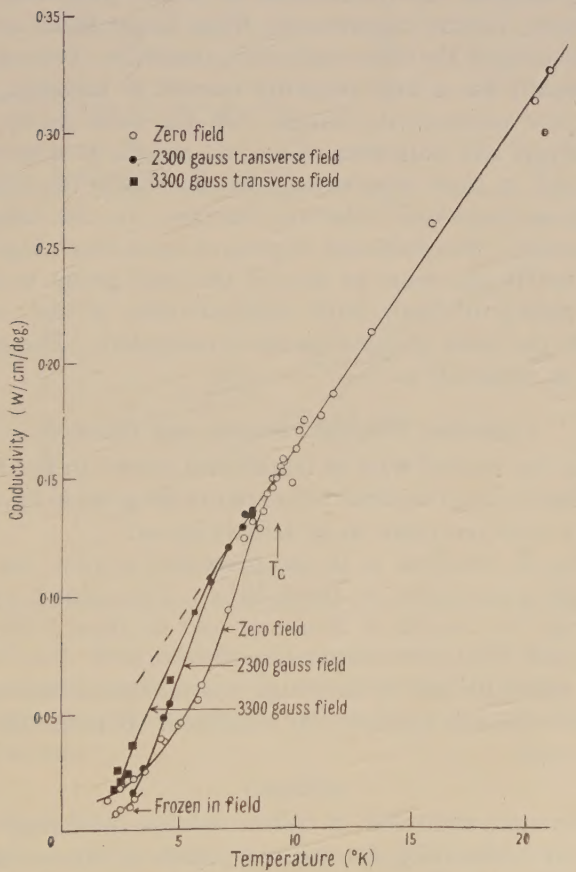

Fig. 4. The thermal conductivity of columbium.

Zirconium, Columbium, Molybdenum, Rhodium and Palladium

Zirconium (fig. 3) and columbium (fig. 4) again have low conductivities followed by the higher values of molybdenum (fig. 2), rhodium (fig. 5) and palladium (fig. 2).

Columbium being a superconductor, a magnetic field has to be applied in order to measure the heat conductivity in the normal state. The curves show that this state is not reached at low temperatures even in a field of 3 300 gauss, which is much higher than the published values of the transition field. Assuming that the conductivity curve in the normal state is a straight line through the origin, then the 2 300 gauss curve breaks away from this about 6° K and the 3 300 gauss curve at a slightly lower temperature. The 2 300 gauss curve crosses the superconducting state curve at about 3° K. One explanation for this is that the lattice conductivity is decreased because of the extra scattering by the normal electrons produced by the field, and this decrease is not fully compensated by the increase in the electron heat transport. Electrical measurements on this specimen, however, indicate that almost all the heat transport is by electrons, and it may be that it is the electron heat transport itself that is decreased by the magnetic field. A possible mechanism is by the formation of normal and superconducting laminae, the boundaries of which may tend to scatter the electrons. However, further experiments, when larger fields are available, will be necessary to investigate the superconducting transition of columbium properly.

Zirconium usually has a large impurity content of hafnium, and this might account for the low conductivity found. On the other hand, the very great similarity in structure and properties of the two metals, as is shown by the great difficulty presented in their separation, may not cause the conductivity to be reduced as much as one would otherwise suppose, i.e. the hafnium might not act as a true impurity. Molybdenum in group 6 has a much higher conductivity whose value is nearly the same as that of the next group 6 metal, tungsten. Rhodium and palladium both have conductivities of the order of a few watts/cm/deg like the other group 8 metals investigated. The palladium shows a flat maximum at about 24° K.

Tantalum, Tungsten, Iridium and Platinum

The curve for the normal state of tantalum is shown in fig. 3 and the curves below the superconducting transition temperature are given in fig. 6. In this range the normal curve does not seem to be strictly linear.

Tungsten (fig. 2), referred to in the preceding section, has a much higher conductivity, with a maximum at about 28° K. The value for α calculated by Hulm (1950) from the results of Bremmer and de Haas (1936) is $0{\cdot}88 \times 10^{-4}$, and it compares fairly well with our value of $1{\cdot}02 \times 10^{-4}$.

Iridium and platinum (fig. 5) have high conductivities, that of iridium being the highest of the transition metals so far measured. Both metals exhibit maxima in the range covered.

Lead

The presentation to us by Mr. S. Weintroub of a lead single crystal gave us an opportunity of measuring its thermal conductivity in the normal and superconducting states. The specimen was extremely pure, as is shown by its very high and sharp maximum in the normal state (fig. 5). Although readings were taken on the low-temperature side of this maximum in the region of 1·8° K,

the conductivity was changing so rapidly that it was extremely difficult to get any reliable experimental points in this range, and hence only one point is shown on the graph for this side of the curve. The heat conductivity in the superconducting state is shown on a larger scale in fig. 7. This confirms the sudden breaking away of the superconducting from the normal curve and also the shallow minimum in the superconducting curve at about 5° K, as has been found by other workers (de Haas and Rademakers 1940). The rise in conductivity on the low-temperature

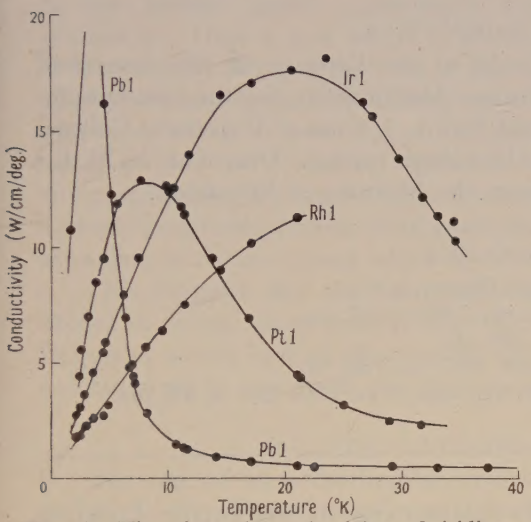

Fig. 5. The thermal conductivity of iridium, rhodium, platinum and a single crystal of lead in the normal state.

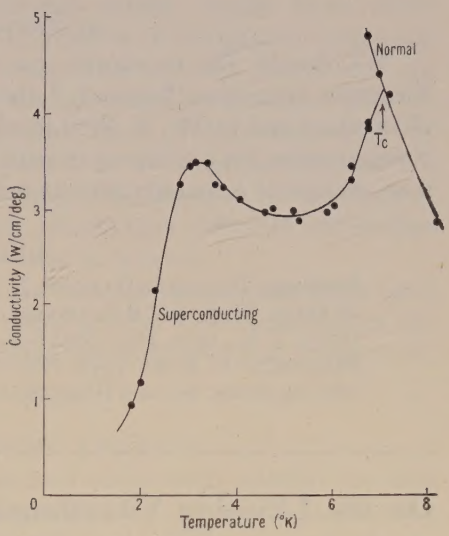

Fig. 7 The thermal conductivity of lead in the superconductive state.

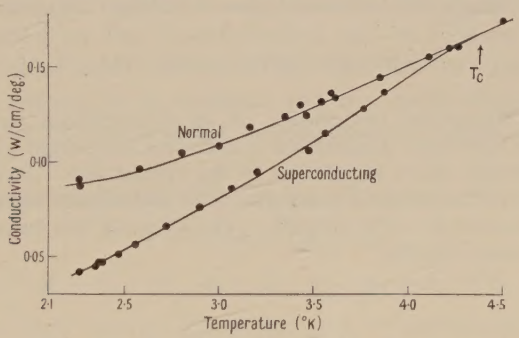

Fig. 6. The thermal conductivity of tantalum in the normal and superconductive states.

side of this minimum has a connection, presumably, with the extremely rapid increase in the normal conductivity in this temperature range.

Magneto-resistance effects, which will be reported separately, have been found in this specimen.

Uranium

The curve for uranium is shown in fig. 1. Although it has a low conductivity it is not linear, whereas all the other metals investigated which have a conductivity of this order are linear in the low-temperature range. Electrical resistance measurements indicate that, within the experimental error, the whole of the heat transport in the uranium is by electrons.

As has been mentioned previously, this paper is only in the nature of a preliminary report, especially as regards the analysis of the results. The graphs of RT against T^3 are by no means linear even at temperatures where the simple formula for R should hold, i.e. below one-tenth of the Debye θ temperature (Makinson 1938), and it is clear that the details of the theory need revising in order that our results may be explained satisfactorily. Extension of the experimental work to higher temperatures is in progress.

ACKNOWLEDGMENTS

We should like to express our thanks to the Director of the Associated Electrical Industries Research Laboratories, Aldermaston, for the two samples of titanium and to Mr. S. Weintroub and Mr. A. J. Goss of University College, Southampton, for presenting us with the lead single crystal. One of us (H. M. R.) is in receipt of a maintenance award from the Ministry of Education.

REFERENCES

Bremmer, H., and de Haas, W. J., 1936, *Physica*, **3**, 672.
de Haas, W. J., and Rademakers, A., 1940, *Physica*, **7**, 992.
Hulm, J. K., 1950, *Proc. Roy. Soc.* A, **204**, 98.
Makinson, R. E. B., 1938, *Proc. Camb. Phil. Soc.*, **34**, 374.
Mendelssohn, K., and Rosenberg, H. M., 1952, *Proc. Phys. Soc.* A, **65**, 385.

On the Limiting Vibrational Frequencies of an Ionic Lattice

By M. BLACKMAN
Physics Department, Imperial College, London

MS. received 30*th November* 1951

ABSTRACT. The vibrational frequencies of an orthorhombic ionic lattice, of the thallium fluoride type, have been worked out in detail for wavelengths long compared with the crystal spacing though short in relation to the crystal size. It is shown that these frequencies are not unique but depend in general on the direction of the wave in the crystal—in contrast to what happens in cubic crystals. The effect of this behaviour on the vibrational spectrum is discussed briefly.

§ 1. INTRODUCTION

It has been shown by Lyddane and Herzfeld (1938) and by Kellermann (1940) that the normal modes of an alkali halide (of the rocksalt type) of long wavelength and high frequency consist of two transverse vibrations of equal frequency and a longitudinal vibration of much higher frequency. The term *long* wavelength here means long compared with the crystal spacing, though short compared with the size of the crystal. Further, the frequencies are calculated on the assumption that Coulomb forces (as well as repulsive forces) would suffice; this excludes cases where the crystal radiates electromagnetic waves—at any rate pending a special consideration—but, as far as those frequencies are concerned which play an important part in the vibrational spectrum, this restriction is not significant.

The existence of the two types of limiting frequencies is linked on the one hand with the existence of a long high-frequency tail to the vibrational spectrum (composed of mainly longitudinal vibrations), on the other hand with a large peak in the vibrational spectrum (associated with mainly transverse vibrations), as can be seen from the work of Kellermann and of Iona (1941).

The large difference in the frequencies of the transverse and the longitudinal waves is a characteristic ionic effect. This effect is considered in some detail in the present paper, particularly for crystals which depart from cubic symmetry. Here a new aspect is found. If a lattice is considered containing two oppositely charged particles in the unit cell, three non-zero frequencies are always obtained in the limit of long waves; if the lattice has, for example, different properties along its axes (e.g. different spacings), some of the solutions of the equations for the frequency would be expected to be different if cases are compared where the wave vector is chosen along different axes. For instance, a purely longitudinal wave, of long wavelength, should have different frequencies according to the axis along which the wave vector is directed.

This suggests that the frequencies are not unique in the long-wave limit except in special cases such as that of the cubic crystal. As variability in the frequency would have an effect on the vibrational spectrum, which is unexpected, a detailed study was made of a special case.

§ 2. THE ORTHORHOMBIC CRYSTAL

The case of an orthorhombic crystal seemed particularly suitable for this investigation. The particular model chosen was based on thallium fluoride, which contains four molecules per orthorhombic cell. This cell is similar to that of rocksalt and can be produced from it by appropriate dilatations along the orthogonal axes. Furthermore, a smaller cell containing two particles can be chosen, as suggested by the rhombohedral cell in rocksalt, and this cell will be used in the calculations below. The definition of the lattice vector also follows the same pattern as in rocksalt, and the mathematical descriptions and formulae can always be reduced, for the purposes of checking results, to that of the rocksalt case.

The lattice vector of the cell $\mathbf{r}^{l_1 l_2 l_3}$ can be written as

$$\mathbf{r}^{l_1 l_2 l_3} = l_1\mathbf{a}_1 + l_2\mathbf{a}_2 + l_3\mathbf{a}_3, \qquad \ldots\ldots(1)$$

where

$$\mathbf{a}_1 = b\mathbf{i}_2 + c\mathbf{i}_3;\ \mathbf{a}_2 = c\mathbf{i}_3 + a\mathbf{i}_1;\ \mathbf{a}_3 = a\mathbf{i}_1 + b\mathbf{i}_2. \qquad \ldots\ldots(2)$$

Here $\mathbf{i}_1$, $\mathbf{i}_2$, $\mathbf{i}_3$ are unit vectors along the x, y, z directions respectively, these being parallel to the orthorhombic axes. The smallest distance between similar particles along these axes are respectively $2a$, $2b$, $2c$, where in thallium fluoride

$$2a = 5{\cdot}18\,\text{Å},\ 2b = 5{\cdot}50\,\text{Å},\ 2c = 6{\cdot}08\,\text{Å}. \qquad \ldots\ldots(3)$$

The particle vectors $\mathbf{r}_k$ in the basic cell and the charges ϵ_k are given by

$$\mathbf{r}_1 = 0,\ \mathbf{r}_2 = \tfrac{1}{2}(\mathbf{a}_1 + \mathbf{a}_2 + \mathbf{a}_3)$$
$$\epsilon_1 = |\boldsymbol{e}|,\ \epsilon_2 = -|\boldsymbol{e}|, \qquad \ldots\ldots(4)$$

where $\boldsymbol{e}$ is the electronic charge.

The vibrational frequencies of long wavelength can be obtained as a special case in the general calculation of lattice frequencies. The method of doing this is well known (Born 1923). Taking a particular wave of wave vector $\mathbf{s}$,

wavelength λ, and angular frequency ω, the displacement $\mathbf{u}_k{}^l$ of a particle k in the lth cell, where $l \equiv (l_1 l_2 l_3)$, is given by

$$\mathbf{u}_k{}^l = \mathbf{U}_k \exp(-i\omega t) \exp\{2\pi i(\mathbf{r}_k{}^l \cdot \mathbf{s}/\lambda)\}. \qquad \ldots\ldots(5)$$

The usual boundary conditions (of the periodic type) will determine the possible values of $\mathbf{s}/\lambda$.

The equations of motion are

$$\omega^2 m_k U_{k\alpha} + \sum_{k'} \sum_{\gamma} \begin{bmatrix} kk' \\ x\gamma \end{bmatrix} U_{k'\gamma} = 0, \qquad \ldots\ldots(6)$$

where

$$\begin{bmatrix} kk' \\ x\gamma \end{bmatrix} = \sum_{l} (\phi^l_{kk'})_{x\gamma} \exp\{2\pi i(\mathbf{r}^l_{k'k} \cdot \mathbf{s}/\lambda)\}. \qquad \ldots\ldots(7)$$

Here $\mathbf{r}^l_{k'k} = \mathbf{r}^l_{k'} - \mathbf{r}_k{}^0$ is the vectorial distance between particles of type k' and type k, the first being in the lth cell, the second in the reference cell $l=0$. The quantity $\phi^l_{k'k}$ is the potential energy of this pair of particles, and the suffixes x, y denote differentiation with respect to these directions. The masses of the particles are given by m_k. Further, in the calculation of $\begin{bmatrix} kk \\ x\gamma \end{bmatrix}$ the terms $(\phi^0_{kk})_{x\gamma}$ are determined by the condition

$$\sum_{l} \sum_{k'} (\phi^l_{kk'})_{x\gamma} = 0. \qquad \ldots\ldots(8)$$

As there are two particles per cell, the angular frequencies can be determined from a sixth-order determinant (cf. eqn. (6)), once the lattice sums (7) have been evaluated. For the special case of long wavelength, three of the solutions will be zero; hence the determinant is reducible to the third order, or even further if waves are chosen in special directions.

§ 3. CALCULATION OF ELECTROSTATIC LATTICE SUMS

In the calculation of the lattice sums, the electrostatic part needs special methods; equivalent methods are known, one due to Ewald (1938), the other using Epstein zeta functions (Epstein 1903). The latter method has been used by Broch (1937) in treating the linear ionic lattice, the former by Kellermann (1940) in connection with the vibrational spectrum of rocksalt. As the Epstein functions seem to lead to a more direct calculation and deserve to be better known, they have been preferred here.

The function which we shall use is defined as

$$Z\left|\begin{matrix} g \\ h \end{matrix}\right|(s) = \sum_{l} \frac{\exp(2\pi i \sum l_\mu h_\mu)}{[\psi(l+g)]^{s/2}}, \qquad \ldots\ldots(9)$$

where

$$\psi(l+g) = \sum_{\mu,\nu} C_{\mu\nu}(l_\mu + g_\mu)(l_\nu + g_\nu)$$

and $\mu, \nu = 1, 2, 3$. The $C_{\mu\nu}$ are constants, the l_μ are integers ranging from $-\infty$ to $+\infty$. The h_μ range from 0 to 1, and s is an integer. The denominator in (9) is in the form of a power of the lattice distance $(|\mathbf{r}^l_{k'k}|)^s$ where $C_{\mu\nu} = C_{\nu\mu}$ and the g_μ are numerically equal to the coordinates of the particles in the cell. If, further, we put $h_i = (\mathbf{a}_i \cdot \mathbf{s}/\lambda)$, then the zeta functions, suitably differentiated with respect to the h_μ, will be in the form required for the evaluation of the electrostatic part of the lattice sums (7). To achieve this evaluation numerically

we need the zeta function in a quickly convergent form, which has been given by Epstein (1903):

$$\pi^{-s/2}\Gamma\left(\frac{s}{2}\right)Z\left|\begin{matrix}g\\h\end{matrix}\right|(s)=\int_1^\infty dz\, z^{(s-2)/2}\sum_l \exp\{-\pi z\psi(g+l)+2\pi i\sum l_\mu h_\mu\}$$
$$+\frac{\exp\{-2\pi i\sum g_\mu h_\mu\}}{\Delta^{1/2}}\int_1^\infty dz\, z^{(p-s-2)/2}\sum_m \exp(-\pi z\Phi(h+m)-2\pi i\sum m_\mu g_\mu). \quad \ldots\ldots(10)$$

Here Γ refers to the gamma function and Δ is the determinant formed by the $C_{\mu\nu}$. The quantity $\psi(g+l)$ has been given above, and $\Phi(h+m)$ is defined by the following expression:

$$\Phi(h+m)=\sum_{\mu\nu} C'_{\mu\nu}(h_\mu+m_\mu)(h_\nu+m_\nu),\ (\mu,\nu=1,2,3), \quad \ldots\ldots(11)$$

where the m_μ are integers ranging from $-\infty$ to $+\infty$, and

$$C'_{\mu\nu}=\frac{1}{\Delta}\frac{\partial\Delta}{\partial C_{\mu\nu}}. \quad \ldots\ldots(12)$$

The transformation (12) is a reciprocal one, and it can be shown that $\Phi(m)$ is the square of the distance in the reciprocal lattice if $\psi(l)$ is the square of the lattice vector. The summation over the integers l_μ, m_μ extends also from $-\infty$ to $+\infty$. In our calculation $p=3$.

The integrals in (10) could be used in a slightly different form by the introduction of the Ewald separating factor ϵ_0, see Born (1923), instead of taking $\epsilon_0=1$, but it has not been found necessary to introduce this modification here.

§ 4. DETAILED EVALUATION OF THE ELECTROSTATIC LATTICE SUMS

We consider first the evaluation of $\left[\begin{matrix}12\\xx\end{matrix}\right]^{\mathrm{E}}$. The lattice distance $|r_{12}{}^l|$ is given by

$$(r_{12}{}^l)^2=2a^2[\tfrac{1}{2}l_1{}^2(\alpha+\beta)+\tfrac{1}{2}l_2{}^2(1+\beta)+\tfrac{1}{2}l_3{}^2(1+\alpha)+l_2l_3+\alpha l_1l_3$$
$$+\beta l_1l_2-l_1(\alpha+\beta)-l_2(1+\beta)-l_3(1+\alpha)+\tfrac{1}{2}+\tfrac{1}{2}\alpha+\tfrac{1}{2}\beta]. \quad \ldots\ldots(13)$$

where
$$\alpha=b^2/a^2,\quad \beta=c^2/a^2. \quad \ldots\ldots(14)$$

It is found convenient to use the Epstein formulae in a dimensionless form, and hence we choose $\psi(l+g)$ equal to the quantity in the bracket of (13). Hence the coefficients $C_{\mu\nu}$, g_μ are given by the following scheme:

$$\left.\begin{aligned} &C_{11}=\tfrac{1}{2}(\alpha+\beta);\ C_{12}=C_{21}=\tfrac{1}{2}\beta;\ g_1=-\tfrac{1}{2};\\ &C_{22}=\tfrac{1}{2}(1+\beta);\ C_{13}=C_{31}=\tfrac{1}{2}\alpha;\ g_2=-\tfrac{1}{2};\\ &C_{33}=\tfrac{1}{2}(1+\alpha);\ C_{23}=C_{32}=\tfrac{1}{2};\ g_3=-\tfrac{1}{2};\end{aligned}\right\} \quad \ldots\ldots(15)$$

and $\Delta=\frac{1}{2}(\alpha\beta)$. We can further determine the coefficients $C'_{\mu\nu}$ using (15). This leads to the following set of relations:

$$\left.\begin{aligned} &C'_{11}=C'_{22}=C'_{33}=\frac{\alpha+\beta+\alpha\beta}{2\alpha\beta};\ C'_{12}=C'_{21}=\frac{\alpha-\beta-\alpha\beta}{2\alpha\beta};\\ &C'_{13}=C'_{31}=\frac{\beta-\alpha-\alpha\beta}{2\alpha\beta};\ C'_{23}=C'_{32}=\frac{\alpha\beta-\alpha-\beta}{2\alpha\beta}.\end{aligned}\right\} \quad \ldots\ldots(16)$$

Finally we can write down $\Phi(h+m)$ in terms of the $C'_{\mu\nu}$:

$$\begin{aligned}\Phi(h+m)=&\frac{\beta+\alpha+\alpha\beta}{2\alpha\beta}(h_1^2+h_2^2+h_3^2+m_1^2+m_2^2+m_3^2)\\&+\frac{\alpha-\beta-\alpha\beta}{\alpha\beta}(h_1h_2+m_1m_2+h_1m_2+h_2m_1)\\&+\frac{\beta-\alpha-\alpha\beta}{\alpha\beta}(h_1h_3+m_1m_3+h_3m_1+h_1m_3)\\&+\frac{\alpha\beta-\alpha-\beta}{\alpha\beta}(h_2h_3+m_2m_3+h_2m_3+h_3m_2)\\&+\frac{\beta+\alpha+\alpha\beta}{\alpha\beta}(h_1m_1+h_2m_2+h_3m_3).\end{aligned}\qquad\ldots\ldots(17)$$

With these preliminaries over, it is now necessary to consider how the derivatives of the potential occurring in the lattice sums can be formulated in terms of the zeta function. In $\left[\begin{matrix}12\\xx\end{matrix}\right]^{\mathrm{E}}$ we need the term $\phi^{12}_{xx}(|r_{12}{}^{l}|)$. Now

$$\phi^{12}_{xx}=\frac{-e^2(2x_l{}^2-y_l{}^2-z_l{}^2)}{|r_{12}{}^{l}|^{5/2}}=\frac{-e^2}{2^{5/2}a^3}\frac{H^{12}_{xx}}{[\psi(l+g)]^{5/2}},\qquad\ldots\ldots(18)$$

where

$$\begin{aligned}H^{12}_{xx}=[&-(\alpha+\beta)l_1{}^2+(2-\beta)l_2{}^2+(2-\alpha)l_3{}^2+4l_2l_3-2\alpha l_1l_3-2\beta l_1l_2\\&+2(\alpha+\beta)l_1-2(2-\beta)l_2-2(2-\alpha)l_3+(2-\alpha-\beta)].\end{aligned}\qquad\ldots\ldots(19)$$

Hence (as $s=5$)

$$\left[\begin{matrix}12\\xx\end{matrix}\right]^{\mathrm{E}}=-\frac{e^2}{2^{5/2}a^3}\exp\{\pi i(h_1+h_2+h_3)\}\left[-\frac{F_1}{4\pi^2}+\frac{F_2}{2\pi i}+(2-\alpha-\beta)F_3\right],\qquad\ldots\ldots(20)$$

where

$$F_1=\left\{(2-\alpha)\frac{\partial^2Z}{\partial h_3{}^2}+(2-\beta)\frac{\partial^2Z}{\partial h_2{}^2}-(\alpha+\beta)\frac{\partial^2Z}{\partial h_1{}^2}+4\frac{\partial^2Z}{\partial h_2\partial h_3}-2\alpha\frac{\partial^2Z}{\partial h_1\partial h_3}-2\beta\frac{\partial^2Z}{\partial h_1\partial h_2}\right\},$$

$$F_2=2(\alpha+\beta)\frac{\partial Z}{\partial h_1}-2(2-\beta)\frac{\partial Z}{\partial h_2}-2(2-\alpha)\frac{\partial Z}{\partial h_3},$$

$$F_3=Z.$$

Inserting the values for the derivatives of Z, using (10), we obtain

$$\begin{aligned}\left[\begin{matrix}12\\xx\end{matrix}\right]^{\mathrm{E}}=&-\frac{e^2\pi^{5/2}}{2^{5/2}a^3\Gamma(5/2)}\left[\int_1^\infty dz\, z^{3/2}\sum_l H^{12}_{xx}(l)\exp\{2\pi i\sum_\mu(l_\mu-\tfrac{1}{2})h_\mu\}\right.\\&\times\exp\{-\pi z\psi(l-\tfrac{1}{2})\}-\frac{1}{\Delta^{1/2}}\int_1^\infty dz\sum_m G_{xx}(m,h)\\&\left.\times\exp\{-\pi z\Phi(h+m)+\pi i\sum_\mu m_\mu\}\right],\end{aligned}\qquad\ldots\ldots(21)$$

where H^{12}_{xx} has been defined above (eqn. (19)) and

$$\begin{aligned}G_{xx}(m,h)=&\frac{2\beta\alpha-\alpha-\beta}{\alpha\beta}(h_1{}^2+h_2{}^2+h_3{}^2+m_1{}^2+m_2{}^2+m_3{}^2)\\&-\frac{2(2\alpha\beta+\alpha-\beta)}{\alpha\beta}(h_1h_2+m_1m_2+h_2m_1+h_1m_2)\\&-\frac{2(2\alpha\beta-\alpha+\beta)}{\alpha\beta}(h_1h_3+m_1m_3+h_1m_3+h_3m_1)\\&+\frac{2(2\alpha\beta+\alpha+\beta)}{\alpha\beta}(h_2h_3+m_2m_3+h_2m_3+h_3m_2).\end{aligned}\qquad\ldots\ldots(22)$$

The expression for G_{xx} is independent of k, k', and so these indices are omitted. We shall be concerned only with those cases where the h_μ tend to zero. This is not necessarily the same as putting $h_\mu = 0$, but is, in fact, the same except for the one term in G_{xx} where $m_\mu = 0$. This term is handled separately, i.e.

$$\begin{bmatrix}12\\xx\end{bmatrix}^{\mathrm{E}}_{h=0} = \begin{bmatrix}12\\xx\end{bmatrix}^{\mathrm{E}}_{h=0} + \frac{e^2}{2^{5/2}a^3}\frac{\pi^{5/2}}{\Gamma(5/2)}\frac{1}{\Delta^{1/2}}\lim_{h\to 0}\int_1^\infty dz\, G_{xx}(h)\exp\{-\pi z\Phi(h)\}, \qquad \ldots\ldots(23)$$

where $\Phi(h)$, $G_{xx}(h)$ are obtained by putting $m_\mu = 0$ in (17) and (22) respectively. In the first term on the right-hand side all $h_\mu = 0$; in dealing with this term numerically it is convenient to transform the summations so as to make use of the orthorhombic cell. Then

$$\begin{aligned}\begin{bmatrix}12\\xx\end{bmatrix}^{\mathrm{E}}_{h=0} = &-\frac{e^2}{a^3}\frac{\pi^{5/2}}{2^{5/2}\Gamma(5/2)}\left[\int_1^\infty dz\, z^{3/2}\sum_p G^{12}_{xx}(p)\right.\\ &\times\exp\{-\tfrac{1}{2}\pi z(p_1^2+\alpha p_2^2+\beta p_3^2)\} - \frac{1}{\Delta^{1/2}}\int_1^\infty dz\sum_m B_{xx}(m)\\ &\left.\times\exp\left\{-\tfrac{1}{2}\pi z\left(m_1^2+\frac{m_2^2}{\alpha}+\frac{m_3^2}{\beta}\right)+\pi i(m_1+m_2+m_3)\right\}\right], \qquad ..(24)\end{aligned}$$

where in the first summation the integers $p \equiv (p_1, p_2, p_3)$ range over the (orthorhombic) face-centred lattice of the particles $k=2$, the origin being taken at one of the particles $k=1$. The second summation $m \equiv (m_1, m_2, m_3)$ is taken over the orthorhombic body-centred reciprocal lattice. The expressions for G^{12}_{xx}, B_{xx} are given below.

The second term in (23) can be evaluated directly, but the result is of interest only when special values are chosen for the h_μ. For instance, if $h_1 = h_2 = h$ and $h_3 = 0$, $G_{xx} = -4h^2/\beta$ and $\Phi(h) = 2h^2/\beta$. The term involving the integral in (23) then becomes

$$-\frac{1}{2^{5/2}}\frac{e^2}{a^3}\frac{\pi^{5/2}}{\Gamma(5/2)}\frac{1}{\Delta^{1/2}}\frac{2}{\pi} = -\frac{4\pi}{3}\frac{e^2}{2a^3}\frac{1}{(\alpha\beta)^{1/2}} \qquad \ldots\ldots(25)$$

since $\Gamma(5/2) = 3\pi^{1/2}/4$ and $\Delta = \frac{1}{2}\alpha\beta$.

This term is typical for Coulomb forces, and for $\alpha = 1$, $\beta = 1$ reduces to the value which appears in the calculation of the limiting frequencies of rocksalt.

The other lattice sums of the above type can be obtained using the following list:

$$\left.\begin{aligned}
&C^{12}_{xx} = (2p_1^2 - \alpha p_2^2 - \beta p_3^2);\ B_{xx} = \left(2m_1^2 + \frac{1}{\alpha}m_2^2 - \frac{1}{\beta}m_3^2\right)\\
&C^{12}_{yy} = (2\alpha p_2^2 - \beta p_3^2 - p_1^2);\ B_{yy} = \left(\frac{2}{\alpha}m_2^2 - \frac{1}{\beta}m_3^2 - m_1^2\right)\\
&C^{12}_{zz} = (2\beta p_3^2 - p_1^2 - \alpha p_2^2);\ B_{zz} = \left(\frac{2}{\beta}m_3^2 - m_1^2 - \frac{1}{\alpha}m_2^2\right)\\
&G_{yy}(h) = \frac{(2\beta-\alpha-\alpha\beta)}{\alpha\beta}(h_1^2+h_2^2+h_3^2) - \frac{2(2\beta+\alpha-\alpha\beta)}{\alpha\beta}h_1h_2\\
&\qquad + \frac{2(2\beta+\alpha+\alpha\beta)}{\alpha\beta}h_1h_3 + \frac{2(\alpha-2\beta-\alpha\beta)}{\alpha\beta}h_2h_3\\
&G_{zz}(h) = \frac{(2\alpha-\beta-\alpha\beta)}{\alpha\beta}(h_1^2+h_2^2+h_3^2) + \frac{2(2\alpha+\beta+\alpha\beta)}{\alpha\beta}h_1h_2\\
&\qquad + \frac{2(\alpha\beta-\beta-2\alpha)}{\alpha\beta}h_1h_3 + \frac{2(\beta-2\alpha-\alpha\beta)}{\alpha\beta}h_2h_3.
\end{aligned}\right\} \qquad \ldots\ldots(26)$$

The next set of lattice sums which need to be considered are of the type $\begin{bmatrix}12\\xy\end{bmatrix}^{\mathrm{E}}$, $x \neq y$. Here it can be shown that $\begin{bmatrix}12\\xy\end{bmatrix}^{\mathrm{E}}_{h=0} = 0$ because of the symmetry properties of the orthorhombic lattice; it is symmetrical on reflection in the xy, yz, zx planes. Using the same methods as in calculating (18),

$$\begin{bmatrix}12\\xy\end{bmatrix}^{\mathrm{E}}_{h\to 0} = -a_{xy}A \lim_{h\to 0} \int_1^\infty G_{xy}(h) \exp\{-\pi z \Phi(h)\}, \quad \ldots\ldots(27)$$

where

$$A = \frac{3e^2}{a^3} \frac{\pi^{5/2}}{2^{5/4}\Gamma(5/2)} \frac{1}{\Delta^{1/2}} = \frac{e^2}{a^3} \frac{\pi^2}{(\alpha\beta)^{1/2}}. \quad \ldots\ldots(28)$$

The other quantities are given below together with their forms in the other cases:

$$\left.\begin{aligned} a_{xy} &= \alpha^{1/2};\ G_{xy}(h) = \frac{1}{\alpha}(h_3^2 - h_1^2 - h_2 + 2h_1h_2) \\ a_{xz} &= \beta^{1/2};\ G_{xz}(h) = \frac{1}{\beta}(h_2^2 - h_3^2 - h_1^2 + 2h_1h_3) \\ a_{yz} &= (\alpha\beta)^{1/2};\ G_{yz}(h) = \frac{1}{\alpha\beta}(h_1^2 - h_2^2 - h_3^2 + 2h_2h_3). \end{aligned}\right\} \quad \ldots\ldots(29)$$

§ 5. THE COMPLETE LATTICE SUM

The contribution from the repulsive forces is considered here in its most elementary form in order to show the effect we wish to demonstrate in its most striking form. We assume that these are nearest neighbour repulsive forces, and further that these are independent of the direction of the bond. The more natural assumption of different force constants for different directions will merely introduce extra, and unknown, parameters. From the above assumptions it follows that

$$\begin{aligned} \begin{bmatrix}12\\xx\end{bmatrix}^{\mathrm{R}}_{h=0} &= \begin{bmatrix}12\\yy\end{bmatrix}^{\mathrm{R}}_{h=0} = \begin{bmatrix}12\\zz\end{bmatrix}^{\mathrm{R}}_{h=0} = D = f\frac{4\pi}{3}\frac{e^2}{2a^3} \\ \begin{bmatrix}12\\xy\end{bmatrix}^{\mathrm{R}}_{h=0} &= \begin{bmatrix}12\\xz\end{bmatrix}^{\mathrm{R}}_{h=0} = \begin{bmatrix}12\\yz\end{bmatrix}^{\mathrm{R}}_{h=0} = 0, \end{aligned} \quad \ldots\ldots(30)$$

where f is a numerical factor. The particular form chosen for D is convenient in that this form occurs naturally in the electrostatic terms. The value of f is chosen so as to bring the frequencies considered into the same region as that of rocksalt ($f = 1{\cdot}88$, cf. § 6). There is also in (30) no difference between $h \to 0$ and $h = 0$. The complete lattice sums can therefore be written as

$$\begin{aligned} \begin{bmatrix}12\\xx\end{bmatrix}_{h\to 0} &= \begin{bmatrix}12\\xx\end{bmatrix}^{\mathrm{E}}_{h\to 0} + \begin{bmatrix}12\\xx\end{bmatrix}^{\mathrm{R}}_{h=0} \\ \begin{bmatrix}12\\xy\end{bmatrix}_{h\to 0} &= \begin{bmatrix}12\\xy\end{bmatrix}^{\mathrm{E}}_{h\to 0}. \end{aligned} \quad \ldots\ldots(31)$$

The calculation of the lattice sums of the type $\begin{bmatrix}11\\xy\end{bmatrix}$ is carried out in the same manner as the type we have been discussing, except that there is an extra term in the summation, involving $(\phi^0_{kk})_{xy}$. This has to be determined using (8). It can then be shown, for instance, that

$$\begin{bmatrix}11\\xx\end{bmatrix}_{h\to 0} = \begin{Bmatrix}11\\xx\end{Bmatrix}_{h\to 0} - \begin{Bmatrix}11\\xx\end{Bmatrix}_{h=0} - \begin{bmatrix}12\\xx\end{bmatrix}_{h=0}, \quad \ldots\ldots(32)$$

where the terms in curly brackets include all those occurring in $\begin{bmatrix}11\\xx\end{bmatrix}$ except

that containing $(\phi^0_{11})_{xx}$. The difference of these two terms is a single expression, that involving G_{xx}, as in eqn. (23), and differs from that expression only in having the negative sign. Hence

$$\left[\begin{matrix}11\\xx\end{matrix}\right]_{h\to 0} = -\left[\begin{matrix}12\\xx\end{matrix}\right]_{h\to 0} \qquad \ldots\ldots(33)$$

and generally

$$\left[\begin{matrix}11\\xy\end{matrix}\right]_{h\to 0} = -\left[\begin{matrix}12\\xy\end{matrix}\right]_{h\to 0}. \qquad \ldots\ldots(34)$$

These descriptions suffice to determine all the lattice sums we shall need. Since the lattice under discussion is symmetrical in the positive and negative charges, and as there are only nearest neighbour repulsive forces, it follows that

$$\left[\begin{matrix}11\\\gamma\delta\end{matrix}\right]_{h\to 0} = \left[\begin{matrix}22\\\gamma\delta\end{matrix}\right]_{h\to 0} \qquad \ldots\ldots(35)$$

where γ, δ take any of the values x, y, z. It can further be shown from the form of the lattice sums that

$$\left[\begin{matrix}12\\\gamma\delta\end{matrix}\right]_{h\to 0} = \left[\begin{matrix}21\\\gamma\delta\end{matrix}\right]_{h\to 0}. \qquad \ldots\ldots(36)$$

§ 6. SPECIAL WAVE DIRECTIONS

The main purpose of this paper is to evaluate the 'limiting' frequencies associated with long waves travelling in different directions in the crystal. To specify these directions we fix certain relations between the values of h_1, h_2 and h_3. These directions are then defined in terms of the vectors of the basic cell, but the direction of the wave vector $\mathbf{s}$ can be expressed without difficulty in terms of the orthogonal axes:

$$\frac{\mathbf{s}}{\lambda} = \mathbf{i}_1\frac{(-h_1+h_2+h_3)}{2a} + \mathbf{i}_2\frac{(h_1-h_2+h_3)}{2b} + \mathbf{i}_3\frac{(h_1+h_2-h_3)}{2c}, \qquad \ldots\ldots(37)$$

where λ is the wavelength and the unit vectors $\mathbf{i}$ are, as in § 2, taken parallel to the orthogonal axes of the orthorhombic cell.

The three cases which will be considered are chosen with a view to simple solutions of the determinantal equation for the frequencies (which follow from (6)) and are in simple directions in reciprocal space.

(*a*) 1. $h_1 = h_2 = h \to 0$; $h_3 = 0$.
2. $h_2 = h_3 = h \to 0$; $h_1 = 0$.
3. $h_3 = h_1 = h \to 0$; $h_2 = 0$.

These represent waves travelling along the orthorhombic axes in reciprocal space, and hence also in the crystal.

(*b*) 1. $h_2 = -h_1 = h \to 0$; $h_3 = 0$.
2. $h_3 = -h_2 = h \to 0$; $h_1 = 0$.
3. $h_1 = -h_3 = h \to 0$; $h_2 = 0$.

Here the waves are directed along the face diagonals of the orthorhombic reciprocal lattice cell. This does not coincide with the corresponding direction in the real cell.

(*c*) 1. $h_1 = h_2 = h_3 = h \to 0$.
2. $h_1 = h_2 = 0$; $h_3 = h \to 0$.
3. $h_1 = h_3 = 0$; $h_2 = h \to 0$.
4. $h_2 = h_3 = 0$; $h_1 = h \to 0$.

Here the directions are parallel to the (four) space diagonals in the reciprocal lattice, which again differ from the corresponding directions in the crystal.

The solution of the equation for the frequencies is particularly simple in case (*a*), and only in case (*c*) is it necessary to solve a third-order equation. These latter sets of solutions are all identical—which can also be seen from the symmetry of the crystal. The values of α and β are chosen to be the same as for thallium fluoride, i.e. $\alpha = 1{\cdot}13$, $\beta = 1{\cdot}38$ and f is taken as 1·88. The solutions are expressed, in units of $B = \frac{4}{3}\pi e^2/2a^3$, as $\mu\omega^2$, where μ is the reduced mass and ω is the angular frequency. The numerical solutions are given in the table.

	(*a*)			(*b*)			(*c*)
Case	1	2	3	1	2	3	
$\mu\omega_1^2$	4·05	3·42	2·96	3·74	3·19	3·54	3·64
$\mu\omega_2^2$	1·03	1·65	1·03	0·55	0·81	1·04	1·32
$\mu\omega_3^2$	0·56	0·56	1·65	1·32	1·65	1·07	0·68

The above values fall into two groups, one ranging from $2{\cdot}96B$ to $4{\cdot}05B$ and the second from $0{\cdot}55B$ to $1{\cdot}65B$—the first group consisting of the longitudinal vibrations. Inserting the value of μ (the reduced mass of thallium fluoride), the frequency ranges are respectively $4{\cdot}8 \times 10^{12}$ to $8{\cdot}2 \times 10^{12}$ and $10{\cdot}9 \times 10^{12}$ to $12{\cdot}9 \times 10^{12}$.

The above set of frequencies forms a sufficient demonstration of the main point of this paper—that the 'limiting' frequencies are dependent in general on the direction of the wave. Even when no distinction is made in the repulsive forces between bonds along the different axes, the spread in the frequency of the longitudinal vibrations, for instance, is about 15%.

§7. RELATION TO INFRA-RED FREQUENCIES

As has been pointed out in the introduction, the above calculations apply insofar as only Coulomb interactions need be considered, and do not necessarily include those vibrations which are associated with electromagnetic waves. The particular vibrations of the lattice which are 'optically active' (in the sense of being associated with electromagnetic waves inside, and outside, the crystal) have been considered by Born (1923, p. 728) who has given a general method of calculating the electromagnetic lattice sums. In the particular case of crystals of the rocksalt type, these optical frequencies coincide with the 'limiting' frequency for transverse waves (cf. Kellermann 1940 and Born 1923). It might therefore be expected that the corresponding calculation for the orthorhombic lattice would lead to (three) frequencies which would coincide with certain of the frequencies listed in the above table. For the orthorhombic crystal one would further expect these limiting frequencies to be associated with those directions which lie along the principal axes of the dielectric ellipsoid, i.e. along the orthogonal axes of the crystal (case (*a*), §6).

Since the lattice sums used by Born are calculated using the formulation of Ewald, these lattice sums can also be used as a check on the accuracy of the numerical calculations used in the table. The electromagnetic lattice sums are given by

$$\left[\frac{kk'}{xy}\right]^{\mathrm{EM}} = \frac{\epsilon_k \epsilon_{k'}}{v}\left[\frac{\partial^2 \psi_0}{\partial x \partial y}\right]_{\mathbf{r}_{kk'}}, \qquad \ldots\ldots(38)$$

where v is the cell volume, ϵ_k the ionic charge and $\psi_0 = \psi_1 + \psi_2$, where

$$\psi_1 = \frac{4\pi}{v} \sum_l{}' \exp\left\{ -\frac{|\mathbf{q}^l|^2}{4\epsilon_0^2} + i(\mathbf{q}^l \cdot \mathbf{r}) \right\},$$

$$\psi_2 = \sum_l \frac{G(\epsilon_0 |\mathbf{r}^l - \mathbf{r}|)}{|\mathbf{r}^l - \mathbf{r}|} - \frac{\pi}{\epsilon_0^2 v}. \qquad \ldots\ldots(39)$$

Here $G(x) = 1 - F(x)$, where F is the error function. The lattice vector is $\mathbf{r}^l$ and the reciprocal lattice vector $\mathbf{q}^l$. The Ewald separating parameter ϵ_0 is taken as a^{-1} in the calculation. In the summation for ψ_1 the zero term is to be omitted. With the same notation and lattice constants as before, the calculation for the orthorhombic lattice leads to

$$\left[\begin{matrix}12\\xx\end{matrix}\right]^{\mathrm{EM}} = -1{\cdot}33B; \quad \left[\begin{matrix}12\\yy\end{matrix}\right]^{\mathrm{EM}} = -0{\cdot}83\,B; \quad \left[\begin{matrix}12\\zz\end{matrix}\right]^{\mathrm{EM}} = -0{\cdot}222\,B. \qquad \ldots\ldots(40)$$

Using the same repulsive forces as before, the three optical (angular) frequencies follow immediately (cf. Born 1923) as

$$\mu\omega^2 = \left[\begin{matrix}12\\\gamma\gamma\end{matrix}\right]^{\mathrm{R}}_{h=0} + \left[\begin{matrix}12\\\gamma\gamma\end{matrix}\right]^{\mathrm{EM}}.$$

These are $\mu\omega_1^2 = 0{\cdot}550B$; $\mu\omega_2^2 = 1{\cdot}05B$; $\mu\omega_3^2 = 1{\cdot}66B$, which agree within the error of calculation with the transverse frequencies listed in the table, case (*a*).

§ 8. OTHER CRYSTAL TYPES

A number of other lattices have been considered. Cubic ionic lattices of the calcium chloride and zinc blende types yield, in the long wave limit, two transverse waves of equal frequency (ν_t) and one longitudinal wave of frequency ν_l, as in the case of rocksalt. The relation between the frequencies of these waves is the same as that deduced by Mott and Fröhlich (1939) from electromagnetic considerations:

$$\nu_l^2 = \nu_t^2 + \epsilon^2/\pi\mu v, \qquad \ldots\ldots(41)$$

where v is the volume of the rhombohedral cell, μ is the reduced mass, and ϵ is the ionic charge.

In calcium fluoride we have a more interesting case, as there are three particles in the rhombohedral cell and the determinant from which the frequencies are to be obtained is of the ninth order. The solutions for wavelengths long compared with the size of the crystal have been given by Born (1923, p. 627) as two triply degenerate vibrations, one of which is optically active. Calculations were carried out using a power law for the repulsive forces, and the results were formulated in the terminology used by Born. The following limiting (angular) frequencies were obtained:

$$\left.\begin{aligned}
\omega_1^2 &= v(D - A')\left(\frac{2}{m_1} + \frac{1}{m_2}\right) \text{ (twice)}\\
\omega_2^2 &= v(2A' + D)\left(\frac{2}{m_1} + \frac{1}{m_2}\right) \text{ (once)}\\
\omega_3^2 &= v(D + 2D')\frac{1}{m_2} \text{ (three times)}
\end{aligned}\right\} \qquad \ldots\ldots(42)$$

where $A' = 8\pi\mathbf{e}^2/3v^2$, m_1 and m_2 are the masses of calcium and fluorine ions, D and D' are the lattice sums defined by Born, v is the volume of the rhombohedral cell. The first of these frequencies is associated with transverse waves and is

the same as that found by Born, the third is also that given by Born, the wave being transverse and having zero electric moment per cell. The second frequency is associated with a longitudinal wave (with a definite electric moment in the reference cell) and is analogous to the longitudinal wave in the rocksalt crystal. Terming $\omega_1 = \omega_t$ and $\omega_2 = \omega_l$, it follows from (42) that

$$\omega_l^2 = \omega_t^2 + \frac{8\pi e^2}{v}\left(\frac{2}{m_1} + \frac{1}{m_2}\right). \qquad \ldots\ldots(43)$$

This is a relation of the same form as (41). Applying the method of Mott and Fröhlich (1939) to calcium fluoride, the relation (43) is also found.

Finally, the zinc oxide lattice was examined, as an example of a group of crystals with ionic forces which do not possess cubic symmetry. The simplest cell contains four molecules, and hence the determinant from which the frequencies are to be obtained is of twelfth order. In the long wave limit, and choosing suitable directions in the crystal, the determinant can be split up so that one does not have to deal with more than third-order determinants. The results of the calculation confirmed those obtained for the orthorhombic lattice, namely, that the limiting frequencies are not unique. In view of this and of the rather complicated nature of the calculations, it does not seem desirable to record them in detail.

§9. CONCLUSION

The general conclusion to be drawn from the above calculation for the orthorhombic lattice has already been indicated in the introduction The fact that the limiting frequency, in a particular frequency branch, is not unique means that the surfaces of constant frequency are strongly distorted in this region. The consequence is that where a sharp peak might have been expected in the vibrational spectrum by analogy with the rocksalt case, this peak will be extensively broadened. As regards the longitudinal branch, characterized by a long tail at its high-frequency end, this distortion of the surfaces of constant frequency will mean a more extensive and tenuous tail.

The general features discussed above are expected to apply to all crystals which do not possess cubic symmetry.

REFERENCES

Born, M., 1923, *Atom Theorie des festen Zustandes* (Leipzig : Teubner).
Broch, E. K., 1937, *Proc. Camb. Phil. Soc.*, **33,** 485.
Epstein, P., 1903, *Math. Ann.*, **56,** 615.
Ewald, P. P., 1938, *Nachr. Ges. Wiss. Göttingen*, N.F. II, **3**, 55.
Iona, M., 1941, *Phys. Rev.*, **60,** 822.
Kellermann, W., 1940, *Phil. Trans. Roy. Soc.* A, **238,** 513.
Lyddane, R. H., and Herzfeld, K. F., 1938, *Phys. Rev.*, **54,** 846.
Mott, N. F., and Fröhlich, H., 1939, *Proc. Roy. Soc.* A, **171,** 496.

Free Energy of the Double Layers of Two Parallel Plates in a 1–2 Electrolyte

By S. LEVINE* and A. SUDDABY†

* Department of Mathematics, University of Manchester
† Department of Physics, Sir John Cass College, London

MS. received 10*th October* 1951 *and in final form* 15*th February* 1952

ABSTRACT. By making use of the Poisson–Boltzmann equation an expression is obtained for the free energy of the electric double layers of two parallel plates immersed in a large volume of an electrolyte of the 1–2 valency type. Two cases arise depending on whether or not the divalent ion and the surface charge have the same sign. The formula for the free energy is expressed in terms of elliptic integrals. An approximate form for the free energy, which is more convenient for numerical computations, is also obtained. This is particularly suitable at large surface potentials and is derived for a symmetrical electrolyte as well as for the asymmetrical ones. Numerical tables of the free energy as a function of plate separation are given and some applications are briefly indicated.

§ 1. INTRODUCTION

A derivation of the expression for the free energy of the electrical double layers of two parallel plates immersed in a large volume of an electrolyte of the binary, symmetrical type has been given by Verwey and Overbeek (1948) in their recent book. Their discussion has been restricted to the case of symmetrical electrolytes owing to the mathematical difficulties involved in the asymmetrical case. In the present paper we obtain corresponding expressions for the free energy of the double layers of two parallel plates in the two cases of a 1–2 valency type of electrolyte, namely Case I, when the divalent ion has the opposite charge to the surface ion, and Case II, when the charge on the divalent ion has the same sign as the surface charge. The solution of the Poisson–Boltzmann equation for an electrolyte containing both monovalent and divalent ions has been already given by Wood and Robinson (1946) and we shall use a similar procedure for evaluating the free energy. Robinson (1948, 1949) has shown that if the electrolyte is of the asymmetrical type, then we can express our results in terms of elliptic integrals only if there are present univalent and divalent ions (in any proportion). However, hyperelliptic integrals are encountered in the case of higher valency types of electrolytes.

The exact formulae for the free energy which are derived in this paper are rather involved and their numerical computation proves to be laborious. Consequently it is desirable to seek various types of expansions which are simpler in form and, at the same time, reasonably accurate. One such approximate expansion is suggested by table XI in the book by Verwey and Overbeek (1948, p. 82), which gives the values of the interaction (free) energy of two plates in a symmetrical electrolyte. It is observed that this energy very nearly depends on the value of the electrical potential at the median plane only. We shall obtain a series for the interaction energy, the first term of which is a function of the median potential; the higher terms depend on both the median potential and surface potential and are

quite small, unless either the potential or the separation is small. This series is given by eqn. (20) for the symmetrical case, by (35) for Case I, and by (46) for Case II. Thus the main part of the energy depends on one parameter only, whereas the exact formula for the energy involves two parameters. Consequently, the first two or three terms of the above series are much more convenient for numerical computation than the exact expression and are sufficiently accurate, except at small potentials or separations, particularly in Case I. Verwey and Overbeek do refer to the above property of the interaction energy, but there is no mention of the expansion which we derive both for the symmetrical and 1–2 valency types of electrolytes. In a future paper (to be referred to for convenience as Part II) we shall develop different expansions which correspond to those obtained in previous papers (Levine and Suddaby 1951 a, b) for the case of a symmetrical electrolyte.

In this paper (and also in Part II) we restrict ourselves chiefly to the mathematical proofs and the computations of numerical tables of the free energy. Applications will be dealt with in a still later paper, although some discussion on the major role of the coagulating ion on stability properties of colloids is given.

§ 2. GENERAL EXPRESSION FOR FREE ENERGY

Each of the parallel plates is assumed to have unit area, and the edge effects and the outer faces of the plates are ignored. We introduce the following notation:

R distance between the plates.
x distance measured in the normal direction from the median plane.
ψ potential at position x in the overlapping diffuse layers.
ψ_0 potential at the surface of each plate ($x = \pm \frac{1}{2}R$).
ψ_m potential at the median plane ($x = 0$).
n_i volume density of ions of species i in the bulk of the electrolyte solution ($i = 1, 2$).
v_i valency of an i ion.
D dielectric constant of the dispersion medium.
T temperature. $\boldsymbol{k}$ Boltzmann's constant. $\boldsymbol{e}$ electronic charge.
$\eta = \boldsymbol{e}\psi/\boldsymbol{k}T$, $\eta_0 = \boldsymbol{e}\psi_0/\boldsymbol{k}T$, $\eta_m = \boldsymbol{e}\psi_m/\boldsymbol{k}T$.
$y = \exp(-\eta)$, $y_0 = \exp(-\eta_0)$, $k = \exp(-\eta_m)$.
κ Debye–Huckel parameter given by $\kappa^2 = 4\pi \boldsymbol{e}^2 B, D\boldsymbol{k}T$, $B = \Sigma n_i v_i^2$, where we sum over $i = 1, 2$.
σ surface charge density.
E electrostatic energy per plate associated with the double layer.
Δp difference between the (ideal) osmotic pressure at any position in the diffuse layer and the corresponding pressure in the interior of the solution.
$2F$ (electrical) free energy of the double layers of the two plates.
$2F_\infty$ free energy of the double layers when plates are at infinite separation.
$V(R) = 2F - 2F_\infty$ interaction or mutual free energy of the plates, i.e. the change in free energy when plates are brought to position R from infinite separation.

$\Delta(k, \phi) = (1 - k^2 \sin^2\phi)^{1/2}$, $R(k, z) = [(1 - z^2)(1 - k^2 z^2)]^{1/2}$.

$$F(k, \phi) = \int_0^{\varphi} \frac{d\phi}{\Delta(k, \phi)} = \int_0^{z} \frac{dz}{R(k, z)}, \quad z = \sin\phi, \text{ elliptic integral of the first kind.}$$

$$E(k, \phi) = \int_0^{\varphi} \Delta(k, \phi)\, d\phi = \int_0^{z} \frac{R(k, z)}{(1 - z^2)}\, dz, \text{ elliptic integral of the second kind.}$$

The form of the electrical free energy employed is derived from the Lippmann equation,

$$2F = -2\int_0^{\psi_0} \sigma\, d\psi = -2E - 2\int_0^{R/2} \Delta p\, dx. \qquad \ldots\ldots(1)$$

The second relation in (1) follows immediately from a more general formula derived by Levine (1951) which applies to a single colloidal particle of arbitrary shape. An equivalent equation was derived by Verwey and Overbeek (1948, pp. 78–81) in the case of a symmetrical electrolyte.

The Poisson–Boltzmann equation for ψ reads

$$\frac{d^2\psi}{dx^2} = -\frac{4\pi \boldsymbol{e}}{D}\Sigma n_i v_i y^{v_i}, \qquad \ldots\ldots(2)$$

a first integral which is

$$\left(\frac{d\psi}{dx}\right)^2 = \frac{8\pi \boldsymbol{k}T}{D}\Sigma n_i (y^{v_i} - k^{v_i}), \qquad \ldots\ldots(3)$$

since $d\psi/dx = 0$ at $x = 0$. It is convenient to express (3) in the form

$$\frac{1}{\kappa}\frac{dy}{dx} = -\frac{y}{\kappa}\frac{d\eta}{dx} = \pm y\left[\frac{2}{B}\Sigma n_i (y^{v_i} - k^{v_i})\right]^{1/2} = \pm pQ(y), \qquad \ldots\ldots(4)$$

where p is so chosen that the coefficient of the highest power of y in $Q^2(y)$ is unity. The positive root is taken if $\sigma < 0$, the negative if $\sigma > 0$. Then the solution of (2) is

$$\tfrac{1}{2}\kappa R = \pm\frac{1}{p}\int_k^{y_0} \frac{dy}{Q(y)}. \qquad \ldots\ldots(5)$$

The electrostatic energy per plate is written as

$$E = \frac{D}{8\pi}\int_0^{R/2}\left(\frac{d\psi}{dx}\right)^2 dx = \frac{D}{8\pi}\int_{\psi_m}^{\psi_0}\frac{d\psi}{dx}\,d\psi = \pm\frac{D\kappa}{4\pi}\left(\frac{\boldsymbol{k}T}{\boldsymbol{e}}\right)^2 pI, \qquad \ldots\ldots(6)$$

where

$$I = \int_k^{y_0}\frac{Q(y)}{y^2}\,d_y, \qquad \ldots\ldots(7)$$

which follows from (4) on transforming from ψ to y. The corresponding expression for the second energy term on the right of (1) is

$$-2\boldsymbol{k}T\Sigma n_i\int_0^{R/2}(y^{v_i} - 1)\,dx. \qquad \ldots\ldots(8)$$

Substituting (3) into the first integral expression for E in (6), it immediately follows that (1) can be expressed as

$$2F = -4E - \boldsymbol{k}TR\Sigma n_i (k^{v_i} - 1). \qquad \ldots\ldots(9)$$

§ 3. SYMMETRICAL ELECTROLYTE

In this case we put the valencies of the ion types $v_1 = -v_2 = v\,(>0)$, the volume densities $n_1 = n_2 = n$, and choose $\sigma > 0$. Then

$$B = 2nv^2,\quad \kappa^2 = 8\pi n v^2 \boldsymbol{e}^2/D\boldsymbol{k}T,\quad p = 1/v, \qquad \ldots\ldots(10)$$

$$Q(y) = y[y^v + y^{-v} - k^v - k^{-v}]^{1/2}, \qquad \ldots\ldots(11)$$

and (5) yields

$$\tfrac{1}{4}\kappa R = k^{v/2}\{F(k^v, \tfrac{1}{2}\pi) - F(k^v, \alpha)\}, \qquad \ldots\ldots(12)$$

where

$$\xi = \sin\alpha = (y_0/k)^{v/2}. \qquad \ldots\ldots(13)$$

The free energy (9) is

$$2F = -\frac{4n\boldsymbol{k}T}{\kappa}\left[\tfrac{1}{4}\kappa R(3k^{-v} - 2 - k^v) + \frac{2}{y_0}Q(y_0) - 4k^{-v/2}\{E(k^v, \tfrac{1}{2}\pi) - E(k^v, \alpha)\}\right], \qquad \ldots\ldots(14)$$

and when $R\to\infty$ this becomes

$$2F_\infty = -\frac{8nkT}{\kappa}[y_0{}^{v/2}+y_0{}^{-v/2}-2]. \qquad \ldots\ldots(15)$$

The solution (12) was originally given by Langmuir (1938). The electrostatic energy E was first evaluated by Corkill and Rosenhead (1939) and the free energy expression (14) was derived by Verwey and Overbeek (1948, pp. 78–81).

It is possible to express (12) and (14) somewhat differently. In the following sections corresponding alternative forms will also be obtained for the 1–2 electrolyte cases and the method of arriving at these results will be essentially the same as for the symmetrical case. This method is based on the substitution

$$z'^2 = \frac{1-z^2}{1-k^2z^2}, \quad z=\sin\phi,\ z'=\sin\phi', \qquad \ldots\ldots(16)$$

which leads to the relations

$$F(k,\tfrac{1}{2}\pi)-F(k,\phi)=F(k,\phi'), \qquad \ldots\ldots(17)$$

$$E(k,\tfrac{1}{2}\pi)-E(k,\phi)=E(k,\phi')-k^2\sin\phi'\cos\phi'/\Delta(k,\phi'). \qquad \ldots\ldots(18)$$

These can be derived from the properties of elliptic integrals (Jahnke and Emde 1945). In the symmetrical case we replace k by k^v and ϕ by α. Then (12) becomes

$$\tfrac{1}{4}\kappa R = k^{v/2}F(k^v,\alpha'), \quad \sin\alpha'=\cos\alpha/\Delta(k^v,\alpha), \qquad \ldots\ldots(12a)$$

and it is readily verified that the second and third terms in the brackets in (14) may be replaced by

$$2\left\{\frac{1+(ky_0)^v}{1-(ky_0)^v}\right\}\frac{Q(y_0)}{y_0}-4k^{-v/2}E(k^v,\alpha'). \qquad \ldots\ldots(14a)$$

To obtain the convenient expansion referred to in the introduction, the form (14) for $2F$ is expanded in powers of ξ. Firstly, the Taylor series for $F(k^v,\alpha)$ in powers of ξ is readily obtained, and then substitution into (12) leads to the relation

$$\tfrac{1}{4}\kappa R = k^{v/2}[F(k^v,\tfrac{1}{2}\pi)-\xi-\tfrac{1}{6}(1+k^{2v})\xi^3-\tfrac{1}{5}\{\tfrac{3}{8}(1+k^{4v})+\tfrac{1}{4}k^{2v}\}\xi^5+\ldots]. \quad \ldots(19)$$

The corresponding series for $E(k^v,\alpha)$ and $Q(y_0)$ in powers of ξ are also derived and, making use of (14), (15) and (19), we obtain

$$V(R)=\frac{4nkT}{\kappa}[f_0(k)+\tfrac{1}{12}k^{v/2}(1-k^v)\xi^3+\tfrac{1}{20}k^{v/2}(1-k^v)^3(1-k^{3v})\xi^5+\ldots], \quad \ldots(20)$$

where $$f_0(k)=k^{v/2}(2-k^v-3k^{-2v})F(k^v,\tfrac{1}{2}\pi)+4k^{-v/2}E(k^v,\tfrac{1}{2}\pi)-4. \qquad \ldots\ldots(21)$$

If k is fixed and $\xi\to 0$, which means that $\eta_0\to\infty$, the first term in the brackets on the right of both (19) and (20) remains, the higher terms becoming negligible. If y_0 (or η_0) is fixed and $\kappa R\to\infty$, then $k\to 1$, $F(k^v,\tfrac{1}{2}\pi)\to\infty$, and again these higher terms can be neglected; in this case $f_0(k)\to 0$, but it does not vanish as rapidly as the higher terms.

An examination of Verwey and Overbeek's table XI shows that at $v\eta_0=4$ and $\kappa R=0{\cdot}8$, for example, the contribution to $V(R)$ from the higher terms is less than 3%; at $v\eta_0=2$ and $\kappa R=2{\cdot}3$ it is about 2%. We therefore reach the following conclusions. The free energy $2F$ can be written as the sum of three terms, namely (i) $2F_\infty$, which depends only on y_0 or η_0, (ii) the part of $V(R)$ which is a function of k or η_m only, and (iii) a correction term which varies with both k and y_0 and which is very small unless η_0 or κR is small. If, according to Verwey and Overbeek, stability properties of colloidal plates depend in the main on the properties of $2F$ for κR equal to or greater than 2, then the first two terms in the

brackets on the right of (20) will usually give sufficient accuracy. Table 1 gives the values of $f_0(k)$ and $\kappa R = (\kappa R)_\infty$ when $\xi = 0$ ($\eta_0 = \infty$) for various k^v. We have used the tables of the complete elliptic integrals of Fletcher (1940), who chooses intervals of the modulus (here k^v) instead of the usual angle $\sin^{-1} k^v$. We have not tabulated the higher terms in (19) or (20), but these are readily computed. It is noted that the series (19) and (20) converge for all $\kappa R > 0$, $\eta_0 > 0$.

Table 1

k^v	$(\kappa R)_\infty$	$f_0(k)$	k^v	$(\kappa R)_\infty$	$f_0(k)$
0·0025	0·3142	27·573	0·4	4·1489	0·23455
0·005	0·4443	18·436	0·45	4·4566	0·17450
0·01	0·6283	12·021	0·5	4·7680	0·12920
0·025	0·9936	6·427	0·55	5·0886	0·09468
0·05	1·4058	3·715	0·6	5·4245	0·06824
0·075	1·7231	2·573	0·65	5·7837	0·04801
0·1	1·9919	1·9259	0·7	6·1769	0·03261
0·15	2·4473	1·2103	0·75	6·6199	0·02106
0·2	2·8387	0·8243	0·8	7·1386	0·01259
0·25	3·1925	0·5860	0·85	7·7813	0·006646
0·3	3·5231	0·4270	0·9	8·6545	0·002784
0·35	3·8396	0·3154	0·95	10·099	0·0006583

§ 4. CASE I. DIVALENT ION OF OPPOSITE CHARGE TO SURFACE

We assume the surface charge density σ is positive and consider a 1–2 electrolyte with a negative divalent ion, for example K_2SO_4. Taking K^+ as species 1, $v_1 = 1$ and SO_4^{2-} as species 2, $v_2 = 2$, $n_1 = 2n_2$. Then

$$B = 6n_2,\ \kappa^2 = 24\pi n_2 \mathbf{e}^2/D\mathbf{k}T,\ p = (2/3)^{1/2}, \qquad \ldots\ldots(22)$$

$$Q(y) = (y^3 - hy^2 + \tfrac{1}{2})^{1/2} = \{(y-a)(y-b)(y-c)\}^{1/2}, \qquad \ldots\ldots(23)$$

where

$$h = k + \tfrac{1}{2}k^{-2},\ a = k,\ \begin{matrix} b \\ c \end{matrix} = \frac{1}{4k^2} \pm \tfrac{1}{2}\left(\frac{1}{4k^4} + \frac{2}{k}\right)^{1/2},\ ab + bc + ca = 0,\ abc = -\tfrac{1}{2}. \qquad (24)$$

Since ψ is positive, $\psi_m < \psi_0$ and hence $y < k < 1$ ($y_0 = k$ at $R = 0$). The disposition of the roots and the range of y are $b > 1 > a = k \geqslant y \geqslant y_0 > 0 > c$. If we introduce the substitution

$$u = \sin\Phi = \{(y-c)/(a-c)\}^{1/2} \qquad \ldots\ldots(25)$$

and put

$$u_0 = \sin\Phi_0 = \{(y_0-c)/(a-c)\}^{1/2},\ k_1 = \{(a-c)/(b-c)\}^{1/2}, \qquad \ldots\ldots(26)$$

then (5) becomes

$$\tfrac{1}{2}\kappa R = \{6/(b-c)\}^{1/2}\ \{F(k_1, \tfrac{1}{2}\pi) - F(k_1, \Phi_0)\}, \qquad \ldots\ldots(27)$$

which is the solution of the Poisson–Boltzmann equation. The formula (9) for the free energy becomes

$$2F = -4E - \mathbf{k}TRn_2(2h-3), \qquad \ldots\ldots(9a)$$

and in Appendix I this is evaluated, giving

$$2F = -\frac{4n_2\mathbf{k}T}{\kappa}\left[\tfrac{1}{4}\kappa R(6b - 2h - 3) + \frac{\sqrt{6}\,Q(y_0)}{y_0} - 3\sqrt{6}\,(b-c)^{1/2}\{E(k_1, \tfrac{1}{2}\pi) - E(k_1, \Phi_0)\}\right], \qquad \ldots\ldots(28)$$

where $Q(y_0)$ is given by (23). The value of $2F_\infty$, the free energy of the two plates at infinite separation, is readily found. When $R\to\infty$, then $k\to 1$, $E(k_1, \frac{1}{2}\pi)\to 1$, $E(k_1, \Phi_0)\to \sin\Phi_0$, the first term on the right of (28) vanishes and the last two terms yield

$$2F_\infty = -\frac{4n_2kT}{\kappa}\left[\sqrt{3}\left(2+\frac{1}{y_0}\right)(1+2y_0)^{1/2}-9\right]. \quad \ldots\ldots(29)$$

The same expression may also be obtained directly by putting $k=1$ in the expression for $Q(y)$ in the integral (7) and evaluating (9). If the surface charge density $\sigma<0$ and the 1–2 electrolyte present has a positive divalent ion, it is clear on physical grounds that the free energy (28) remains unchanged. It is readily verified that the preceding analysis is reproduced exactly if we replace y and k by their reciprocals (which is equivalent to changing the signs of σ and of the divalent ion).

In the preceding section we made reference to an alternative form for the free energy based on the substitution (16) and the use of the relations (17) and (18). For the case under consideration this substitution will be written

$$u' = \sin\Phi' = \left(\frac{1-u^2}{1-k_1^2u^2}\right)^{1/2} = \frac{1}{k_1}\left(\frac{y-a}{y-b}\right)^{1/2}. \quad \ldots\ldots(30)$$

Then (27) can be expressed as

$$\tfrac{1}{2}\kappa R = \left(\frac{6}{b-c}\right)^{1/2} F(k_1, \Phi_0'), \quad \sin\Phi_0' = \frac{1}{k_1}\left(\frac{y_0-a}{y_0-b}\right)^{1/2}, \quad \ldots\ldots(27a)$$

and the second and third terms in the brackets in (28) become

$$\frac{\sqrt{6}\,(b+2y_0)}{y_0(b-y_0)}\,Q(y_0) - 3\sqrt{6}\,(b-c)^{1/2}\,E(k_1, \Phi_0'). \quad \ldots\ldots(28a)$$

It is also possible, although more laborious, to obtain the above results directly from (5) and (9) by employing the substitution (30).

Finally we derive an expansion for the free energy difference $V(R)$ which corresponds to (20). Firstly,

$$F(k_1, \Phi_0) = \int_0^{u_0}\frac{du}{R(k_1, u)} = F(k_1, \Omega) + \frac{(b-c)^{1/2}}{2}\int_0^{y_0}\frac{dy}{Q(y)}$$

$$= F(k_1, \Omega) + \left(\frac{b-c}{2}\right)^{1/2}(y_0 + \tfrac{1}{3}hy_0^3 - \tfrac{1}{4}y_0^4 + \tfrac{3}{10}h^2y_0^5 + \ldots), \quad \ldots\ldots(31)$$

where $\sin\Omega = -c/(a-c)$. This expansion is obtained if we transform from u to y, making use of (25) and (26), and then we expand the integrand in (31) in powers of y. Similarly

$$E(k_1, \Phi_0) = E(k_1, \Omega) + \frac{1}{\{2(b-c)\}^{1/2}}\{by_0 - \tfrac{1}{2}y_0^2 + \tfrac{1}{3}bhy_0^3$$

$$-\tfrac{1}{4}(b+h)y_0^4 + \tfrac{1}{5}(\tfrac{3}{2}bh^2+1)y_0^5 + \ldots\}, \quad \ldots\ldots(32)$$

noting that $(b-y)/Q(y)$ replaces the integrand $1/Q(y)$ in (31). It is now convenient to introduce the substitution (16) where $z = \sin\Omega$, i.e.

$$\sin\Omega' = \frac{\cos\Omega}{\Delta(k_1, \Omega)} = \left\{\frac{a(b-c)}{b(a-c)}\right\}^{1/2} = \left(\frac{2a+b}{a+2b}\right)^{1/2}, \quad \ldots\ldots(33)$$

which follows from (24). Making use of (17) and (31), (27) becomes

$$\tfrac{1}{2}\kappa R = \sqrt{6}\left[\frac{F(k_1,\Omega')}{(b-c)^{1/2}} - \frac{y_0}{\sqrt{2}} - \frac{hy_0^3}{3\sqrt{2}} + \frac{y_0^4}{4\sqrt{2}} - \frac{3y_0^5}{10\sqrt{2}} + \dots\right]. \quad \dots\dots(34)$$

To obtain $V(R)$, the quantities $Q(y_0)$ and $2F_\infty$, defined by (23) and (29) respectively, are expanded in powers of y_0 and use is made of the substitution (33) and of the relations (17), (18) and (32). Then it follows from (28), (29) and (34) that

$$V(R) = \frac{4n_2kT}{\kappa}\left[f_1(k) + \frac{1}{2\sqrt{3}}(h-\tfrac{3}{2})^2 y_0^3 + \frac{\sqrt{3}}{5}(h-\tfrac{3}{2})^2(4h+3)y_0^5 + \dots\right]$$

$$= \frac{4n_2kT}{\kappa} g_1(k,y_0), \text{ say,} \quad \dots\dots(35)$$

where $$f_1(k) = \left(\frac{3}{2(b-c)}\right)^{1/2}(2h+3-6b)\,F(k_1,\Omega')$$

$$+ 3\sqrt{6}(b-c)^{1/2}E(k_1,\Omega') + 3\sqrt{6}(1-b^{-1}) - 9. \quad \dots\dots(36)$$

The equivalent form for $f_1(k)$ in terms of Ω is readily obtained.

Just as in the symmetrical case, $f_1(k)$ is the main contribution to $g_1(k,y_0)$ provided κR or η_0 is not too small. Indeed, the expansions (31), (34) and (35) converge only if $y_0 < |c|$, and this condition implies that κR must be greater than 0·71, 0·17, 0·07, 0·03, 0·01 and 0·004 approximately when $\eta_0 = 1$, 2, 3, 4, 5 and 6 respectively. Tables 2 and 3 give the values of κR and the function $g_1(k,y_0)$ for the above range of η_0. When $\eta_0 = 2$ and $\kappa R > 1$, the first three terms in the expansion (35) yield $V(R)$ with an error of less than $\frac{1}{2}\%$. As either κR or η_0 increases, the accuracy of these terms improves; thus we have at least four-figure accuracy when $\eta_0 = 2$, $\kappa R > 3$, or $\eta_0 = 3$, $\kappa R > 1$ or $\eta_0 = 4$, $\kappa R > \frac{1}{2}$. When $\eta_0 = 1$, $\kappa R = 1$ the error is about 5% and, although this diminishes as κR increases, the third term in (35) is larger than the second, which means that we require the higher terms in the expansion. The corresponding first five terms in the series (34) for κR are even more accurate; thus when $\eta_0 = 1$, $\kappa R = 1$ we have an error of less than 3%, and when $\eta_0 = 2$, $\kappa R > 1$ at least four-figure accuracy. It is convenient to divide table 2 into two sections; in the upper section we need not tabulate $g_1(k,y_0)$ since it is identical with $g_1(k,\infty) = f_1(k)$ if we retain only four figures. In table 3 the values of $g_1(k,y_0)$ are calculated for small κR. We used the exact formulae (27) and (28) for both $\eta_0 = 1$ and small κR and also as a check in the range where the expansions (34) and (35) are applicable. Where the values of k are not given in table 3, we have applied another series for $g_1(k,y_0)$, which is suitable at small separations and which will be derived in Part II. Also in the case $\eta_0 = 1$ and large κR still another expansion for $g_1(k,y_0)$ has been used; this will also be given in Part II.

It is observed that the correction to the limiting function $f_1(k)$ is of order $y_0^3 = \exp(-3\eta_0)$, which is very small for η_0 equal to or greater than 2. This is to be compared with the corresponding correction in the case of a 2–2 valency type of electrolyte, given in (20), where we find the same factor in $\xi^3 = k^{-3}\exp(-3\eta_0)$ since $v = 2$. The range of κR and η_0 over which the series (35) can be applied is much greater than that of the expansions developed in Part II. However, these other series can be generalized to higher valency electrolyte types, whereas the corresponding extension of (35) would involve hyperelliptic integrals. Also, to obtain $f_1(k)$ for large κR, we subtract two quantities which are very nearly equal and this requires a double interpolation of the tabulated values of elliptic integrals, which is found to be rather laborious.

Table 2

η_0	k	0·025	0·050	0·075	0·10	0·15	0·20	0·25	0·30	0·35	0·40	0·45	0·50	0·55	0·60	0·65	0·70	0·80	0·90
∞	$g_1(k,\infty)=f_1(k)$	50·71	23·60	14·63	10·19	5·830	3·731	2·530	1·773	1·266	0·9125	0·6602	0·4760	0·3403	0·2395	0·1648	0·1094	0·04061	0·008645
	$\kappa R=(\kappa R)_\infty$	0·1360	0·2721	0·4082	0·5443	0·8170	1·091	1·366	1·645	1·927	2·216	2·513	2·821	3·144	3·486	3·855	4·260	5·250	6·798
6		0·1274	0·2635	0·3996	0·5357	0·8084	1·082	1·358	1·636	1·919	2·208	2·504	2·812	3·135	3·477	3·846	4·251	5·241	6·789
5	κR^*		0·2487	0·3848	0·5209	0·7936	1·067	1·343	1·621	1·904	2·193	2·490	2·798	3·120	3·463	3·831	4·236	5·227	6·775
4					0·4805	0·7534	1·027	1·303	1·581	1·864	2·153	2·450	2·758	3·080	3·422	3·791	4·196	5·186	6·734
3	$g_1(k,y_0)$				10·28	5·850	3·736	2·532	1·774	1·266	0·9127	0·6603							
	κR				0·3638	0·6412	0·9164	1·193	1·471	1·754	2·043	2·340	2·648	2·971	3·313	3·682	4·087	5·077	6·625
2	$g_1(k,y_\bullet)$						3·860	2·570	1·788	1·273	0·9158	0·6621	0·4768	0·3407	0·2397	0·1649			
	κR						0·5753	0·8703	1·158	1·445	1·737	2·036	2·345	2·669	3·012	3·381	3·786	4·777	6·325
1	$g_1(k,y_0)$										1·0840	0·7220	0·5025	0·3523	0·2449	0·1671	0·1104		
	κR										0·5771	0·9991	1·365	1·722	2·086	2·469	2·884		

* $g_1(k,y_0)=f_1(k)$ in group $\eta_0=4, 5, 6$.

Table 3

η_0								
	k	0·00248	—	—	0·00048	0·0095	0·0185	0·036
6	$g_1(k, y_0)$	694·96	615·0	542·$_3$	282·1	139·6	69·81	34·13
	κR	0	0·002	0·004	0·01710	0·04301	0·09206	0·1873
	k	0·00674	—	—	0·011	0·0185	0·025	0·03
5	$g_1(k, y_0)$	253·27	226·2	201·2	121·9	70·01	50·64	41·69
	κR	0	0·005	0·01	0·03473	0·07678	0·1124	0·1399
	k	0·0183	—	—	0·032	0·050	0·057	0·075
4	$g_1(k, y_0)$	90·810	79·84	69·9_0	39·36	23·69	20·33	14·64
	κR	0	0·015	0·03	0·1066	0·2071	0·2456	0·3441
	k	0·0498	—	—	0·07	0·1	0·15	
3	$g_1(k, y_0)$	31·113	27·18	23·60	16·44	10·28	5·850	
	κR	0	0·04	0·08	0·1891	0·3638	0·6412	
	k	0·1353	—	—	0·17			
2	$g_1(k, y_0)$	9·3315	8·055	6·883	5·148			
	κR	0	0·1	0·2	0·3836			
	k	0·3679	—	—		0·75	—	—
1	$g_1(k, y_0)$	1·7669	1·5133	1·2747		0·06968	0·03638	0·01341
	κR	0	0·2	0·4		3·348	4	5

§ 5. CASE II. DIVALENT ION OF SAME CHARGE AS SURFACE

It is convenient to consider again a 1–2 electrolyte with a negative divalent ion, but this time to take the surface charge as negative. Since the potential ψ is negative, the distribution of the roots a, b, c and the range of y are now $y_0 \geqslant y \geqslant a = k > 1 > b > 0 > c$. From physical considerations one would expect Case II to follow directly from Case I by replacing η_0 by $-\eta_0$. The details of this method of treating Case II are as follows. We introduce the (real) substitution

$$v = \sin\beta = \left(\frac{a-c}{y-c}\right)^{1/2} = \frac{1}{u}, \qquad \ldots\ldots(37)$$

and put

$$v_0 = \sin\beta_0 = \left(\frac{a-c}{y_0-c}\right)^{1/2}, \quad k_2 = \left(\frac{b-c}{a-c}\right)^{1/2} = \frac{1}{k_1}. \qquad \ldots\ldots(38)$$

Then, making use of the first equation in (31), we can write

$$F(k_1, \tfrac{1}{2}\pi) - F(k_1, \Phi_0) = k_2 \int_{v_0}^{1} \frac{dv}{R(k_2, v)} = k_2[F(k_2, \tfrac{1}{2}\pi) - F(k_2, \beta_0)]. \qquad \ldots\ldots(39)$$

Thus (27) becomes

$$\tfrac{1}{2}\kappa R = \{6/(a-c)\}^{1/2}\{F(k_2, \tfrac{1}{2}\pi) - F(k_2, \beta_0)\}. \qquad \ldots\ldots(40)$$

This can also be obtained by introducing the transformation (37) directly into (5). In equation (27) Φ_0 is real and $k_1 < 1$ if the potential is positive, whereas in equation (40) β_0 is real and $k_2 < 1$ if the potential is negative. Similarly

$$E(k_1, \tfrac{1}{2}\pi) - E(k_1, \Phi_0) = -\frac{1}{k_2}\int_{v_0}^{1} \frac{R(k_2, v)}{v^2(1-v^2)}\,dv = -\frac{1}{k_2}\int_{\beta_0}^{\pi/2} \frac{\Delta(k_2, \beta)}{\sin^2\beta}\,d\beta$$

$$= -\frac{1}{k_2}\Delta(k_2, \beta_0)\cot\beta_0 + \frac{1}{k_2}\{E(k_2, \tfrac{1}{2}\pi) - E(k_2, \beta_0)\}$$

$$+ \frac{(1-k_2^2)}{k_2^2}\{F(k_2, \tfrac{1}{2}\pi) - F(k_2, \beta_0)\}, \qquad \ldots\ldots(41)$$

where the final form is obtained after integrating by parts. Using eqns. (24)–(27), it can be verified that (28) becomes

$$2F = -\frac{4n_2\boldsymbol{k}T}{\kappa}\left[\tfrac{1}{4}\kappa R(6k-3-2h)+\frac{\sqrt{6}}{(y_0-c)}\left(2+\frac{c}{y_0}\right)Q(y_0)\right.$$
$$\left.-3\sqrt{6}\,(a-c)^{1/2}\{E(k_2,\tfrac{1}{2}\pi)-E(k_2,\beta_0)\}\right], \quad \ldots\ldots(42)$$

where $Q(y_0)$ is again given by (23). This is the required formula for the free energy in Case II. We find $2F_\infty$ in the same way as in Case I and obtain a form identical with (29). It is noted, however, that in Case I $\eta_0>\eta_m>0$ and thus $y_0<k<1$, whereas in Case II $\eta_0<\eta_m<0$ and thus $y_0>k>1$. In Appendix II it is shown that we can arrive at the result (42) by starting with the original formulae (9) and employing a method analogous to that used in Case I.

The alternative expression for the free energy is readily obtained. We substitute

$$v'=\sin\beta'=\left(\frac{1-v^2}{1-k_2{}^2v^2}\right)^{1/2}=\left(\frac{y-a}{y-b}\right)^{1/2}. \quad \ldots\ldots(43)$$

Then (40) reads

$$\tfrac{1}{2}\kappa R=\left(\frac{6}{a-c}\right)^{1/2}F(k_2,\beta_0'),\ \sin\beta_0'=\left(\frac{y_0-a}{y_0-b}\right)^{1/2}, \quad \ldots\ldots(44)$$

and the second and third terms in the brackets in (42) are transformed to

$$\frac{\sqrt{6}(2y_0+b)}{y_0(y_0-b)}Q(y_0)-3\{6(a-c)\}^{1/2}E(k_2,\beta_0'), \quad \ldots\ldots(42a)$$

which corresponds to (28*a*). As in Case I, this equivalent form for the free energy has also been derived by the more laborious method of introducing the substitution (43) directly into (5) and (9).

Finally, using (37) and (38), we expand $F(k,\beta_0)$ in powers of $1/y_0$ and then (40) becomes

$$\tfrac{1}{2}\kappa R=\sqrt{6}\left[\frac{F(k_2,\frac{1}{2}\pi)}{(a-c)^{1/2}}+\tfrac{1}{2}\int_{y_0}^{\infty}\frac{dy}{Q(y)}\right]$$
$$=\sqrt{6}\left[\frac{F(k_2,\frac{1}{2}\pi)}{(a-c)^{1/2}}-\frac{1}{y_0{}^{1/2}}-\frac{1}{6}\frac{h}{y_0{}^{3/2}}-\frac{3}{40}\frac{h^2}{y_0{}^{5/2}}-\frac{1}{112}\frac{(5h^3-4)}{y_0{}^{7/2}}-\ldots\right], \quad \ldots(45)$$

which corresponds to (34). Similarly, we may expand $E(k_2,\beta_0)$ in powers of $1/y_0$, noting that in place of $1/Q(y)$ the integrand is now $(y-b)/(y-c)\,Q(y)$. Making use of the latter expansion and of the corresponding ones for $Q(y)_0/(y_0-c)$ and $2F_\infty$, we derive from (29), (42) and (45) that

$$V(R)=\frac{4n_2\boldsymbol{k}T}{\kappa}\left[f_2(k)+\frac{1}{2\sqrt{6}}(h-\tfrac{3}{2})^2\frac{1}{y_0{}^{3/2}}+\frac{\sqrt{6}}{80}(h-\tfrac{3}{2})^2(4h+3)\frac{1}{y_0{}^{5/2}}\right.$$
$$\left.+\frac{15\sqrt{6}}{7\times256}(h-\tfrac{3}{2})^2(4h^2+4h+3)\frac{1}{y_0{}^{7/2}}+\ldots\right]=\frac{4n_2\boldsymbol{k}T}{\kappa}g_2(k,y_0),\ \text{say}, \quad (46)$$

where

$$f_2(k)=\left(\frac{3}{2(a-c)}\right)^{1,2}(2h+2k+3)\,F(k_2,\tfrac{1}{2}\pi)+3\sqrt{6}\,(a-c)\,E(k_2,\tfrac{1}{2}\pi)-9. \quad \ldots(47)$$

Here again $f_2(k)$ is the main contribution to $g_2(k,y_0)$ provided κR or η_0 is not too small. The series (45) and (46) converge for all $\kappa R>0$, $\eta_0>0$ since $|c|<b<a<y_0$. However, the correction to the limiting function $f_2(k)$ is now of order $\exp(-3\eta_0/2)$, so that for large η_0 the series (46) does not converge as rapidly as the corresponding one in Case I. We note that the expansion (46) is to be

Table 4

η_0	k	50	40	30	20	15	10	7·5	6·0	5·0	4·0	3·5	3·0	2·5	2·0	1·75	1·50	1·25
	$g_2(k,\infty)=f_2(k)$	19·02	16·25	13·13	9·496	7·389	4·988	3·635	2·765	2·161	1·542	1·230	0·9215	0·6230	0·3465	0·2231	0·1164	0·03559
∞	$\kappa R-(\kappa R)_\infty$	1·088	1·217	1·405	1·721	1·987	2·430	2·811	3·145	3·448	3·861	4·135	4·480	4·939	5·601	6·083	6·774	7·996
	$g_2(k,y_0)$	19·09	16·29	13·15	9·504	7·394	4·989	3·636					0·9216					
6	κR	0·8391	0·9687	1·158	1·475	1·742	2·189	2·567	2·900	3·203	3·617	3·890	4·236	4·695	5·375	5·838	6·530	7·752
	$g_2(k,y_0)$	19·36	16·45	13·23	9·538	7·411	4·996	3·640	2·767	2·162			0·9218	0·6231	0·3466			
5	κR	0·6593	0·7939	0·9879	1·309	1·578	2·027	2·406	2·740	3·043	3·457	3·731	4·076	4·536	5·198	5·680	6·371	7·593
	$g_2(k,y_0)$		17·71	13·76	9·722	7·501	5·042	3·656	2·776	2·167	1·545	1·232	0·9228	0·6236	0·3467	0·2232		
4	κR		0·4210	0·6582	1·009	1·289	1·749	2·132	2·469	2·774	3·190	3·464	3·810	4·270	4·934	5·416	6·107	7·330
	$g_2(k,y_0)$					8·233	5·243	3·745	2·823	2·195	1·558	1·241	0·9277	0·6259	0·3475	0·2235	0·1165	
3	κR					0·6671	1·221	1·635	1·988	2·303	2·729	3·007	3·357	3·820	4·488	4·971	5·665	6·888
	$g_2(k,y_0)$								3·271	2·407	1·649	1·295	0·9571	0·6392	0·3517	0·2252	0·1170	0·03565
2	κR								0·8988	1·330	1·834	2·144	2·522	3·010	3·700	4·193	4·894	6·124
	$g_2(k,y_0)$													0·8474	0·3948	0·2416	0·1212	0·03624
1	κR													0·9189	1·981	2·576	3·353	4·634

Table 5

η_0								
6	k	403·4	—	—	200	100	90	
	$g_2(k, y_0)$	89·582	79·67	70·49	47·26	30·34	26·23	
	κR	0	0·05	0·1	0·2735	0·5142	0·6075	
5	k	148·4	—	—	100	80		
	$g_2(k, y_0)$	50·984	43·78	$38\cdot3_3$	32·01	27·12		
	κR	0	0·1	0·2	0·2978	0·4088		
4	k	54·60	—	—	—			
	$g_2(k, y_0)$	27·697	25·06	22·54	20·22			
	κR	0	0·1	0·2	0·2			
3	k	20·09	—	—				
	$g_2(k, y_0)$	13·781	11·94	10·23				
	κR	0	0·2	0·4				
2	k	7·389	—	—	—			
	$g_2(k, y_0)$	5·6911	5·106	4·538	4·002			
	κR	0	0·2	0·4	0·6			
1	k	2·718	—	—	—	2·65	2·6	2·25
	$g_2(k, y_0)$	1·4051	1·3409	1·2769	1·2135	1·0940	0·9952	0·5869
	κR	0	0·1	0·2	0·3	0·4922	0·6570	1·458

compared with the series (20) for the case of a 1–1 valency type of electrolyte. In tables 4 and 5 we have calculated κR and $g_2(k, y_0)$ for various η_0. When the values of $g_2(k, y_0)$ are not shown it is understood that $g_2(k, y_0) = f_2(k)$. The rapidity of convergence of the series (45) and (46) follows a similar pattern to Case I, the difference being, of course, that to obtain the same accuracy for a specified η_0 and the same number of terms we need to choose a larger κR. For example, if we retain the first three terms in (46), the error in $V(R)$ is less than $\frac{1}{2}\%$ when $\eta_0 = 2$, $\kappa R > 2{\cdot}5$ and about 5% if $\eta_0 = 1$ and $\kappa R = 2$.

§ 6. APPLICATIONS

Verwey and Overbeek (1948, p. 33) demonstrated the small effect of the ion carrying the same charge as the surface on the capacity of a single flat double layer. In the case of two parallel plates, however, their calculation only shows that this ion has a minor effect on the free energy at infinite separation, or on the repulsive potential $V(0) = -2F_\infty$ at contact. The influence on $V(R)$ at finite R, and particularly at large R, remains to be evaluated. As the above authors point out, the colloid chemical facts show the secondary importance of the ion of the same charge as the particle. This property can be investigated theoretically by applying the results of the present paper, and some tentative conclusions will be described here.

Let the interaction energy for 2–1 and 2–2 valency types of electrolytes be denoted by $V_{21}(R)$ and $V_{22}(R)$, respectively, in the case of a divalent coagulating ion (i.e. the ion carrying the opposite charge to the plates); the corresponding Debye–Huckel parameters are $\kappa(2, 1)$ and $\kappa(2, 2)$. Assuming the same plate potential ψ_0 and the same concentration n_2 of the divalent coagulating ion (so that $\kappa^2(2, 2) = (4/3)\kappa^2(2, 1)$) in these two electrolyte types, we have plotted $V_{21}(R)$ and $V_{22}(R)$ as functions of R. It is found that, except for large R, the two curves obtained do lie quite close together, particularly for large η_0. Thus at $R = 0$ the ratio $V_{22}(0)/V_{21}(0)$ has the approximate values 1·06, 1·024 and 1·01 at $\eta_0 = 1$, 2, 3 respectively, and tends to unity as η_0 increases. As the plates are separated the ratio $V_{22}(R)/V_{21}(R)$ initially increases somewhat, but then the above two curves

cross each other, and for large R ($\kappa(2,2)R<3$, say) we have the approximate relation

$$V_{22}(R)/V_{21}(R)=A(\eta_0)\exp[-0{\cdot}134\kappa(2,2)R], \qquad \ldots\ldots(48)$$

where $A(\eta_0)$ increases from 1·48 to 1·79 as η_0 varies from 1 to 6. The relation (48) yields an upper bound for the value of $\kappa(2,2)R$ at the crossing point where $V_{22}(R)=V_{21}(R)$.

In the case of a univalent coagulating ion we denote the energy functions for 1–2 and 1–1 electrolytes by $V_{12}(R)$ and $V_{11}(R)$ and the parameters by $\kappa(1,2)$ and $\kappa(1,1)$ respectively. Assuming again the same plate potential ψ_0, but now the same concentration n_1 of the univalent coagulating ion (so that $\kappa^2(1,2)=1{\cdot}5\kappa^2(1,1)$), we have plotted $V_{12}(R)$ and $V_{11}(R)$ as functions of R. The two curves are more separated than in the previous case, although still never differing very much except at large R. At $R=0$, $V_{12}(0)/V_{11}(0)$ has the values 1·126, 1·07, 1·04, 1·025, 1·015 and 1·01 at $\eta_0=1$, 2, 3, 4, 5 and 6 respectively, and the behaviour of $V_{12}(R)$, $V_{11}(R)$ as a function of R is similar to that of $V_{22}(R)/V_{21}(R)$. Thus at large separations ($\kappa(1,1)R>4$, say) we have approximately

$$V_{12}(R)/V_{11}(R)=B(\eta_0)\exp[-0{\cdot}225\kappa(1,1)R], \qquad \ldots\ldots(49)$$

where $B(\eta_0)$ increases from 1·63 to 2·64 in the range $1\ldots.6$ for η_0. Again (49) provides an upper bound for the value of $\kappa(1,1)R$ at the crossing point.

ACKNOWLEDGMENT

In conclusion, the authors wish to acknowledge their indebtedness to Mr. D. F. Ferguson of the Department of Mathematics, University of Manchester, who carried out most of the very laborious computations.

APPENDIX I

In obtaining (28) we simplify the notation by considering the indefinite integral, J say, which corresponds to the definite integral I, as defined by (7). Then J can be written as

$$J=J_1-hJ_2+\tfrac{1}{2}J_3, \qquad \ldots\ldots(A1)$$

where

$$J_1=\int\frac{y\,dy}{Q(y)}=\frac{2b}{(b-c)^{1/2}}\int\frac{d\Phi}{\Delta_1}-2(b-c)^{1/2}\int\Delta_1 d\Phi, \qquad \ldots\ldots(A2)$$

$$J_2=\int\frac{dy}{Q(y)}=\frac{2}{(b-c)^{1/2}}\int\frac{d\Phi}{\Delta_1}, \qquad \ldots\ldots(A3)$$

$$J_3=\int\frac{dy}{y^2Q(y)}=\frac{2}{c^2(b-c)^{1/2}}\int\frac{du}{(1+mu^2)\,R(k_1,u)}, \qquad \ldots\ldots(A4)$$

$$\Delta_1=\Delta(k_1,\Phi),\quad m=(a-c)/c.$$

J_3 is not yet in a standard form but, adopting the usual procedure, we differentiate the expression $uR(k_1,u)/(1+mu^2)$ and then integrate to obtain a reduction formula which expresses J_3 in terms of the three kinds of elliptic integrals. Writing the result in terms of the variable Φ, the integral in (A4) reads

$$\int\frac{d\Phi}{(1+m\sin^2\Phi)^2\Delta_1}=\frac{1}{2D}\left[-\frac{(m+k_1^2)}{m^2}\int\frac{d\Phi}{\Delta_1}+\frac{1}{m}\int\Delta_1 d\Phi\right.$$
$$\left.+C\int\frac{d\Phi}{(1+m\sin^2\Phi)\Delta_1}+\frac{\Delta_1\sin\Phi\cos\Phi}{(1+m\sin^2\Phi)}\right], \qquad \ldots\ldots(A5)$$

where

$$D=1+\frac{1+k_1^2}{m}+\frac{k_1^2}{m^2},\quad C=1+\frac{1+k_1^2}{2m}+\frac{3k_1^2}{m^2}. \qquad \ldots\ldots(A6)$$

If we substitute for k_1 and m we find that $ab+bc+ca=0$ appears as a factor in C and hence $C=0$; also J_3 simplifies to

$$J_3=\frac{2b}{(b-c)^{1/2}}\int\frac{d\Phi}{\Delta_1}-2(b-c)^{1/2}\int\Delta_1 d\Phi+2\frac{Q(y)}{y}. \quad \ldots\ldots(A\,7)$$

The integral (7) for I, and hence the expression (6) for E, are immediately obtained by introducing the limits of integration $\frac{1}{2}\pi\geqslant\Phi\geqslant\Phi_0$ when $k\geqslant y\geqslant y_0$ in the formulae for J_1, J_2 and J_3. It is convenient to eliminate the elliptic integral of the first kind by means of (27), and then it is readily verified that the formula (9 *a*) for the free energy becomes the required expression (28).

APPENDIX II

To determine the integral (7) for I in Case II we substitute $t^2=1/(y-c)=v^2/(a-c)$ and write

$$S(t)=[\{1-(b-c)t^2\}\{1-(a-c)t^2\}]^{1/2}. \quad \ldots\ldots(A\,8)$$

Considering the indefinite integral J, we have

$$J=-2H_1+\frac{2}{c^2}H_2+\frac{1}{c^3}H_3, \quad \ldots\ldots(A\,9)$$

where $H_1=\int\frac{dt}{t^2S(t)}=(a-c)^{1/2}\int\frac{d\beta}{\Delta_2\sin^2\beta}$ $\ldots\ldots(A\,10)$

$$=-(a-c)^{1/2}\left[\Delta_2\cot\beta-\int\frac{d\beta}{\Delta_2}+\int\Delta_2 d\beta\right],\ \Delta_2=\Delta(k_2,\beta),$$

$$H_2=\int\frac{dt}{(1+ct^2)S(t)}=\frac{1}{(a-c)^{1/2}}\int\frac{d\beta}{(1+m^{-1}\sin^2\beta)\Delta_2}, \quad \ldots\ldots(A\,11)$$

which is an elliptic integral of the third kind, and

$$H_3=\int\frac{dt}{(1+ct^2)^2S(t)}=\frac{1}{(a-c)^{1/2}}\int\frac{d\beta}{(1+m^{-1}\sin^2\beta)^2\Delta_2}. \quad \ldots\ldots(A\,12)$$

This can be determined by applying (A 5), and we now find that

$$D=1+(1+k_2^2)m+k_2^2m^2=-c^3,\ C=1+2(1+k_2^2)m+3k_2^2m^2=-2/c^3.$$

Making use of these results, (A 9) becomes

$$J=(a-c)^{1/2}\left(2+\frac{b}{c}\right)\int\frac{d\beta}{\Delta_2}-(a-c)^{1/2}\int\Delta_2 d\beta+\left(2+\frac{c}{y}\right)\frac{Q(y)}{(y-c)}, \quad \ldots\ldots(A\,13)$$

noting that the coefficient of the elliptic integral of the third kind vanishes. Introducing the limits of integration $\frac{1}{2}\pi\geqslant\beta\geqslant\Phi_0$ when $k\leqslant y\leqslant y_0$ into (A 13), we readily derive that the formula (9) for $2F$ leads to the required result (42).

REFERENCES

Corkill, A. J., and Rosenhead, L., 1939, *Proc. Roy. Soc.* A, **172**, 410.

Fletcher, A., 1940, *Phil. Mag.*, **30**, 516.

Jahnke, E., and Emde, F., 1945, *Tables of Functions*, 4th edn. (New York : Dover).

Langmuir, L., 1938, *J. Chem. Phys.*, **6**, 893.

Levine, S., 1951, *Proc. Phys. Soc.* A, **64**, 781.

Levine, S., and Suddaby, A., 1951 a, *Proc. Phys. Soc.* A, **64**, 287 ; 1951 b, *Ibid.*, **64**, 431.

Robinson, L. B., 1948, *J. Chem. Phys.*, **16**, 734 ; 1949, *Ibid.*, **17**, 960.

Verwey, E. J. W., and Overbeek, J. Th. G., 1948, *Theory of Stability of Lyophobic Colloids* (Amsterdam and New York : Elsevier).

Wood, L. A., and Robinson, L. B., 1946, *J. Chem. Phys.*, **14**, 258.

The Near Ultra-Violet Band-System (D–X) of Silicon Monosulphide

By A. LAGERQVIST*, G. NILHEDEN* and R. F. BARROW†

* Physics Department, University of Stockholm

† Physical Chemistry Laboratory, University of Oxford

MS. received 29*th October* 1951, *and in final form* 21*st January* 1952

ABSTRACT. The rotational analysis of the near ultra-violet band-system, $D^1\Pi - X^1\Sigma^+$, has been extended. Twelve bands have been analysed, namely the 7,1, 6,0, 6,1, 5,0, 5,1, 4,0, 4,1, 3,0, 2,0, 1,0, 1,1 and 0,0 bands. The constants derived for $D^1\Pi$ are

$$B_v' = 0{\cdot}2664_7 - 0{\cdot}0021_6\,(v'+\tfrac{1}{2})\,;\quad D_v' = [2{\cdot}91 - 0{\cdot}03(v'+\tfrac{1}{2})]\times 10^{-7},$$

$$G_{v'} = 513{\cdot}1_2(v'+\tfrac{1}{2}) - 2{\cdot}9_3(v'+\tfrac{1}{2})^2\,;\quad \nu_e = 35026{\cdot}8_6\ \mathrm{cm}^{-1}\,;\quad r_e' = 2{\cdot}058_9\ \text{Å}.$$

A number of perturbations have been found in the upper state. They appear to arise from interactions with two electronic states, a $^3\Sigma^-$ state and a singlet state, $^1\Pi$ or $^1\Delta$. It has not been possible to determine the absolute numbering of the vibrational levels of the perturbing states, but in all other respects fairly complete information has been obtained about the $^3\Sigma^-$ state. The perturbations are similar to those already known in the spectrum of CO, and the analogy between the electronic states of the molecules is thus strengthened.

§ 1. INTRODUCTION

Three band-systems ascribed to the SiS molecule are known. Two are situated in the ultra-violet region of the spectrum; the E–X system, which lies in the region 2050–2600 Å (Vago and Barrow 1946), and the D–X system, which extends from about 2500 to 3900 Å (Barrow and Jevons 1938). These are both obtained in absorption, and the D–X system has also been obtained in emission. Vibrational analyses are given in the papers mentioned above. A further system has been obtained in emission in the visible region (Barrow and Jevons 1938), but it has not been analysed. A rotational analysis of the 0,1, 0,2, 0,3, 0,4 and 1,5 bands of the D–X system (Barrow 1946) showed that the transition was $D^1\Pi$–$X^1\Sigma^+$.

The vibrational analysis of the D–X system suggested that the heads of the bands with $v'=7$ are abnormally situated, indicating a perturbation in this level. An extension of the rotational analysis of this system to higher vibrational levels in $D^1\Pi$ was therefore undertaken with the object of getting information about this perturbation and at the same time of determining better values of the constants. This paper presents the analysis for all the upper levels from $v'=0$ to 7: it shows that two electronic states perturb the $^1\Pi$ state, one of which is a $^3\Sigma^-$ state, the other a singlet state. The $^3\Sigma^-$ state perturbs the $^1\Pi$ level in such a way that the interactions from the substates $^3\Sigma_{J-1}$ and $^3\Sigma_{J+1}$ are visible

in the R and P branches and the interactions from the substate $^3\Sigma_J^-$ in the Q branches. The very strong perturbation causing the head-displacement of the level $v'=7$ arises from interactions between the $^1\Pi$ and the $^3\Sigma^-$ states.

§ 2. EXPERIMENTAL

The spectrograms were taken in absorption in a first order of a 21-ft Wood concave grating (165 000 lines) having a dispersion of about 1·25 Å/mm. The absorption tube was made of quartz, with quartz windows. The length of the tube was 75 cm, of which 50 cm were heated in an electric furnace. The temperature of operation was about 1 000° c. The tube contained initially a mixture of Al_2S_3 powder and quartz sand, which gives SiS on heating. A hydrogen lamp was used as source of continuum. The exposure time on Ilford Zenith plates was about 30 minutes. The band-lines were compared against Fe arc lines whose wavelengths were taken from the M.I.T. tables (1939).

§ 3. STRUCTURE OF THE BANDS

The appearance of the structure of some of the bands is shown in the spectrograms reproduced in fig. 1. A Deslandres scheme of band-origins is given in table 1. The wave-numbers of the band-lines are given in tables 2–5, where overlapped lines are indicated with an asterisk. Perturbations have been found in all the upper state vibrational levels examined from $v'=0$ to $v'=7$. Those in the level $v'=0$ are, however, very weak, and they were not detected

Table 1. Deslandres Scheme of Band-Origins

v'	$v''=0$		$v''=1$	$v''=2$	$v''=3$	$v''=4$	$v''=5$
7			37596·41				
			476·67				
6	37864·08	744·23	37119·74				
	477·68		478·10				
5	37386·40	744·76	36641·64				
	483·86		483·50				
4	36902·54	744·40	36158·14				
	489·74						
3	36412·80						
	495·98						
2	35916·82						
	501·23						
1	35415·59	744·45	34671·14				31744·61
	506·95		507·26				
0	34908·64	744·76	34163·88	739·34	33424·54	734·23	32690·31	729·04	31961·27	

in the original analysis (Barrow 1946). A strong perturbation in $v'=7$ displaces the origins of bands with $v'=7$ by about 5 cm^{-1}. In tables 2–5 romans and italics are used to distinguish interacting levels—except that the type is not altered at the weak perturbations in $v'=0$. For the weak 4,1 band only the Q branch is given.

Silicon has three stable isotopes, sulphur four, but of these ^{28}Si (92·2 %) and ^{32}S (95·1 %) are much the most abundant. We have made no effort to measure lines other than those attributed to these isotopes.

Table 2. Wave-numbers for the 0,0, 1,0 and 1,1 Bands

	0,0 Band			1,0 Band			1,1 Band		
J	Q(*J*)	R(*J*)	P(*J*)	Q(*J*)	R(*J*)	P(*J*)	Q(*J*)	R(*J*)	P(*J*)
4	34908·81*								
5	08·27*								
6	07·74*								
7	07·01*			35413·30					
8	06·23*			12·77*					
9	05·49*			11·99*					
10	04·68*			11·02*					
11	03·43*			10·28					
12	02·54*			09·39			34665·09*		
13	01·47*	34908·81*		08·33	35415·65		64·08*		
14	00·24*	08·27*		07·37*	15·03		63·19		
15	899·08*	07·74*	34891·36*	06·09*	14·51		61·92		34654·07
16	98·03	07·01*	89·59*	04·74*	13·77	35396·31	60·73		52·23
17	96·76	06·23*	87·66*	03·42*	12·77*	94·48	59·39		50·42
18	95·45	05·49*	85·80*	01·96*	11·99*	92·39	58·12	34668·14	48·44
19	93·96	04·68*	83·92*	00·36*	11·02*	90·42	56·60	67·02	46·72
20	92·48	03·43*	81·89*	398·86	09·86	88·35	55·07*	66·13	44·73
21	90·89	02·54*	79·84*	97·12	08·76	86·16	53·45*	65·09*	42·32*
22	89·27	01·47*	77·70*	95·47	07·37*	83·95	51·78*	64·08*	40·10*
23	87·66*	00·24*	75·56*	93·62	06·09*	81·52	49·94*	62·72	37·83*
24	85·80*	899·08*	73·18*	91·70	04·74*	79·10	48·10*	61·53	35·55*
25	83·92*	97·50	870·79*	89·67	03·42*	76·61	46·12*	59·89	33·14*
26	81·89*	95·98	68·11*	87·65	01·96*	74·04	44·29	58·56	30·67*
27	79·84*	94·62	65·55*	85·45	00·36*	71·35	42·32*	56·97	28·18*
28	77·70*	93·03	62·92*	83·28	398·54	68·57	40·10*	55·07*	25·52*
29	75·56*	91·36*	60·24*	80·96	96·70	65·65	37·83*	53·45*	22·77*
30	73·18*	89·59*	57·44*	78·62	94·88	62·88*	35·55*	51·78*	19·70
31	70·79*	87·66*	54·55*	76·15	92·97	59·76*	33·14*	49·94*	16·96
32	68·51	85·80*	51·65*	73·60	90·89	56·69*	30·67*	48·10*	13·94
33	66·06	83·92*	48·52*	70·95	88·79	53·54*	28·18*	46·12*	10·83
34	63·45	81·89*	45·46*	68·29	86·60	50·30*	25·52*	44·00	07·76
35	60·91	79·84*	42·28*	65·65	84·35	47·03*	22·77*	41·68	04·50
36	58·15	77·70*	39·01*	62·88*	82·04	43·62*	20·09	39·52	01·20
37	55·39	75·56*	35·66*	59·76*	79·57	40·19*	17·32	37·11	597·91
38	52·45	73·18*	32·25*	56·69*	77·06	36·75*	14·45	34·77	94·42
39	49·48	70·79*	28·83*	53·54*	74·45	33·02*	11·37	32·26	90·90
40	46·56	68·11*	25·22*	50·30*	71·75	29·33*	08·28	29·76	87·38
41	43·43	65·55*	21·73	47·03*	68·99	25·56*	05·08	27·09	83·56
42	40·17	62·92*	18·07	43·62*	66·11	21·67*	01·85	24·41	79·81
43	37·03	60·24*	14·24	40·19*	62·88*	17·68*	598·53	21·55	76·02
44	33·61	57·44*	10·38	36·75*	*60·47*	13·47*	95·18	*18·95*	72·14
45	30·28	54·55*	06·51	33·02*	*57·29*	09·35	91·62	*15·95*	67·91
46	26·73	51·65*	02·50	29·33*	*54·07*	*05·55**	88·11	*12·83*	*64·32*
47	23·19	48·52*	798·33	25·56*	*50·86*	*01·14**	84·47	*09·80*	*60·02*
48	19·57	45·46*	94·23	21·67*	*47·53*	*296·74**	80·76	*06·50*	*55·73*
49	15·88	42·28*	90·08	17·68*	*44·07*	*92·27**	76·82	*03·25*	*51·38*
50	12·00	39·01*	85·73	13·47*			72·73		
50				*17·68**	*40·53*	*87·72**		*599·90*	*47·07*
51	08·15	35·66*	81·35	07·18					
51				*10·56*	*36·75**	*83·06**	*69·97*	*96·40*	*42·48*
52	04·22	32·25*	76·85	*05·96*	*33·02**	*78·34**	*65·55*	*92·63*	*38·10*
53	00·18	28·83*	72·16	*01·55*	30·15	*73·49**	*61·42*	90·02	*33·34*
54	796·13	25·22*	67·70	*297·14*	25·97	*68·49**	*57·12*	85·90	*28·34*
55	91·92	21·41	63·07	*92·76*	22·02	64·43*	*52·80*	82·17	24·59
56	87·71	17·66	58·16	*88·27*	18·12	59·09	*48·54*	78·36	19·36
57	83·32	13·84	53·24	*83·66*	13·98	53·88	*44·05*	74·53	14·36
58	78·97	10·01	48·32	*78·97*	09·85	48·72	*39·53*	70·46	09·30
59	74·39	05·94	43·22	*74·20*	05·55*	43·41	*35·03*	66·33	04·26
60	69·82	02·08	38·35	*69·38*	01·14*	38·02	*30·34*	62·24	499·14
61	65·20	797·76	33·11	*64·43**	296·74*	32·62	*25·63*	57·92	93·70
62	60·54	93·60	27·93	*59·38*	92·27*	27·09	*20·80*	53·68	88·39
63	55·69	89·20	22·54	*54·35*	87·72*	21·53	*15·87*	49·22	83·10

Table 2 (*cont.*)

	0,0 Band			1,0 Band			1,1 Band		
J	Q(*J*)	R(*J*)	P(*J*)	Q(*J*)	R(*J*)	P(*J*)	Q(*J*)	R(*J*)	P(*J*)
64	50·79	84·91	17·12	*49·22*	83·06*	15.74	*10·93*	44·79	77·51
65	45·74	80·52	11·62	*43·93*	78·34*	10·05	*05·82*	40·21	71·99
66	40·63	76·02	06·12	*38·61*	73·49*	04·14	*00·79**	35·52	66·39
67	35·67	71·28	00·31	*33·16*	68·49*	198·22	*495·57**	30·88	60·59
68	30·34	66·59	694·67	*27·63*	63·59	92·21	*90·26**	26·09	54·84
69	25·19	61·97	88·92	*22·06*	58·56	86·14	*84·85**	21·30	48·92
70	19·77	57·04	83·03	*16·41*	53·37	79·94	*79·36**	16·37	42·95
71	14·24	52·03	77·28	*10·60*	48·12	73·71	*73·66**	11·35	36·77
72	08·83	47·16	70·95	*04·80*	42·80	67·43	*68·13*	06·03	30·78
73	03·20	41·69	65·09*	*198·87*	37·45	61·01	*62·39*	00·79*	24·35
74	697·40	36·81	58·56	*92·86*	31·88	54·40	*56·66*	495·57*	18·16
75	91·72	31·48	52·23	*86·76*	26·25	47·64	*50·78*	90·26*	11·87
76	85·90	26·16		*80·53*	20·64	41·17	*44·95*	84·85*	05·48
77	79·85	20·59		*74·39*	14·87	34·32	*38·79*	79·36*	398·82
78	73·84	15·14		*68·03*	09·09	27·49	*32·67*	73·66*	92·13
79	67·70	09·61		*61·53*	03·06	20·50	*26·48*		85·37
80	61·53*	04·03		*55·05*	197·01	13·49	*20·24*		78·75
81	55·07*	698·23		*48·46*	90·87	06·39	*13·97*		
82	49·01	92·49		*41·70*	84·81	099·32	*07·38*		
83	42·32*	86·57		*34·90*	78·46	91·97	*00·85*		
84	36·03			*28·07*	72·10	84·54	*394·24*		
85	29·38			*21·14*	65·72		*87·51*		
86				*14·03*	59·05		*80·71*		
87				*06·89*	52·49		*74·09*		
88				*099·79*	45·51		*66·88*		
89				*92·42*	38·97		*59·72*		
90				*85·12*	31·94		*52·96*		
91				*77·30*	24·97		*45·47*		
92				*69·77*	17·86				
93				*62·15*	10·84				
94				*54·37*	03·50				
95				*46·63*	096·10				
96				*38·60*	88·88				
97				*30·65*	81·28				
98				*22·49*	73·68				
99				*14·15*					
100				*05·89*					
101				*34997·56*					
102				*89·20*					
103				*80·59*					
104				*71·98*					
105				*63·24*					
106				*54·40*					
107				*45·45*					
108				*36·70*					
109				*27·60*					
110				*18·04*					

Table 3. Wave-numbers for the 2,0, 3,0 and 4,0 Bands

	2,0 Band			3,0 Band			4,0 Band		
J	Q(*J*)	R(*J*)	P(*J*)	Q(*J*)	R(*J*)	P(*J*)	Q(*J*)	R(*J*)	P(*J*
5							36901·25		
6							00·54		
7							899·81		
8							99·25		
9							98·55*		
10	35912·07						97·54*		
11	11·21	35917·61					96·50*		
12	10·24*	16·97	35903·92*				95·27*		
13	09·01*	16·37	02·31*				93·99*		

Table 3 (*cont.*)

	2,0 Band			3,0 Band			4,0 Band		
J	Q(*J*)	R(*J*)	P(*J*)	Q(*J*)	R(*J*)	P(*J*)	Q(*J*)	R(*J*)	P(*J*)
14	08·04	15·65	00·83*				92·90		
15	06·70	14·98	898·94*				91·45		
16	05·33	13·95	97·16*				89·95	36898·55*	
17	03·92*		95·06	36399·41			88·39	97·54*	
18	02·31*	*13·02*	92·91	97·79		36388·64*	86·72	96·50*	36877·72*
19	00·83*	*11·62*		96·13		86·43*	84·99	95·27*	75·41*
20	898·94*	*10·24**	*89·54*	94·25		84·20*	83·17	93·99*	73·07*
21	97·16*	*09·01**	*86·81*	92·49		81·89*	81·31	92·38	70·65*
22	95·39*	*07·54*	*84·23*	90·40		79·16	79·16	90·75	68·10*
23	93·33	*05·99*	*81·84**	88·64*		76·60	76·96	89·27	65·11*
24	91·08	*04·52*	*79·13**	86·43*		74·42*	74·81	87·59	62·48*
25	88·79	*02·86*	*76·28**	84·20*		71·34	72·54	85·85	59·82*
26	86·30	*00·83**	*73·46*	81·89*		68·52	70·19	83·88	56·81*
27	83·17*			79·62		65·61	67·72	81·92	53·90*
27	*88·79*	*898·94**	*70·86*						
28	79·13*			77·16		62·67	65·11*	79·90	50·82*
28	*84·98*	*96·53*	*67·61**						
29	74·67	98·29		74·42*	36390·11	59·57	62·48*	77·72*	47·62*
29	*81·84**		*64·56**						
30	*79·13**	95·39*	*60·71*	71·91	87·92	56·48	59·82*	75·41*	44·37*
31	*76·28**	92·91	61·44	69·19	85·65	53·19	56·81*	73·07*	40·95*
32	*73·28*	90·59	57·40*	66·36	83·45	49·82	53·90*	70·65*	37·51*
33	*70·53*	88·19	53·60	63·47	81·04	46·38	50·82*	68·10*	34·02*
34	*67·61**	85·85	50·12	60·47	78·48	42·85	47·62*	65·50	30·35*
35	*64·56**	83·17*	46·49	57·30	75·97	39·28	44·37*	62·48*	26·63*
36	*61·44*	80·75	42·89	54·18	73·32	35·63	40·95*	59·82*	22·78*
37	*58·38*	78·16	39·20	50·89	70·50	31·84	37·51*	56·81*	18·88*
38	*55·11*	75·47	35·47	47·51	67·65	27·89	34·02*	53·90*	14·65*
39	*51·83*	72·61	31·63	44·00	64·72	23·94	30·35*	50·82*	10·57*
40	*48·44*	69·77	27·70	40·57	61·74	19·95	26·63*	47·62*	06·35*
41	*45·01*	66·86	23·75	36·92	58·55	15·81	22·78*	44·37*	01·99*
42	*41·50*	63·81	19·66	33·15	55·38	11·56	18·88*	40·95*	797·60*
43	*37·78*	60·71	15·50	29·35	52·15	07·22	15·06*	37·51*	93·03*
44	*34·06*	57·40*	11·27	25·52	48·74	02·89	10·88*	34·02*	88·45*
45	*30·22*	54·11	06·93	21·51	45·28	298·36	06·91*	30·35*	83·74*
46	*26·40*	50·82	02·55	17·50	41·71	93·80	02·51*	26·63*	78·92*
47	*22·47*	47·42	798·05	13·26	38·05	89·09	798·21*	22·78*	74·04*
48	*18·41*	43·87	93·50	09·09	34·29	84·33	93·76*	18·88*	69·09
49	*14·30*	40·29	88·92	04·72	30·49	79·49	89·24*	14·65*	64·15
50	*10·11*	36·55	84·14	00·29	26·53	74·58	84·55*	10·57*	59·05
51	*05·79*	32·79	79·32	295·78	22·46	69·55	79·80*	06·35*	53·78
52	*01·39*	28·86	74·37	91·21	18·45	64·43	74·96*	01·99*	48·43
53	*796·88*	24·88	69·40	86·42	14·22	59·17	69·95*	797·60*	42·91
54	*92·33*	20·83	64·27	81·64	09·98	53·85	64·98*	93·03*	37·55*
55	*87·64*	16·69	59·09	76·75	05·46	48·52	59·83*	88·45*	31·80*
56	*82·90*	12·46	53·83	71·79	01·07	43·00	54·59*	83·74*	25·92*
57	*78·06*	08·18	48·53	66·72	296·58	37·32	49·34*	78·92*	20·36
58	*73·14*	03·80	43·14	61·51	91·90	31·76	43·87*	74·04*	14·32
59	*68·14*	799·25	37·57	56·27	87·11	26·01	38·38	68·77	08·37
60	*63·04*	94·70	32·01	50·96	82·31	20·30	32·79	63·68	02·24
61	*57·90*	90·01	26·15	45·53	77·47	14·21	27·03	58·48	695·91
62	*52·63*	85·27	20·56	40·10*	72·36	08·21	21·24	52·89	89·62
63	*47·29*	80·38	14·73	34·48*	67·26	02·00	15·33	46·88	83·03
64		75·48	08·75	28·68*	62·12	195·78	09·31	39·87	76·32*
64	*41·83*							*44·37*	
65	*36·33*	70·45	02·71	22·85*	56·70	89·54	03·09	*37·55**	69·12
66		65·31	696·57	16·94*	51·32	83·11	696·77		61·16
66	*30·68*							*31·80**	*65·40*
67	*25·03*	60·08	90·40	11·05*	45·97	76·62	90·33	*25·92**	*57·63**
68	*19·20*	54·94	84·07	04·80*	40·10*	70·09	83·62	*19·72*	*50·49*
69	*13·34*	49·45	77·77*	198·75	34·48*	63·32	76·32*	*13·55*	*43·55*

Table 3 (*cont.*)

	2,0 Band			3,0 Band			4,0 Band		
J	Q(*J*)	R(*J*)	P(*J*)	Q(*J*)	R(*J*)	P(*J*)	Q(*J*)	R(*J*)	P(*J*)
70		44·14	71·31*	92·41	28·68*	56·52	67·83*		
70	*07·31*						*86·06*	*07·26*	*36·18*
71		38·40	64·67*	86·13*	22·85*	49·86	57·63*		
71	*01·30*						*76·32**	*00·50*	*28·94*
72	*695·14*	32·89	58·00*	79·59*	16·94*	42·78	*67·83**	*692·61*	*21·20**
73	*88·92*	27·14	51·18*	72·92*	11·05*	35·58*	*60·11*	91·36	*13·26*
74	*82·59*	21·29	44·41*	66·38*	04·80*	28·47	*52·72*	83·80*	*04·33*
75	*76·19*	15·43	37·46*	59·66	197·95	21·28	*45·50*	77·20	01·75*
76	*69·64*	09·35	30·39*	52·78	*93·11*	13·84*	*38·42*	70·15	593·20
77	*63·11*	03·24	23·22*	45·86	*86·13**	06·28	*31·11*	63·31	85·05
78	*56·35*	697·08	16·28	38·72	*79·59**	*00·05*	*23·92**	56·51	77·08
79	*49·53*	90·91	09·01	31·38	*72·92**	*091·84**	*16·50*	49·26	68·82*
80	*42·75*	84·29	01·62	24·27	*66·38**	*83·94*	*08·99**	42·57	61·04*
81		77·77*	594·08	16·48*			01·75*		52·89*
81	*35·76*				*59·14*	*76·13*	*01·16*		
82		71·31*	86·56	08·02			593·81		44·64*
82	*28·72*				*52·03*	*68·29*	*93·20*		
83		64·67*	78·74	098·55			86·01*		
83	*21·50*			*114·78*	*44·96*	*60·17*			
84	*14·30*	58·00*	71·12	*04·30*	*37·49*	*51·86*	77·98		
85	*06·97*	51·18*	63·36	*095·48**	*27·73*	*43·94*	70·06		
86	*599·64*	44·41*	55·55	*87·66*		*34·57*	62·06		
87	*92·12*	37·46*	47·39	*79·95*		*23·47*	53·88		
88	*84·52*	30·39*	38·66	*71·91*			45·57		
89	*76·74*	23·22*		*64·00*			37·24		
90	*68·96*			*55·79*			28·89		
91	*60·94*			*47·64*			20·30		
92	*52·09*			*39·39**			11·67*		
93	54·20						02·93		
93	*39·79*			*30·98*					
94	45·61			*22·53*			493·86*		
95	37·25			*14·05*			84·94*		
96	29·05			*05·34*			76·02		
97	20·58			*35996·54*					
98	12·15			*88·03**					
99	03·59			*78·80*					
100	495·00			*69·96*					
101	86·30			*60·72*					
102	77·56			*51·49*					
103	68·62			*42·17*					
104	59·61			*32·57*					
105	50·47			*23·28*					
106	41·18								

Table 4. Wave-numbers for the 4,1, 5,0 and 5,1 Bands

	4, 1 Band	5, 0 Band			5, 1 Band		
J	Q(*J*)	Q(*J*)	R(*J*)	P(*J*)	Q(*J*)	R(*J*)	P(*J*)
11			37386·09				
12			85·38				
13			84·63	37370·89			
14			83·69	69·09			
15			82·85	67·12*			
16			81·95	65·13			
17		37371·70*	80·89	63·02	36627·65		
18		69·98*	79·49	60·81	25·87		
19		68·07*	78·19	58·45	23·92		
20		66·15*	76·75	55·93	22·17		
21	36137·49	64·11*	75·22	53·22	20·20		
22	35·58*	61·96*	73·92	50·70	18·16		

Table 4 (*cont.*)

	4, 1 Band	5, 0 Band			5, 1 Band		
J	Q(*J*)	Q(*J*)	R(*J*)	P(*J*)	Q(*J*)	R(*J*)	P(*J*)
23	33·55	59·68*	71·70*	48·02	16·20*		
24	31·38	57·31*	69·98*	45·23	14·06*		
25	29·11	54·83*	68·07*	42·31	11·56*		
26	26·73	52·42	66·15*	39·15	08·99*		
27	24·27	49·91	64·11*	36·08	06·56*		
28	21·84	47·16	61·96*	32·88	03·86*		
29	19·18	44·33	59·68*	29·62	01·16*	36616·20*	
30	16·48*	41·46	57·31*	26·22	598·30*	14·06*	36582·93*
31	13·84*	38·49	54·83*	22·73	95·32*	11·56*	79·52*
32	10·93	35·32	52·00	19·20	92·36*	08·99*	76·03*
33	08·02	32·17	49·32	15·36	89·21*	06·56*	72·42*
34	04·89	28·86	46·55	11·64	86·01	03·86*	68·82*
35	01·74	25·49	43·72	07·68	82·93*	01·16*	65·02*
36	098·55	21·98	40·72	03·57	79·52*	598·30*	61·04*
37	95·48*	18·41	37·58	299·56	76·03*	95·32*	57·15*
38	91·84*	14·69	34·49	95·31	72·42*	92·36*	52·89*
39	88·35	10·94	31·29	90·95	68·82*	89·21*	48·80*
40	84·80	06·97	27·83	86·69	65·02*	85·80	44·64*
41	81·02	03·02	24·10	82·51	61·04*	82·24	40·24*
42	77·29	298·92	20·58	77·57	57·15*	78·80	35·67*
43	73·37	94·73	16·96	72·83	52·89*	75·13	31·11*
44	69·45	90·45	13·03	67·96	48·80*	71·51	26·38*
45	65·61	85·99	09·00	63·13	44·64*	67·65	21·53*
46	61·38	81·44	04·89	57·95	40·24*	63·67	16·51*
47	57·24	76·82	00·69	52·97	35·67*	59·29	11·67*
48	52·78	72·05	295·95	47·52	31·11*		06·61
49	48·42	67·10		41·96	26·38*		01·25
50	43·94	62·30	*90·45**	36·07	21·53*		
51	39·39*	56·96	*84·66*		16·51*		
52	34·57*	51·69	*80·24*	*28·03*	11·31		
53	29·79	46·08	*75·25*	*22·03*	05·91	*34·77*	
54	24·92	40·10			00·08		
54		*57·68*	*70·17*	*15·64*		*29·99*	
55	19·98	33·61			493·86*		
55		*48·08*	*64·71*	*09·56*		*24·85*	*468·90*
56	14·95	26·08			86·28		
56		*39·23*		*03·05*			*63·28*
57	09·77	17·38					
57		*31·25*		*196·62*	*491·99*		*56·71*
58	04·45	06·97*	56·46*			17·45	
58		*24·27*			*84·94**		
59	35999·34	*17·59*	49·27		*78·33*	10·22	
60	93·78	*11·26*	42·67	84·98	*72·19*	03·73	45·84
61	88·03*	*04·87*	36·62	76·34	*66·04*	497·94	37·53
62	82·46	*198·70*	30·58	68·71*	*59·99*		29·54
63	76·83	*92·25*	24·85	61·15	*53·76*		23·03
64	70·99	*86·02*	19·01	54·12	*47·77*		
65	64·95	*79·58*	12·99	47·11	*41·43*		
66	58·78	*72·98*	06·97*	40·02	*34·86*		
67	52·63	*66·35*	00·67	32·98	*28·66*		
68	46·04	*59·65*	194·52	25·56	*22·18*		
69	38·89	*52·69*	88·47	18·32			
70	30·67	46·24	81·98	10·80			
70	*48·37*						
71	20·59	39·26	75·30	03·71*			
71	*39·17*						
72	*31·08*	32·09	68·71*	095·88			
73	*23·28*	24·92	61·69	88·29*			
74	*16·37**	17·46		80·31*			
75		10·30*		72·36*			
76		02·58*					

Table 5. Wave-numbers for the 6,0, 6,1 and 7,1 Bands

	6,0 Band			6,1 Band			7,1 Band		
J	Q(J)	R(J)	P(J)	Q(J)	R(J)	P(J)	Q(J)	R(J)	P(J)
11	37857·14								
12	55·91								
13	54·52			37110·30*			37586·72		
14	52·98*			08·92*			85·31		
15	51·62			07·38*			83·75		
16	49·84			05·75	37114·15		81·90		
17	48·08			04·15	13·03		80·10		
18	46·26			02·58	11·71*	37093·29	78·18		
19	44·55			00·44	10·30*	90·98	76·04	37585·99	
20	42·50	37852·98*		098·52	08·92*	88·29*	73·95	84·42	
21	40·21	51·06	37830·22*	96·44	07·38*	85·76*	71·69	82·59	37561·54*
22	37·95*	49·18	26·95	94·13	05·61*	83·08	69·34	80·55	58·39
23	35·47*	47·16	23·72	91·81	03·71	80·31*	66·87	78·84	55·41
24	32·93	45·01	20·62*	89·47	01·67	77·18	64·11	76·66*	52·59
25	30·22*	42·85	17·48	86·92	099·63	74·00	61·54*	74·66	49·29
26	27·54	40·74	14·31	84·15	97·24	71·02	58·88	72·41	46·05
27	24·71	37·95*	10·98	81·41	94·69	67·67	56·00	70·05	42·81*
28	21·78	35·47	07·44	78·59	92·10	63·99	53·16	67·55	39·35
29	18·65		03·66*	75·52	89·10	60·49	50·07	65·07	35·72
30	15·33		00·20	72·36*	85·76*	56·74	47·05*	62·45	32·03
31	11·88			69·06		52·49	43·61	59·63	28·21
32	08·52*			65·53		48·18	40·33	56·65	24·57*
33	04·57			61·88*			36·81	53·63	20·35
34	00·52	*20·62**		57·74	*78·13*		33·19	50·54	16·44
35	795·97	*16·84*		53·51	*74·49*		29·43	47·05*	12·21
36	91·24	*12·94*	*777·67*	48·93	*70·47*	*35·36**	25·48	43·27	07·97
37	85·90*			43·70			21·05	38·85*	03·32
37		*08·57**	*72·38**	*61·21*	*66·45**	*30·45*	*24·57**	*42·81**	
38	80·07			37·99					498·18
38			*67·61**	*55·75*	*61·88**	*25·17*	*19·92**	*38·85**	
39	73·84	13·66		31·63*	71·64				92·67
39			*62·60**	*50·32*	*56·92*	*20·25*	*15·31**	*34·93*	*96·52*
40		08·57*			66·45*				
40	*86·96*			*45·00*	*51·38*	*14·53*	*10·92*	*31·04*	*91·32*
41		03·66*	64·76		61·88*	22·58*			
41	*82·05*			*40·10**		*08·32**	*06·49*	*27·42*	*86·31*
42		799·10	58·27*		57·74*	16·64*			
42	*77·12**			*35·36**		*01·35*	*02·14*	*23·58*	*81·40*
43	*72·38**	94·61	52·39	*30·80*	53·30	10·77	*497·53*	*19·49*	*76·21*
44	*67·61**	90·36	46·19	*26·07*	48·93*	05·10	*93·16*	*15·31**	*71·28*
45	*62·60**	85·90*	41·18	*21·32*	44·51	36999·74*	*88·42*	*11·37*	*66·13*
46	*57·73*	81·47	35·30	*16·64*	40·20*	94·02*	*83·65*	*07·21*	*60·77*
47	*52·86*	77·12*	29·78	*11·83*	36·10	88·66*	*78·78*	*02·79*	*55·44*
48	*47·78*	72·38*	24·02	*06·95*	31·63*	83·26*	*73·83*	*498·18*	*50·00*
49	*42·67*	67·61*	18·39	*02·04*	27·19	77·72*	*68·75*	*93·55*	*44·34*
50	*37·51*	63·20	12·71	*36997·03*	22·58*	72·26	*63·59*	*89·22*	*38·76*
51	*32·17*	58·27*	06·93	*91·78*	18·05	66·57	*58·41*	*84·25*	*32·98*
52	*26·88*	53·58	01·15	*86·70*	13·19	60·96	*52·98*	*79·49*	*27·10*
53	*21·32*		694·94	*81·25*	08·32*	54·88	*47·57*	*74·53*	*21·26*
54	*15·75*		89·05	*75·94*	03·35	49·04	*41·97*	*69·41*	*15·11*
55				72·91	36997·70	43·02			
55	*09·82*			*70·17*	*99·74**		*36·50*	*64·10*	*08·95*
56	05·58			65·96		36·66			
56		*33·36*		*62·75*	*94·18**		*30·63*	*59·04*	*02·83*
57	699·07			59·62		29·70*			
57		*28·05*		*54·58*	*88·66**	*31·99*	*24·87*	*53·54*	*396·39*
58	92·78	*22·51*	*64·16*	53·72	*83·23**	*24·99*	*18·75*	*47·95*	*89·96*
59	86·90	*16·99*	*57·64*	47·86	*78·01**	*18·53*	*12·66*		
60	80·72	*11·32*	*50·71*	41·85	*72·68*	*11·91*	*06·51*		
61	74·28		*44·13*	35·74	*66·89*	*05·39*	*00·48*		
62	68·10		*37·54*	29·70*	*61·24*		*393·83*		
63	61·83			23·37	*55·44*				
64	55·27			17·14	*49·71*				

Table 5 (*cont.*)

	6,0 Band			6,1 Band			7,1 Band		
J	Q(*J*)	R(*J*)	P(*J*)	Q(*J*)	R(*J*)	P(*J*)	Q(*J*)	R(*J*)	P(*J*)
65	48·51			10·73	*43·65*				
66	41·76				*37·56*				
67	35·07				*31·63*				
68	27·97								
69	21·03								
70	13·87								
71	06·50								
72	599·23								
73	91·79								
74	84·42*								
75	76·66*								
76	68·66								
77	60·75								
78	52·59*								
79	44·61								
80	36·36								
81	27·42*								
82	18·24								

§ 4. DETERMINATION OF ROTATIONAL CONSTANTS

The rotational constants for the ground state have already been determined (Barrow 1946). The values of B'' and D'' were found to follow the equations

$$B_v'' = 0{\cdot}3036_3 - 0{\cdot}0014_9(v''+\tfrac{1}{2}); \quad D_v'' = [2{\cdot}01_5 - 0{\cdot}01(v''+\tfrac{1}{2})]\times 10^{-7}.$$

In order to calculate the rotational constants for the upper perturbed levels we have used the method introduced by Gerö (1935). The following expressions are formed:

$$\frac{Q(J-1)-Q(J)}{2J} = B''-B'-2J^2(D''-D'), \qquad \ldots\ldots(1)$$

$$\frac{R(J-2)-R(J-1)+P(J)-P(J+1)}{4J} = B''-B'+6D''-2J^2(D''-D'). \qquad \ldots\ldots(2)$$

If the left-hand sides of these expressions are plotted against J^2, ΔB is obtained as the intercept at $J=0$. Only the unperturbed regions, where the points lie on almost horizontal lines, are used for the extrapolation. These values of ΔB and

Table 6. Rotational Constants for the $D^1\Pi$ State

v'	B_{obs}	B_{calc}	D_{obs}	D_{calc}
0	$0{\cdot}2653_7$	$0{\cdot}2653_9$	$2{\cdot}85\times10^{-7}$	$2{\cdot}90\times10^{-7}$
1	$0{\cdot}2632_3$	$0{\cdot}2632_3$	2·90	2·87
2	$0{\cdot}2610_7$	$0{\cdot}2610_7$	2·87	2·84
3	$0{\cdot}2589_3$	$0{\cdot}2589_1$	2·82	2·81
4	$0{\cdot}2567_8$	$0{\cdot}2567_5$	2·73	2·78
5	0·2546	$0{\cdot}2545_9$		2·75
6	0·2524	$0{\cdot}2524_3$		2·72
7	0·2503	$0{\cdot}2502_7$		2·69

of ΔD were used to obtain values of B' and of D' with the aid of values of B'' and D'' already known. The perturbations in $v'=5$, 6 and 7 are, however, so considerable that no reliable values of D' can be obtained for these levels.

The constants are given in table 6. The calculated values are from the smoothed expressions

$$B_v' = 0{\cdot}2664_7 - 0{\cdot}0021_6(v' + \tfrac{1}{2}),\ D_v' = [2{\cdot}91 - 0{\cdot}03(v' + \tfrac{1}{2})] \times 10^{-7}.$$

We estimate the errors in the B'-values to be about $\pm 0{\cdot}00005$ for the levels $v' = 0$ to $v' = 4$: for B_5', B_6' and B_7' they are about $\pm 0{\cdot}0001\ \mathrm{cm}^{-1}$.

With the values for ω_e'' and ω_e' in §5 we obtain, from Kratzer's relation ($D = 4B^3/\omega^2$), $D'' = 1{\cdot}99 \times 10^{-7}$, $D' = 2{\cdot}87 \times 10^{-7}$, in satisfactory agreement with the experimental values.

§5. DETERMINATION OF VIBRATIONAL CONSTANTS

The origins of the bands analysed have been given in table 1. The vibrational constants have been calculated in the usual way, omitting the perturbed origin of the 7,1 band from consideration. We obtain $\omega_e'' = 749{\cdot}69$, $\omega_e' = 513{\cdot}12$, $x_e''\omega_e'' = 2{\cdot}58$, $x_e'\omega_e' = 2{\cdot}93$, $\nu_e = 35026{\cdot}86$. With these values the calculated origin of the 7,1 band is found to be 37591·72; this is $4{\cdot}69\ \mathrm{cm}^{-1}$ lower than the value observed.

§6. PERTURBATIONS

It is found that all the upper vibrational levels are perturbed: the lower levels are unperturbed. The perturbations have been detected by forming the expressions (1) and (2) and plotting them against J (fig. 2). Information about the perturbations is summarized in table 7 and in fig. 3. The figure shows the upper vibrational levels in a plot against $J(J+1)$: circles, squares and triangles indicate the positions where the perturbations culminate.

The Perturbing States

The appearance of the perturbations shows that they are caused by interactions of two perturbing states, a triplet one and a singlet one. These states are here called e and f. Both states lie lower than the $D\,^1\Pi$ state. It is not possible to decide whether the state f is $^1\Pi$ or $^1\Delta$. It cannot be $^1\Sigma$ as both the Λ-type terms of $D\,^1\Pi$ are perturbed. State e is probably $^3\Sigma^-$, as in the CO spectrum (Coster and Brons 1934, Budó and Kovács 1938). There are three interactions at a $^3\Sigma$.$^1\Pi$ perturbation: the c terms in $^1\Pi$ are perturbed by the $^3\Sigma_J^-$ component and the d terms by the $^3\Sigma_{J-1}^-$ and $^3\Sigma_{J+1}^-$ components. This means that at a $^3\Sigma^-.{}^1\Pi$ interaction one perturbation may be found in the Q branch at a certain J value, two in the R and P branches, one at a lower, the other at a higher J value than that for the Q branch. In fig. 3 the $^3\Sigma_J^-.{}^1\Pi$ perturbations are indicated by squares, the $^3\Sigma_{J\pm1}^-.{}^1\Pi$ perturbations by circles and the f.$^1\Pi$ interactions by triangles.

Determination of Constants for Perturbing States

At several perturbations extra lines have been found. If extra lines are found at least at two consecutive J values, it is possible to determine the B and C values of the perturbing states (Kovács 1937, 1951: for practical examples see also Lagerqvist, Lind and Barrow 1950 and Hultin and Lagerqvist 1951). The ordinate of an intersection point in fig. 2 gives, for a singlet–singlet perturbation, $\frac{1}{2}(B_s + B') - B''$, where B_s is the B value of the perturbing state. Kovács (1951) has shown that if the terms of a $^3\Sigma$ state can be written as

$$\left.\begin{aligned} F_{J+1} &= C + B_{^3\Sigma}(J+1)(J+2),\ F_J = C + B_{^3\Sigma}J(J+1), \\ F_{J-1} &= C + B_{^3\Sigma}(J-1)J \end{aligned}\right\} \quad \ldots\ldots (3)$$

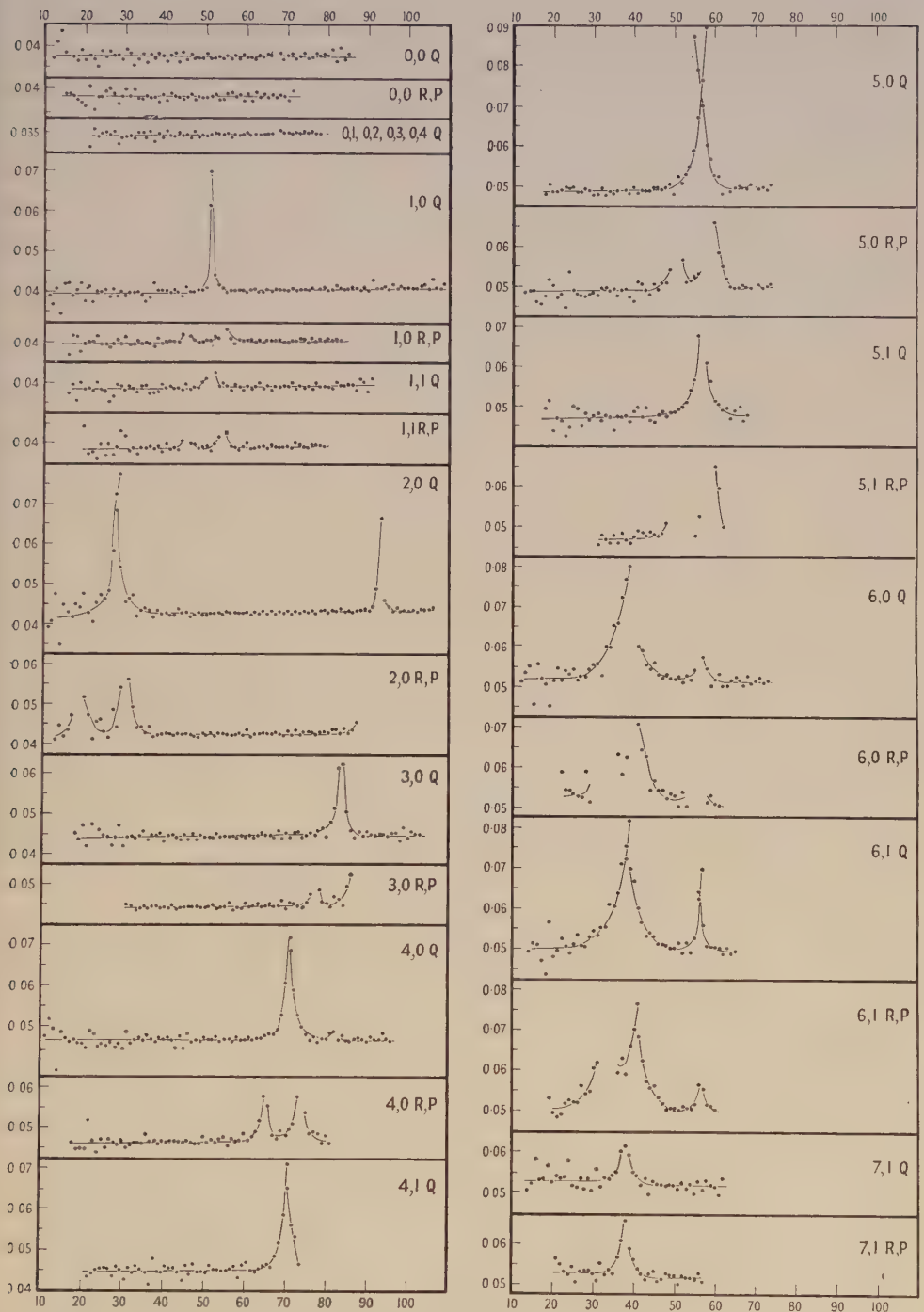

Fig. 2. $[Q(J-1)-Q(J)]/2J$ and $[R(J-2)-R(J-1)+P(J)-P(J+1)]/4J$ plotted against J.

then the middle component of a $^3\Sigma.^1\Pi$ perturbation may be treated in the same way as for a singlet–singlet interaction. The B values for the other components are

$$B_{^3\Sigma}(\mathrm{P}) = \{J/(J+1)\}B_s(\mathrm{P}) \text{ for } K = J+1,$$
$$B_{^3\Sigma}(\mathrm{P}) = \{J/(J-1)\}B_s(\mathrm{P}) \text{ for } K = J-1.$$

The values of C (the separation at $J=0$ between the perturbed and perturbing states) are given by

$$C_s(\mathrm{Q}) = -2\nu_0 + B' - \tfrac{1}{2}\{(J-1)[\mathrm{Q}(J) + \mathrm{Q}'(J)] - (J+1)[\mathrm{Q}(J-1) + \mathrm{Q}'(J-1)]\} \quad \ldots\ldots(4)$$

$$C_s(\mathrm{P}) = -2\nu_0 + 2B'' + B' - \tfrac{1}{4}\{(J-1)[\mathrm{P}(J+1) + \mathrm{P}'(J+1) + \mathrm{R}(J-1) + \mathrm{R}'(J-1)] - (J+1)[\mathrm{P}(J) + \mathrm{P}'(J) + \mathrm{R}(J-2) + \mathrm{R}'(J-2)]\}. \quad \ldots\ldots(5)$$

An approximate value for C can be found from

$$C_s(\mathrm{Q}) = B'(J^{*2} - 1) - B_s J^{*2}, \quad \ldots\ldots(6)$$

where J^* is the J value where the curves in fig. 2 cut each other.

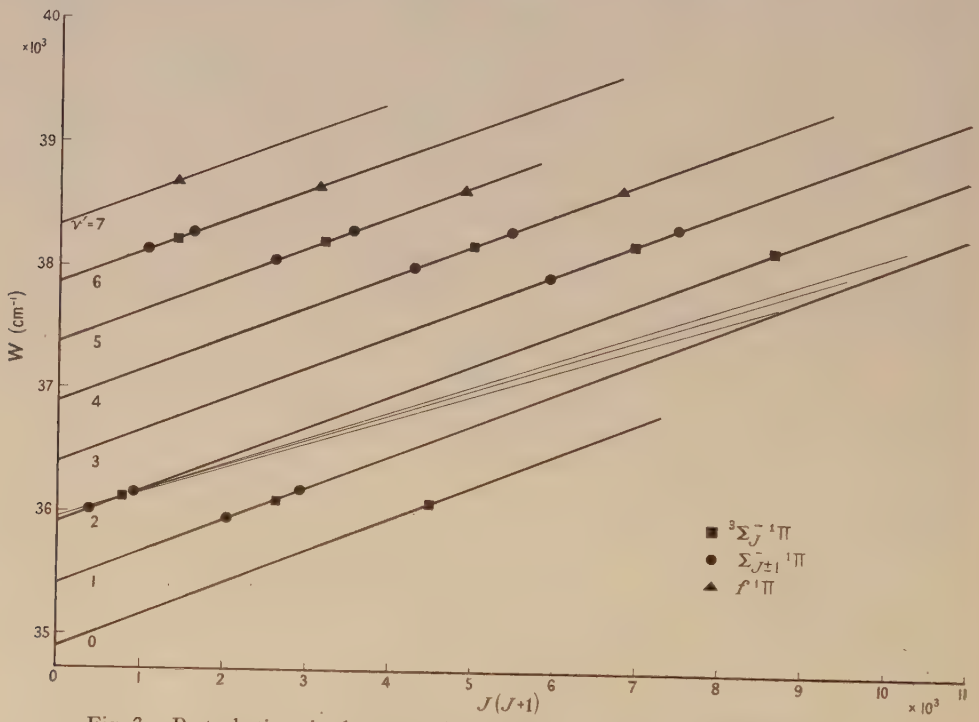

Fig. 3. Perturbations in the state D $^1\Pi$ of SiS; term values plotted against $J(J+1)$.

The results of the treatment of the perturbations are collected in table 7. The B_s values given there are the means of the observed values (the number of observed values is given in brackets). Only at one $^3\Sigma^-$ perturbation has an intersection been found in the R and P branches, namely at $J \sim 40$ in the 6,1 band: the values of $C + \nu_0$ in table 7 are therefore those calculated from the Q lines, using eqns. (4) and (6). It has not been possible to determine the absolute numbering of the vibrational levels of the perturbing states. The lowest observed levels have therefore been given the vibrational quantum numbers *e* and *f*.

The perturbation between $e^3\Sigma^-$ and $D^1\Pi$ in $v'=0$ at $J\sim66{\cdot}5$ in the Q branch is very weak, but it is clear enough to be detected. This can be seen from the behaviour of the Q branch of the 0,0 band in fig. 2. The perturbation can also be traced in the bands analysed earlier, as may be seen from the plot of the mean value of $[Q(J-1)-Q(J)]/2J$ for the 0,1, 0,2 0,3 and 0,4 bands given in fig. 2. The corresponding perturbations in the R and P branches have not been detected: presumably the perturbing matrix elements are too small. We have

Table 7. Summary of the Perturbations

v'	J^*			B_s	ν_s	$C_s+\nu_0$		Perturbing state
	RP	Q	RP			eqn. (4)	eqn. (6)	
0	—	66·5	—	—	e	—	35139·8	$^3\Sigma^-$
1	45	51·2	54	0·2111(1)	$e+1$	35551·1	35548·7	$^3\Sigma^-$
1	—	>100	—	—	$e+2$	—	—	$^3\Sigma^-$
2	19	27·8	30	0·2092(2)	$e+2$	35957·7	35955·4	$^3\Sigma^-$
2	—	93	—	—	$e+3$	—	36364·3	$^3\Sigma^-$
3	77	83·5	(86·5)	—	$e+4$	—	36769·0	$^3\Sigma^-$
4	65·5	70·8	74	0·2094(2)	$e+5$	37144·9	37155·3	$^3\Sigma^-$
4	—	82·5	—	—	f	—	—	$^1\Pi$ or $^1\Delta$
5	51	56·5	59·5	0·2056(4)	$e+6$	37546·1	37545·0	$^3\Sigma^-$
5	70	70	—	—	$f+1$	—	—	$^1\Pi$ or $^1\Delta$
6	32·5	37·5	40	0·2013(3)	$e+7$	37940·1	37932·9	$^3\Sigma^-$
6	56·5	56·5	—	0·224(2)	$f+2$	—	—	$^1\Pi$ or $^1\Delta$
7	38	38	—	—	$f+3$	—	—	$^1\Pi$ or $^1\Delta$

also been unable to find the $^3\Sigma^-.{}^1\Pi$ perturbation between the levels $v'=1(D^1\Pi)$ and $v_e=e+2/(^3\Sigma^-)$, which also seems to be too weak for detection. It should be situated at $J\sim102$.

The B values for $e^3\Sigma^-$ may be summarized: $B_{e+v}=0{\cdot}213_8-0{\cdot}001_5v$. For the state f only one value has been computed: $B_{f+2}=0{\cdot}22_5$. Since the absolute v-numbering is unknown, the vibrational constants must be left as follows

$$e^3\Sigma^-:\ \omega_e\geqslant415,\ x_e\omega_e=1{\cdot}9,\quad f:\ \omega\sim450\ \mathrm{cm}^{-1}.$$

§ 7. CONCLUSION: COMPARISON OF SiS WITH CO

The information at present available about the electronic states of SiS is summarized in table 8, and in table 9 a comparison is made between SiS and CO, the first member of this group of molecules. It is clear that the analogy between the states of these molecules has been considerably strengthened by the results of the present work. The two states, $e^3\Sigma^-$, both of which are known only through their interactions with other states, are certainly very similar in properties. Much less is known about the perturbing states $f^1\Pi$ or $^1\Delta$, both in CO and in SiS, but from what is known they too appear to be similar. Thus four of the six known states of SiS appear to have their counterparts in the term-scheme for CO. It seems however that it may be dangerous to attempt to take the analogy much further at the moment. Thus, a third perturbing state, $I^1\Sigma^-$, is known from its interactions with $A^1\Pi$ in CO, but no corresponding state has yet been found in SiS. It is of course possible that such a state will be revealed by perturbations in the D–X system of SiS lying outside the range of the present measurements, although such work is likely to be very difficult on account of

the weakness of the bands concerned. More striking is the difficulty of finding a counterpart to the E state of SiS in CO. The behaviour of the force constants has led to the suggestion that this state may correspond either to $d^3\Pi_i$ or to a $a'^3\Sigma^+$ of CO (Vago and Barrow 1946). Neither identification can, however, be accepted very readily, for the E–X system seems to be stronger in absorption than would be expected for a forbidden transition. It may therefore be that a

Table 8. Summary of Constants for SiS

State	ν_e	ω_e	$x_e\omega_e$	B_e	α_e	$D_e\times10^7$	$\beta\times10^9$	r_e(Å)	D(ev)
E	41923·5	$403{\cdot}5_4$	1·40*	$<0{\cdot}30$	—	—	—	$>1{\cdot}93$	$1{\cdot}2_9$†
f $^1\Pi$ or $^1\Delta$	$\leqslant$37150	(450)	—	$\geqslant0{\cdot}224$	—	—	—	$\leqslant2{\cdot}24$	—
$e^3\Sigma^-$	$\leqslant$35310	$\geqslant$415	1·9	$\geqslant0{\cdot}214$	$0{\cdot}001_5$	—	—	$\leqslant2{\cdot}30$	—
D $^1\Pi$	35026·8$_6$	$513{\cdot}1_2$	$2{\cdot}9_3$	$0{\cdot}2664_7$	$0{\cdot}0021_6$	2·91	3	$2{\cdot}058_9$	$2{\cdot}1_3$†
a^3_+	(15000)	(650)	—	—	—	—	—	—	—
X $^1\Sigma^+$	0	$749{\cdot}6_9$	2·58	$0{\cdot}3036_3$	$0{\cdot}0014_9$	$2{\cdot}01_5$	1	$1{\cdot}928_8$	$6{\cdot}4_7$†

* $-0{\cdot}032_9(v+\frac{1}{2})^3-1{\cdot}1_5\times10^{-5}(v+\frac{1}{2})^5$ (Thomas 1947).

† By extrapolation of the vibrational levels in state E, and assuming that states X, D and E all dissociate into ground-state atoms, Si(^{3}P)+S(^{3}P) : the multiplet separations in these atomic states introduce a maximum uncertainty in the values of D_0 of about 0·1 ev.

‡ This state is very uncertain at present. It is included here on the assumption that the visible system attributed to SiS arises from a transition E—a. No satisfactory analysis of this system has yet been made, however, and the visible bands may well arise from a transition between two states of SiS, neither of which is yet known to take part in other transitions.

Table 9. States of SiS compared with the Lowest States of CO

	CO				SiS		
State	T_0	ω/ω_X	B/B_X	State	T_0	ω/ω_X	B/B_X
$d\ ^3\Pi_i$	61785	0·52	0·65				
$e\ ^3\Sigma^-$	$\leqslant$64800	$\geqslant$0·49	$\geqslant$0·64	$e\ ^3\Sigma^-$	$\leqslant$35140	$\geqslant$0·55	$\geqslant$0·70
$a'\ ^3\Sigma^+$	(55380)	0·56	0·69				
$a\ ^3\Pi_r$	48474	0·80	0·87				
				E ?	41751	0·54	—
B $^1\Sigma^+$	86918	0·96	1·02				
I $^1\Sigma^-$	$\leqslant$66380	$\geqslant$0·48	$\geqslant$0·75				
$^1\Pi$ or $^1\Delta$	$\leqslant$66230	—	$<0{\cdot}83$	f $^1\Pi$ or $^1\Delta$	$\leqslant$37000	$\geqslant$0·60	$\geqslant$0·74
A $^1\Pi$	64747	0·70	0·83	D $^1\Pi$	34909	0·68	0·88
				(a) ?	(15000)	(0·87)	—
X $^1\Sigma^+$	0	1·00	1·00	X $^1\Sigma^+$	0	1·00	1·00

The data for CO have been taken from Herzberg (1950), except for the constants for the perturbing states. The figures for $e\ ^3\Sigma^-$ and $I\ ^1\Sigma^-$ are derived from Schmid and Gerö (1937). The existence of the $^1\Pi$ or $^1\Delta$ state of CO at $v\leqslant66230$ is based on the observation of a perturbation near the beginning of $v=1$ in A $^1\Pi$ by Gerö (1935) and Schmid and Gerö (1935).

real difference between the electronic schemes of the two molecules is appearing here, and that the counterpart to the E state of SiS is to be found, not in CO but, for example, in the isoelectronic molecule P_2, which has an excited $^1\Sigma^+$ state of weaker binding than in the ground state. A rotational analysis of the E–X system of SiS which has been begun by one of us (G. N.) should throw light on this question. Too little is known about the only state of SiS remaining, the lower state, a, of the visible bands, to justify much consideration now. The most likely interpretation, on the basis of table 9, is that it may correspond to $a^3\Pi_r$ of CO.

REFERENCES

BARROW, R. F., 1946, *Proc. Phys. Soc.*, **58**, 606.
BARROW, R. F., and JEVONS, W., 1938, *Proc. Roy. Soc.* A, **169**, 45.
BUDÓ, A., and KOVÁCS, I., 1938, *Z. Phys.*, **109**, 393.
GERÖ, L., 1935, *Z. Phys.*, **93**, 669.
HERZBERG, G., 1950, *Molecular Spectra and Molecular Structure*: I. *Spectra of Diatomic Molecules* (New York: van Nostrand).
HULTIN, M., and LAGERQVIST, A., 1951, *Ark. Fys.*, **2**, 471.
KOVÁCS, I., 1937, *Z. Phys.*, **106**, 431; 1951, *Acta Phys. Hung.*, **1**, 97.
LAGERQVIST, A., LIND, E., and BARROW, R. F., 1950, *Proc. Phys. Soc.* A, **63**, 1132.
M.I.T. Wavelength Tables, 1939 (London: Chapman and Hall).
SCHMID, R., and GERÖ, L., 1935, *Z. Phys.*, **94**, 386; 1937, *Z. Phys.*, **106**, 205.
THOMAS, D. M., 1947, *Thesis*, Oxford.
VAGO, E. E., and BARROW, R. F., 1946, *Proc. Phys. Soc.*, **58**, 538.

Dissociation of Molecular Hydrogen Ions in the Cyclotron

BY K. E. A. EFFAT
Department of Physics, The University of Birmingham

Communicated by J. H. Fremlin; *MS. received 28th January* 1952

ABSTRACT. The dissociation of H_2^+ ions by collision with gas molecules greatly reduces the current of these ions that can be obtained from a cyclotron. The current has been measured at two distances from the ion source corresponding to energies of 9 and 18 MEV and with various pressures of air and argon in the tank; the loss of ions in expanding from the smaller to the larger radius is somewhat less than is predicted by Salpeter's calculations of the dissociation cross section. Assuming this cross section to be inversely proportional to the kinetic energy of the ion, the product σE is found experimentally to be $(1{\cdot}9 \pm 0{\cdot}4) \times 10^{-16}$ cm² MEV per 'atom' of air and $(7{\cdot}0 \pm 1{\cdot}4) \times 10^{-16}$ cm² MEV per atom of argon.

THE Birmingham 60-inch cyclotron (Fremlin and Gooden 1950) is a fixed machine which is normally used to accelerate molecular hydrogen ions H_2^+, deuterons D^+ or alpha-particles He^{2+}, using nearly the same magnetic field in each case. The beam of 20 MEV molecular hydrogen ions is equivalent when incident on a target or when emerging through a window to a beam of 10 MEV protons. The acceleration of H_2^+ ions has therefore the advantage that the proton beam is obtained with the same magnetic field as for deuterons and alpha-particles; the re-shimming of the magnetic field which would be necessary if protons were to be accelerated directly is therefore avoided.

With H_2^+ ions the circulating beam current at full energy is, however, some 10 to 15 times less than would be expected from comparable observations with deuterons, and this suggests, as pointed out to the author by Dr. J. H. Fremlin, that dissociation of the H_2^+ ions occurs as a result of collisions with gas molecules during acceleration.

Since the energy required to dissociate a molecular hydrogen ion is only a few electron volts, the dissociation cross section cannot be studied by the usual method of interposing foils into the beam. In collisions between high-energy molecular ions and gas molecules in which such small amounts of energy are

transferred, a proton and a neutral hydrogen atom or two protons each of half the incident energy will be formed. The protons will then move in circular orbits of radius half that of the orbit of the incident H_2^+ ion as shown in fig. 1. This should cause most of the protons so formed to strike the ion source situated at the centre of the cyclotron. Visual observations through the optical system arranged so that the inside of the vacuum chamber can be viewed from the control room show that the ion source tip becomes white hot when H_2^+ ions are accelerated, but not during the acceleration of either deuterons or alpha-particles. If the gas pressure in the cyclotron tank is increased, more H_2^+ ions are dissociated and the ion current therefore decreases. For ions of energy above a few MeV dissociation is much the most probable cause of removal of ions from the beam owing to the small energy transfer required; and the

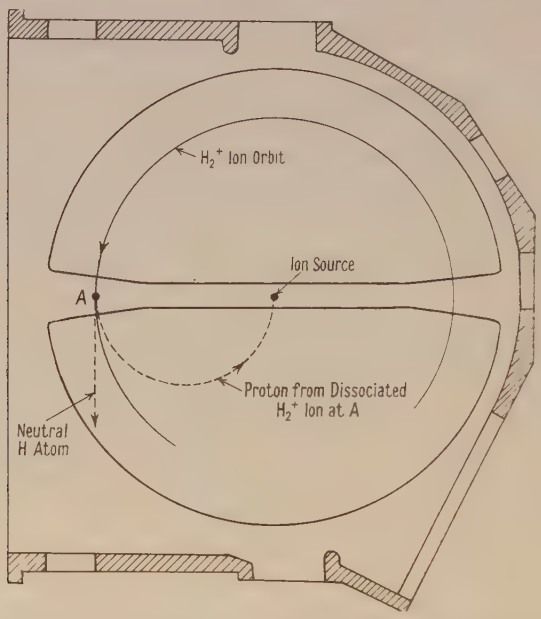

Fig. 1. Diagrammatic representation of dissociation of H_2^+ ions in the cyclotron.

dependence of ion current on gas pressure can therefore be used to measure the dissociation cross section. A calculation made by Salpeter (1950) shows that the cross section for dissociation of an H_2^+ ion of energy E is expected to have the form $\sigma = \sigma_0/E$.

If then the ion current is found under steady conditions at a radius R_1 from the centre of the cyclotron and then at a greater radius R_2, the two currents I_1 and I_2 will be given by

$$\ln \frac{I_1}{I_2} = K \frac{\sigma_0 (R_2 - R_1)}{\Delta E} p, \qquad \ldots\ldots(1)$$

where p is the gas pressure in the tank in microns, and I_1 and I_2 are the ion currents at the radii R_1, R_2 respectively, σ_0 (cm^2 MeV) is a constant for a given gas which equals numerically the dissociation cross section for an H_2^+ ion at an energy of 1 MeV, and ΔE is the energy gain per revolution in MeV, assumed to be equivalent to an acceleration of twice the peak voltage between the dees; $K = 4{\cdot}45 \times 10^{13}$ for a monatomic gas.

Ion currents were measured calorimetrically so that uncertainties due to radio-frequency pick-up and secondary electron emission were eliminated. Measurements were carried out at radii of 18 in. and 25½ in. from the centre of the cyclotron, corresponding to nominal H_2^+ ion energies of 9 and 18 MeV respectively. Over this region the loss of ions is mostly due to dissociation; other processes, such as electron capture, scattering, etc., are not important because momentum transfer in ionizing collisions is small and nuclear collisions are rare.

Dry air or 99% argon was admitted to the cyclotron tank through a needle valve to vary the pressure between the ultimate vacuum, $3\text{–}4 \times 10^{-5}$ mm, with the cyclotron running and 10^{-4} mm Hg, which was the highest pressure at which the accelerating voltage could be maintained on the dees. The pressure was measured by a B.A.R. ionization gauge connected by a wide tube to the cyclotron tank and located in a position where the effect of the pressure gradient due to the pumping manifold and baffling is not important. Pressure changes

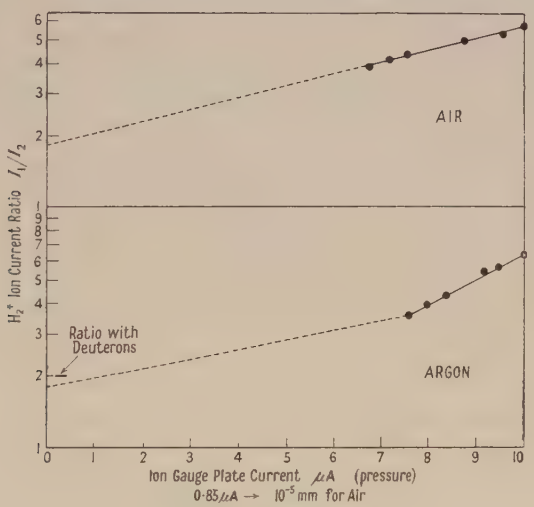

Fig. 2. Plots of the H_2^+ ion current ratios at 9 and 18 MeV against tank pressure.

of 10^{-6} mm could be obtained with the leak system and detected by the microammeter (sensitivity of 10^{-7} amp/div.) measuring the positive ion current of the ion gauge. Absolute pressures were obtained using conversion factors of the ionization gauge (Riddiford 1951). The r.m.s. voltage between each dee and earth was measured by diode rectifiers connected by quarter-wave transmission lines to circular probes placed near the dee surfaces.

The results of typical runs for air and for argon are shown in fig. 2, and confirm the linear relation between $\ln I_1/I_2$ and p predicted by eqn. (1). The intercepts obtained by extrapolation indicate that, in addition to the losses due to dissociation, there are losses which are independent of the pressure. These losses appear to be a function of the operating conditions of the machine, and may be caused by deceleration of the ions by excessive phase change since it is found that the ratio of the currents obtained at the same radii with deuterons agrees reasonably well with the intercept obtained by extrapolation of the curve for air. In the case of argon, the background pressure is due to the gases present

in the tank when the argon is introduced; extrapolation is therefore carried out with a slope corresponding to the air cross section as indicated by the dotted line on the curve for argon. This also gives an intercept in agreement with the ratio of currents obtained with deuterons. The absolute average cross sections deduced from independent sets of observations and the corresponding values of the mean free path for dissociation at a pressure of one micron are compared with the two estimates given by the theory (Salpeter 1950) in the table.

Gas	σ_0 (cm² MeV) per atom $\times 10^{18}$		(Mean free path)/E (cm/MeV) for $p=1$ micron	
	Theoretical	Experimental	Theoretical	Experimental
Air	220–350	$190 \pm 20\%$	41–66*	$75 \pm 20\%$
Argon	990–1300	$700 \pm 20\%$	22–31	$40 \pm 20\%$

* In the preparation of the table given by Salpeter (1950) some factors of two were inadvertently omitted. The results quoted in Salpeter's letter for (mean free path)/E for hydrogen, nitrogen and oxygen should be divided by 2.

The theoretical values for air is obtained from the values given for nitrogen and oxygen.

The difference between the cross sections is about 30% with an estimated experimental error of 20%, which is reasonable in view of the uncertainties of the theory. The ratio of the cross sections of air and argon agrees with the theoretical value to within 5%. Previous investigations have only been carried out at low energies, up to a few kev, and were not intended for measurement of the dissociation cross section. Estimates of 5 to 300 collisions per cm path, at 1 mm pressure for 1160 ev H_2^+ ion were given by Lamar *et al.* (1935). These values cannot be compared with the present results because the inverse proportionality between σ and E will not be valid in this energy region.

It is clear from these experiments that good vacuum conditions are of great importance for the acceleration of molecular ions. In this cyclotron, with a pressure of 4×10^{-5} mm, 70% of the H_2^+ ions reaching an energy of 1 MeV are later lost by dissociation. This loss is reduced to 3% at a pressure of 10^{-6} mm, which can be obtained in large vacuum systems. It is interesting to note that in the case of a synchro-cyclotron, the vacuum required for efficient acceleration of H_2^+ ions would be better than is obtainable with present techniques. In a typical 200 MeV synchro-cyclotron, with a total path length of about 100 km 50% of the H_2^+ ions would be lost by dissociation at a pressure of about 2×10^{-7} mm. In a 1 000 MeV proton synchrotron where the path length is much greater the loss of particles would be virtually 100%.

ACKNOWLEDGMENTS

The author wishes to record his appreciation to Dr. J. H. Fremlin for his continuous interest and advice during the course of these experiments, and to the members of the cyclotron team for their willing co-operation.

REFERENCES

Fremlin, J. H., and Gooden, J. S., 1950, *Rep. Prog. Phys.*, **13,** 295 (London : Physical Society).

Lamar, E. S., Samson, E. W., and Compton, K. T., 1935, *Phys. Rev.*, **48,** 886.

Riddiford, L., 1951, *J. Sci. Instrum.*, **28,** 375.

Salpeter, E. E., 1950, *Proc. Phys. Soc.* A, **63,** 1295.

The Increase of Ionization with Momentum for Energetic Cosmic-Ray Particles

By J. BECKER*, P. CHANSON*, E. NAGEOTTE*, P. TREILLE*, B. T. PRICE† and P. ROTHWELL†

* Centre National de la Recherche Scientifique, France
† Atomic Energy Research Establishment, Harwell, Berks.

MS. received 6th September 1951, and in amended form 9th January 1952

ABSTRACT. An experiment is described in which the momentum and specific ionization of cosmic-ray mesons were simultaneously measured, the momentum by means of a cloud chamber in a magnetic field, and the specific ionization by rectangular proportional counters. The difficulties inherent in the use of proportional counters for such measurements are discussed.

The experimental results are in satisfactory agreement with theoretical predictions of an increase of specific ionization for very energetic μ-mesons.

§ 1. INTRODUCTION

1.1. *Theoretical Background*

The average specific ionization produced by fast charged particles in their passage through matter has been discussed by Bohr (1915), Bethe (1933) and Bloch (1933 a, b). They conclude that the ionization should decrease with increasing particle momentum until a minimum value is reached at a velocity given by $v/\boldsymbol{c}=\beta\simeq 0{\cdot}96$; this minimum should be the same for all particles with equal charges. When the momentum is raised still further, the ionization should slowly increase. For convenience this effect will be referred to as the 'logarithmic increase of ionization'. It is a relativistic effect, due to the Lorentz contraction of the electric field, and the consequent increase in the maximum distance at which a particle is able to ionize.

Swann (1938) and Fermi (1940) pointed out that polarization effects in the medium should screen the more distant atoms from the electric field of the particle. As a result, the ionization should not increase indefinitely as $\beta=v/\boldsymbol{c}>1$, but should reach a limiting value, and then remain constant. Fermi's one-electron theory has been generalized by Halpern and Hall (1948). For low energies their results agree with those of Bethe and Bloch, but differences between the two theories become important when the particle velocity exceeds the velocity of light in the medium. The differences are, however, negligible when μ-mesons of momentum less than about 10^{10} ev/c pass through the proportional counters used in the experiment described below.

The polarization effect (which is more usually referred to as the 'density effect') should be particularly important in solids and liquids. Detectors such as crystal counters and photographic plates are therefore rather less suitable for investigations of the logarithmic increase than cloud chambers or gas-filled counters.

So far we have referred to the average ionization, which is the quantity usually considered theoretically. There are good reasons, however, for

preferring to deal in experimental work with the most probable ionization. The statistics of the ionization process were first considered by Bohr (1915) and Williams (1929). They pointed out that large fluctuations in the rate of loss of energy must occur from point to point along the track of a particle. These fluctuations arise partly from the Poisson distribution of the number of collisions per unit length, and partly from the widely different energies which can be given to the secondary (δ) electrons at each collision. The probability of any particular energy-loss occurring in a given track-length has been calculated by Landau (1944). His results show a broad distribution for which the most probable ionization (the peak of the distribution) shows the same kind of dependence on $v/\boldsymbol{c}$ as the mean ionization*. Either value could equally well be used to verify the existence of the logarithmic increase. From the experimental point of view, however, the determination of the mean presents several difficulties, of which saturation of the detector or amplifier by large pulses is an obvious example. These difficulties are avoided by measuring the most probable specific ionization.

1.2. *Previous Experimental Results*

A considerable number of attempts have been made to observe the logarithmic increase and the density effect experimentally, with rather contradictory results. In experiments using cloud chambers the ionization is measured by drop-counting. Occasional high-energy collisions cause dense clusters of drops which cannot be counted accurately, and have therefore to be excluded from the results. However, there is no serious objection to this procedure provided the most probable, and not the average ionization is being measured. Corson and Brode (1938), Sen Gupta (1940) and Hazen (1945) made such measurements on electrons, and all detected an increase of ionization with momentum. Similar experiments on μ-mesons by Sen Gupta (1943) and Hazen (1945) suggested that the rise was smaller than had been predicted. On the other hand, Ghosh, Jones and Wilson (1952) obtained results which agreed very well with theory. They were able to extend their measurements to sufficiently high momenta (3×10^{10} ev/c) for the polarization effect to be detectable.

Low-efficiency Geiger counters, the efficiency of which depends on the primary ionization, have been used by Hereford (1948) to measure the ionization of electrons. He found a small rise as momentum increased. Experiments using proportional counters to measure the ionization of mesons of momenta up to 5×10^{10} ev/c have been made by Goodman *et al.* (1951). They failed to detect any increase above the minimum, and concluded that mesons behaved in this respect differently from electrons.

The results obtained with gaseous detectors therefore seem to be in favour of a logarithmic increase for electrons, but leave room for doubt in the case of μ-mesons.

The evidence provided by solid detectors is also not unanimous. Whittemore and Street (1949) measured the energy-loss of mesons in a crystal ionization chamber, and found a small increase of ionization with momentum. It was less than expected, however, even after allowance had been made for the density effect. Bowen and Roser (1951), using an anthracene scintillator, failed to

* It is now known that Landau's theory underestimates the width of the distribution for heavy gases. Blunck and Leisegang (1950) show that, by taking the shell structure of the atom into account, a broader distribution can be obtained.

detect any change in ionization for μ-mesons between 3×10^8 and 3×10^9 ev/c. They concluded that the density effect prevented any rise from taking place, although their results were equally compatible with the view that the logarithmic increase does not occur for μ-mesons. Pickup and Voyvodic (1950) used photographic plates to measure meson energies by scattering and ionization by grain counting. They found a 10% rise in ionization above the minimum, and evidence for a density-effect 'plateau' at high energies.

In the present experiment we have used a proportional counter to measure the energy-loss of cosmic-ray mesons, and a cloud chamber to determine their momentum. Our results show an increase which is in reasonable agreement with the theoretical predictions. The work was carried out at the Aiguille du Midi laboratory (3 650 metres) during the course of some experiments designed to measure the vertical slow proton intensity. These experiments will be described elsewhere.

§ 2. APPARATUS

2.1. *General Description*

The experimental arrangement is shown in fig. 1. A simple telescope defined the cosmic-ray beam, which passed through a double proportional

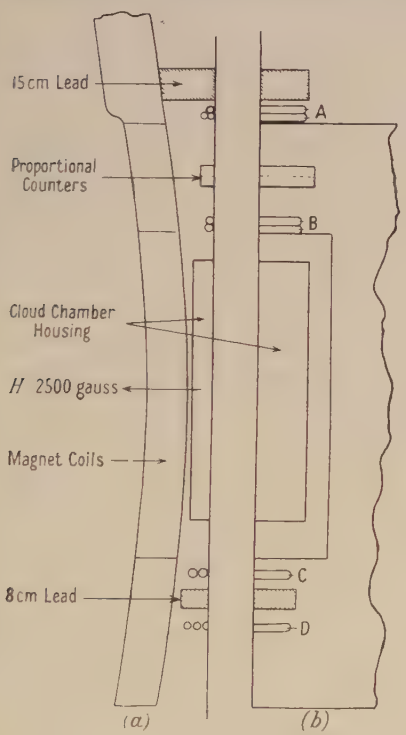

Fig. 1. (*a*) Section perpendicular to counter axes. (*b*) Section parallel to counter axes.

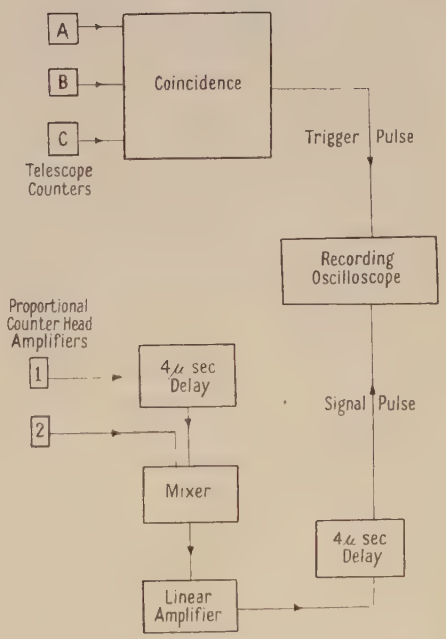

Fig. 2. Block diagram of circuit used for recording proportional counter pulses.

counter and then through a cloud chamber. A filter consisting of 15 cm of lead was placed above tray A, in order to cut out the soft component. Below tray C was a fourth counter tray D, the two being separated by 8 cm of lead.

The cloud chamber was expanded and the proportional counter pulses recorded whenever a triple coincidence (A + B + C) occurred. In addition a telephone register indicated when events of the type (A + B + C − D) took place. This information was used to estimate the number of particles stopped by the absorber.

The cloud chamber, of dimensions 56 cm × 16 cm × 15·5 cm, was situated in a very uniform magnetic field of about 2 500 gauss. This field, which was produced by a large air-cored electromagnet, enabled momenta of up to 5×10^9 ev/c to be measured. The cloud chamber, and the associated apparatus (not shown in the figure), were designed by Nageotte, and are described in a paper by Bastin *et al.* (1950).

2.2. *Proportional Counters*

(*a*) *Construction.* The double counter used throughout the experiment consisted of two rectangular chambers, placed one above the other in the same envelope. The common dividing wall was made of thin ($\frac{1}{32}$ inch) brass, perforated to allow the same gas filling to be used for both counters. The gas used was a mixture of 40·6 cm Hg of krypton and 4·2 cm Hg of methane (at 18° C). The depth of the counters in the direction of the cosmic-ray beam was 3·19 cm in one case and 3·42 cm in the other; the internal width was 7·2 cm and the useful length 25 cm. The wires, placed centrally in the two compartments, were of 0·004 inch diameter tungsten. The counters were operated at 2 200 volts.

The rectangular shape of the counter, chosen to give equal path-lengths for all particles, led to some difficulties in the preparation of the filling gas. It was found necessary to work with very pure gases in order to avoid recombination in the low-field regions near the corners.

To test that a filling was suitable, calibration x-rays (Rothwell and West 1950) were introduced into each counter through five thin windows. Two of the windows were close to a low-field region, while the other three were on the centre-line of the counter, where the electric field was strong. A good filling gave substantially identical calibrations for each of the five windows. Impurities caused the two 'low-field' windows to give x-ray peaks that were too low and too broad.

With argon practically identical curves were easily obtained for all five windows, but with krypton more difficulty was found. The filling chosen for the experiment, using krypton that had been purified by standing over heated calcium for 24 hours, gave a 4% difference in most probable pulse-size between windows, and a 9% half-width at half-height for the 8 kev K x-ray of zinc. (A good cylindrical counter gives a half-width of 7½%.) This was considered admissible in view of the large fluctuations known to exist in the ionization of cosmic-ray particles, but, as a precaution, the counter telescope was arranged to include only the central 5 cm of the proportional counter width.

(*b*) *Routine calibration.* X-ray calibrations were carried out regularly throughout the course of the experiment, using a series of artificially prepared radioactive sources. Lines at 8·1, 10·5, 20·2 and 41·6 kev, given by zinc, selenium, palladium and gadolinium respectively enabled non-linearities in the counter and amplifiers to be corrected, and the output pulse-height converted to an energy-loss. This set of calibrations enabled us to measure energy-losses of up to eight times the most probable value for minimally ionizing mesons.

The mean value of the calibrations for the five windows was used, in order to reduce errors due to variations of sensitivity within the counter.

(*c*) *Recording of counter pulses.* Figure 2 shows the block diagram of the circuit used to record the proportional counter pulses. The signals from the head-amplifiers were separated in time by a delay-line operating on one pulse only, then mixed and amplified. The amplified pulse was fed through a further delay-line to the Y plates of a single-sweep recording oscilloscope, which was triggered and photographed whenever a coincidence pulse was received from the counter telescope.

§ 3. EXPERIMENTAL ERRORS

3.1. *Errors associated with Ionization Measurements*

There were three sources of instrumental error that were not eliminated by calibration with X-rays:

(i) Statistical fluctuations in the counter multiplication processes gave rise to a random error with a standard deviation of about $8\frac{1}{2}\%$. This figure was calculated for a release in the counter of 4 kev (roughly the most probable value of the ionization minimum) by assuming that the uncertainty would be the same as that found for an X-ray calibration line of the same energy.

(ii) The uncertainties in calibration, due to variations of sensitivity within the useful volume of the counter, gave a random error of standard deviation not greater than 3%.

(iii) The r.m.s. error in reading the photographic record of the oscilloscope trace was estimated to be not more than 5%, by comparison of the results obtained by two independent observers.

Since these errors were independent, the overall r.m.s. error of a single observation was taken as the root of the sum of the squares, that is, approximately 10%. It will be shown later that random instrumental errors of this magnitude have only a slight effect on the accuracy of the results.

3.2. *Errors in Momentum Measurement*

The errors in momentum measurement vary with the magnetic field and with the quality of the cloud chamber photograph. The principal error, however, arises from turbulence, which causes an apparent curvature of the tracks even in the absence of the magnetic field. This error, and any errors due to multiple scattering, were estimated by taking about ten per cent of all the photographs without field, and measuring the curvature of the tracks. It may be concluded that, for the majority of the observations, the uncertainty in the momentum p is such that $1/p$ is known to better than $\pm 0{\cdot}2$, if p is in units of 10^9 ev/c. The highest value of momentum that could be regarded as measurable was therefore taken as 5×10^9 ev/c, and all particles of momentum greater than this were placed in the 'unresolved group'. At 10^9 ev/c the maximum error was $+25\%$ and -17%; at 5×10^8 ev/c it was $+11\%$ and -9%.

Due to the asymmetry of the momentum error the momentum will, on the average, be overestimated. If the logarithmic increase exists this error will cause the most probable ionization predicted on the basis of the momentum measurements to exceed the observed value by an amount which will be negligible below 2×10^9 ev/c, and less than 6% at 4×10^9 ev/c. The momentum error will therefore cause the observed rise to be a little less than that expected theoretically.

§4. TREATMENT OF RESULTS

4.1. *Rejection of Unwanted Particles*

Almost all the particles recorded by the apparatus were either μ-mesons, π-mesons or protons. As we shall show later, the π-mesons comprised only a small fraction of the total beam. Since their predicted ionization curve is very close to that for μ-mesons, their presence is unimportant. On the other hand, the protons, which differ appreciably from mesons in their ionization properties, were sufficiently numerous at the altitude of the laboratory to make their exclusion essential.

The simplest way of ensuring this was to ignore all positive particles possessing more than the momentum at which protons could just traverse the telescope. This was approximately 5×10^8 ev/c. Below this momentum there was no objection to using both positive and negative particles, since the ionization of mesons is independent of their sign.

At momenta greater than about 5×10^9 ev/c the tracks were so little curved that it was impossible to decide whether the particles were positive or negative. There was therefore no way of selecting only mesons from the 'unresolved group' of very energetic particles.

4.2. *Rejection of Multiple Events*

Approximately two-thirds of the cloud chamber photographs showed single particle tracks, the remainder being confused by showers or the accidental passage of two particles during the sensitive time of the chamber. Proportional counter observations were accepted only if the particles were definitely single. It is realized that this method of rejecting multiple events is not completely certain. For instance, two diverging particles could pass through the proportional counters and give rise to only one track in the cloud chamber. It is difficult, however, to imagine a mechanism whereby this kind of event could imitate a logarithmic increase. For this to happen the angular divergence of the associated particles would have to be greater the greater their energy. In fact the opposite is known to be true. The rise we have observed cannot, therefore, be explained in this manner.

4.3. *Fluctuations in the Ionization Process and their Effect on the Treatment of Results*

The existence of fluctuations in the rate of ionization of fast charged particles has already been briefly mentioned. The probability distribution for the ionization liberated in a layer of matter having a thickness much smaller than the range of the particle has been calculated (with the aid of some simplifying assumptions) by Landau (1944). He finds that on the low-energy side of the peak the curve should fall rapidly to zero, while on the high-energy side it should fall much less sharply and show a pronounced 'high-energy tail'. The values predicted by his theory for the ratio of the full width of the distribution (at half-height) to the most probable ionization range from 0·25 to 0·45 for many commonly used counter gases. However, it has since been pointed out by Blunck and Leisegang (1950) that for heavy gases the widths should be even greater than those predicted by Landau. This is confirmed by some

recent work (Rothwell 1951) on the ionization losses of fast electrons in argon and krypton, according to which the widths for the counters used in the present experiment would be expected to be 0·53 and 0·7 respectively.*

These large fluctuations would present no real difficulty if an unlimited number of observations were available. When, however, there are only comparatively few observations, ordinary statistical fluctuations are superimposed on those resulting from the physical nature of the ionization process. It is then necessary to adopt a fairly elaborate method of treating the results.

The results of the present experiment were first grouped into seven momentum intervals, and a statistical procedure (summarized below) was then used for fitting curves to the experimental ionization distributions. This enabled us to make use of all the observations, duly weighted, including those in the 'high-energy tail' at some distance from the peak, and to quote values for the most probable ionization and the r.m.s. error which were statistically valid. The curve which was fitted to the observations was based on Rothwell's curve for krypton, modified by varying the width (without otherwise changing the shape) until the best fit was obtained. With the statistical procedure which was adopted the dependence of the computed value of the most probable ionization on the width of the fitted curve was very slight. For instance, changing the width by 20% altered the computed value by only 2%. The width found for the distribution was, in any case, not significantly different from that quoted for electrons in krypton.

It would have been possible, of course, to have chosen any one of a number of analytical formulae representing single-peaked skew curves with a 'high-energy tail', but the curve for electrons seemed physically a more reasonable choice.

In treating the results no use was made of the fact that two ionization measurements were made simultaneously on each particle. The combination of these pairs of observations into some kind of mean is useful only when more than one kind of particle is being observed. When, as in the present case, the particles are very nearly all of one kind, such a procedure does not give any increased accuracy. It has therefore been assumed that the observations can be treated as though they were independent measurements on two identical particles. For this particular experiment the only advantage of the double counter was that information was collected twice as quickly.

4.4. *Summary of the Method of Curve-fitting*

The following is a summary of Behrens' (1951) method of curve-fitting. We start with a large number n of observed values of a function Δ (in this case the energy-loss), together with a probability curve ϕ, as a function of $x=(\Delta-\Delta_0)/\xi$, which it is believed should correspond to the probability distribution of the Δ's. The purpose of the method is to calculate the best-fitting values of the parameters Δ_0 and ξ, and also the r.m.s. errors in these values.

In the present case Δ_0 is equal to the most probable value of the ionization and ξ determines the width of the distribution.

Let $(\Delta_1, \Delta_2, \ldots, \Delta_j, \ldots \Delta_{n-1}, \Delta_n)$ represent the set of observed values, and define $\phi_j=\phi[(\Delta_j-\Delta_0)/\xi]$.

* It therefore now seems that krypton was an unsuitable choice for this experiment. This is confirmed by Cranshaw (1951), who used an argon counter in an essentially similar experiment, and obtained a narrower distribution.

If we fix Δ_0 and ξ, the probability of any given value of Δ arising will be proportional to $[\phi(x)]/\xi$. The probability P of any particular combination of Δ's arising is therefore

$$P \propto \prod_{j=1}^{n} (\phi_j)/\xi^n.$$

Then $$\log P = \text{constant} - n \log \xi + \sum_{1}^{n} \log \phi_j,$$

whence $$-\partial \frac{(\log P)}{\partial \xi} = \xi^{-1} \sum_{1}^{n} \{x_j \phi_j'/\phi_j) + 1\} = Y, \qquad \ldots\ldots(1)$$

where ϕ_j' denotes $d\phi/dx$ at $x = x_j$.

Similarly, $$-\frac{\partial (\log P)}{\partial \Delta_0} = \xi^{-1} \sum_{1}^{n} (\phi_j'/\phi_j) = Z. \qquad \ldots\ldots(2)$$

The most probable values of ξ and Δ_0 are found by making both Y and Z simultaneously equal to zero. These two auxiliary functions, defined in eqns. (1) and (2), are first tabulated for various values of the two parameters. The best values of ξ and Δ_0 are then found by interpolation. This stage of the calculation is very simple in practice, since Y depends sensitively on ξ, and hardly at all on Δ_0, while the reverse is true for Z. The mean square error in Δ_0 can be shown to be $E_1^2 = (\partial Z/\partial \Delta_0)^{-1}$. The differentiation must be performed at a point in the (ξ, Δ_0) plane corresponding to $Y = Z = 0$, and along a direction defined by $Y = 0$. This expression neglects any contribution from third and higher order terms.

Similarly, the mean square error in ξ is given by $(\partial Y/\partial \xi)^{-1}$, evaluated at the same point along the contour in the (ξ, Δ_0) plane defined by $Z = 0$.

The above treatment is correct only when there are negligible observational errors. The experimental errors can be taken into account by writing the total uncertainty E in the form $E = [E_1^2 + (kE_2^2/n)]^{1/2}$, where n is the number of observations, E_2 is the uncertainty arising from the instrumental error in an individual observation, and k is a constant, greater than unity, whose value depends on the shape of the distribution $\phi(x)$ and on how the errors change with Δ. (For a constant error and gaussian distribution k is equal to one; for the conditions of this experiment it is slightly greater.)

The quantity E has been evaluated numerically for three of the seven momentum groups. In no case does the inclusion of the second term introduce an additional error of more than 0·2%, which is quite negligible in comparison with the error in curve-fitting. It is obvious by inspection that similar results will hold for the other groups.

§ 5. STATEMENT OF EXPERIMENTAL RESULTS

5.1. *Most Probable Ionization of Cosmic-Ray Mesons as a Function of Momentum*

The most probable value of the ionization has been computed for each of the seven momentum groups: Group I (1·7 to $2{\cdot}5 \times 10^8$ ev/c) contains mesons of momentum less than that corresponding to the theoretically predicted minimum of ionization (for convenience we shall refer to such mesons as being 'below' the minimum). In this region the ionization varies rapidly—it is very roughly proportional to the inverse of the momentum—so that the group has been made as narrow as the rather small number of observations permitted. Group II (2·5 to $3{\cdot}5 \times 10^8$ ev/c), and Group III (3·5 to $5{\cdot}0 \times 10^8$ ev/c), both

contain approximately minimally ionizing mesons. Groups IV, V and VI (5·0 to 9·9, 9·9 to 19·5 and 19·5 to 50×10^8 ev/c respectively), being above the proton cut-off, are restricted to negative particles. The momentum intervals were chosen to give approximately the same statistical weight to each group. Group VII contains all the particles of momentum greater than 5×10^9 ev/c.

Figure 3 shows the curves which were fitted to the experimental data for each of the seven groups. The data are summarized in the accompanying histograms.

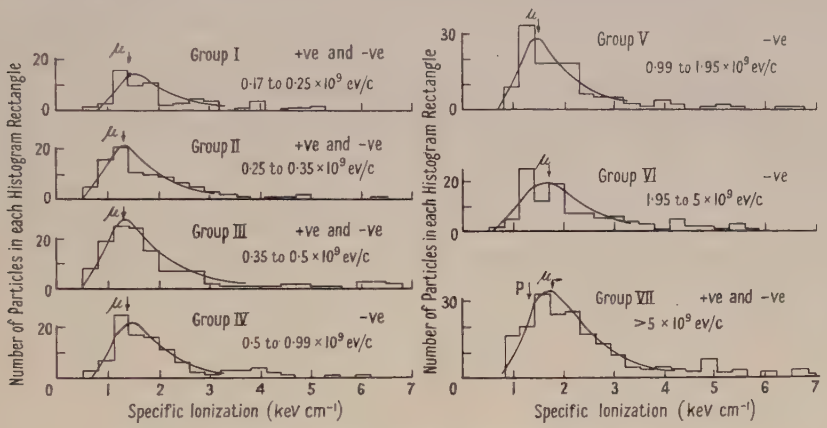

Fig. 3. Variation of pulse-height distribution with momentum.

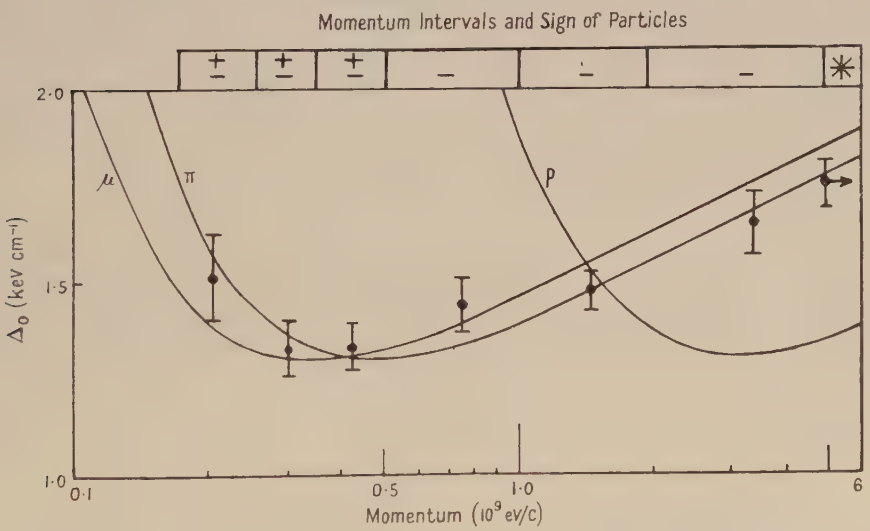

Fig. 4. Values of most probable ionization Δ_0 derived from statistical treatment of results. p, μ, π : Curves calculated from Landau's theory for protons, and μ- and π-mesons. $*$: The arrow on the last point indicates that it refers to all particles of momentum greater than 5×10^9 ev/c.

It is emphasized that these histograms have an illustrative value only; they were not used in the fitting of the curves to the observations, which was done directly. The histograms are included only because the large diagram, in which the observed values of energy-loss were plotted against the observed values of momentum, is not suitable for reproduction on a reduced scale. The small arrows in fig. 3 show the most probable ionization for μ-mesons, and in one case, for protons, calculated from Landau's formula.

In fig. 4 the computed values of the most probable ionization are plotted against momentum; r.m.s. errors are indicated by the vertical extension of the points. For all except the highest momentum group the mean momentum has been chosen as abscissa; the unresolved group, however, has been plotted at 5×10^9 ev/c with an arrow indicating that it refers to all particles of momentum greater than this value. The curves included in this figure show the most probable ionization, according to Landau, for μ-mesons, π-mesons and protons.

5.2. *The Width of the Distribution for Minimally Ionizing Mesons*

Besides giving the most probable ionization, the statistical procedure enabled the most probable width of the distribution to be determined. After taking the average of the results for Groups II and III (both containing mesons which should be approximately minimally ionizing), and correcting for errors, we find

$$\frac{\text{Full width of distribution at half-height}}{\text{Most probable value of specific ionization}} = 0{\cdot}75 \pm 0{\cdot}1.$$

This value agrees, within the experimental error, with the results found by Rothwell for 2 Mev electrons and similar counter conditions.

5.3. *Information obtained from Counter Tray D*

The events which have been described as being of the type (A + B + C − D), and which therefore appear to be associated with the stopping of particles in the bottom 8 cm of lead, fall into two categories. The first comprises particles of momenta less than about $2{\cdot}5 \times 10^8$ ev/c, the momentum below which no μ-mesons should be able to traverse the absorber. For this group the majority (80%) of all the particles which would have been expected to stop in the absorber were recorded as actually having done so. The agreement is not quantitative because, in the restricted space between the supports of the electromagnet coils, it was possible to install only a rather inadequate counter assembly.

The second category contains negative particles with momenta between $2{\cdot}5 \times 10^8$ and 5×10^9 ev/c, and positive particles in the band $2{\cdot}5 \times 10^8$ to 5×10^8 ev/c. The particles recorded as 'stopped' are distributed more or less at random over the whole momentum spectrum, and are interpreted as particles which have suffered catastrophic absorption in the 8 cm of lead, without having given rise to penetrating secondaries. They comprise only 5% of all particles observed within the same momentum limits.

This information is used in the following section to estimate the fraction of π-mesons present in the cosmic-ray beam.

§ 6. DISCUSSION OF RESULTS

6.1. *The Proportion of Particles other than μ-Mesons contained in Groups I–VI*

The statement has been made earlier in this paper that virtually all the particles observed were μ-mesons. The arguments that lead to this conclusion are as follows. Protons and other heavy positive particles can be excluded because of the method of selection (§ 4.1). None of the recently discovered heavy mesons is sufficiently numerous to be worth considering, and no electrons can penetrate the 15 cm of lead placed above the apparatus, so that it is only necessary to show that π-mesons were present in small numbers.

Fast π-mesons have an interaction length in lead which is about 160 g/cm^2. Further, for momenta less than 10^9 ev/c, they give rise to stars with secondaries

capable of penetrating a few centimetres of lead in only about 20% of all interactions (Camerini *et al.* 1951). Combining these two facts, we see that 35% of all incident π-mesons (at least below 10^9 ev/c) should be counted as (A + B + C − D) events. From the figures quoted in § 5.3 it can be concluded that above $2{\cdot}5 \times 10^8$ ev/c π-mesons do not comprise more than about 13% of the total meson component. A very similar conclusion can be reached from rough calculations based on the known properties of stars, if it is assumed that only the stars produced in the 15 cm lead filter contribute to the π-meson component.

6.2. *Results obtained for the Unresolved Group* ($p > 5 \times 10^9$ ev/c)

Much of the value of the results would be lost if the large value of the most probable ionization found for the unresolved group could be given some explanation unconnected with the logarithmic increase, such as, for instance, the presence of heavy particles below the ionization minimum. Quite apart from the fact that such heavy particles are known to be rare in comparison with mesons, it is fortunately very easy to show that there are no particles which have the properties required for such an explanation. Alpha-particles, having a double charge, and therefore a four times greater ionization at the minimum, cannot contribute to the observations which lie in the peak of the ionization distribution. The ionization properties of protons, deuterons and tritons, below the minimum, are sufficiently well established for it to be certain that, at momenta greater than 5×10^9 ev/c, they would have most probable ionizations below the value observed for Group VII. Including them in this group could only depress, and not raise, the observed value. We are therefore forced to the conclusion that for some, or all, of the particles comprising this group the logarithmic increase exists.

6.3. *Statistical Significance of the Results: Conclusion*

To estimate the significance of the results we have used a slightly modified form of the χ^2 test. This test deals with any observations in which the numerical value of the r.m.s. error is equal to the square root of the quantity observed. The tables can therefore be used directly if the results are first scaled so that this condition is satisfied. The test has been used in this manner to check the agreement of the values of the most probable ionization, computed for Groups II to VI, with the predicted curves for μ- and π-mesons. (It did not seem desirable to include Group VII because it comprised a mixture of particles of unknown momentum and doubtful identity.)

It is usually assumed that satisfactory agreement between experiment and hypothesis has been shown when the probability values derived from the test lie within the limits 0·3 and 0·8. The χ^2 value obtained for the μ-meson curve was 4·3, and for the π-meson curve 2·6, corresponding (for five degrees of freedom) to probabilities of 0·5 and 0·75 respectively. The experimental values can therefore be satisfactorily accounted for on the basis of Landau's theory although the results are insufficiently accurate to distinguish between the two kinds of meson. The evidence given earlier that the particles consisted predominantly of μ-mesons is nevertheless still relevant, since it has been suggested that the absence of a logarithmic rise might be a specific property of these particles.

A test has also been made to see whether the results could equally well be in agreement with the hypothesis that no logarithmic increase exists. No constant value of ionization could be found which had a chance of more than one in 10^5 of being in agreement with the results from Groups II–VII.

The results therefore suggest very strongly that a rise similar to the predicted logarithmic increase exists, and therefore disagree with the findings of Goodman *et al.* (1951). There is no obvious reason why there should be this contradiction between two very similar experiments, but in view of the disagreement we are repeating the measurements with substantially increased accuracy.

ACKNOWLEDGMENTS

We wish to acknowledge our indebtedness to Mr. R. Aves, who built the counters; to MM. Bastin and Reposeur and Miss J. Carey for their help in the laboratory; to Mr. R. Preston for his help in the computation of the results; to Mr. W. J. Whitehouse, Mr. T. E. Cranshaw and Dr. J. B. Harding for many valuable discussions; and to Dr. E. Bretscher for his encouragement. Two of us are indebted to Professor Leprince-Ringuet for his invitation to collaborate in the work of the Aiguille du Midi laboratory, and to the Director, Atomic Energy Research Establishment, for permission to participate in the publication of these results.

REFERENCES

Bastin, E., Becker, J., Chanson, P., Nageotte, E., and Treille, P., 1950, *J. Phys. Radium*, **11,** 273.
Behrens, D. J., 1951, *A.E.R.E. Report* T/M 50 (H.M.S.O. Code 70–674–0–42).
Bethe, H. A., 1933, *Handb. Phys.*, **24,** 522.
Bloch, F., 1933 a, *Ann. Phys., Lpz.*, **16,** 285; 1933 b, *Z. Phys.*, **81,** 363.
Blunck, O., and Leisegang, S., 1950, *Z. Phys.*, **128,** 500.
Bohr, N., 1915, *Phil. Mag.*, **30,** 581.
Bowen, T., and Roser, F. X., 1951, *Phys. Rev.*, **83,** 689.
Camerini, U., *et al.*, 1951, *Phil. Mag.*, **42,** 1255.
Corson, D. R., and Brode, R. B., 1938, *Phys. Rev.*, **53,** 773.
Cranshaw, T. E., 1951, *Thesis*, University of Cambridge.
Fermi, E., 1940, *Phys. Rev.*, **57,** 485.
Ghosh, S. K., Jones, G. M. D. B., and Wilson, J. G., 1952, *Proc. Phys. Soc.* A, **65,** 68.
Goodman, P., Nicholson, K. P., and Rathgeber, H. D., 1951, *Proc. Phys. Soc.* A, **64,** 96.
Halpern, O., and Hall, H., 1948, *Phys. Rev.*, **73,** 477.
Hazen, W. E., 1945, *Phys. Rev.*, **67,** 269.
Hereford, F. L., 1948, *Phys. Rev.*, **74,** 574.
Landau, L., 1944, *J. Phys., U.S.S.R.*, **8,** 201.
Pickup, E., and Voyvodic, L., 1950, *Phys. Rev.*, **80,** 89.
Rothwell, P., 1951, *Proc. Phys. Soc.* B, **64,** 911.
Rothwell, P., and West, D., 1950, *Proc. Phys. Soc.* A, **63,** 541.
Sen Gupta, R. L., 1940, *Nature, Lond.*, **146,** 65; 1943, *Proc. Nat. Inst. Sci., India*, **9,** 295.
Swann, W. F. G., 1938, *J. Franklin Inst.*, **226,** 598.
Whittemore, W. L., and Street, J. C., 1949, *Phys. Rev.*, **76,** 1786.
Williams, E. J., 1929, *Proc. Roy. Soc.* A, **125,** 420.

LETTERS TO THE EDITOR

^{83}Kr—The Possible Existence of a Nuclear Level preceding the Metastable State

During cloud-chamber studies of the angular distribution of successive conversion electrons in radioactive isotopes of bromine, many photographs have been obtained showing a fast and a slow electron with a common origin in circumstances where the only bromine isotope present was ^{83}Br. This isotope is known to undergo β-decay to ^{83}Kr, followed by a 32·7 kev gamma-ray from an excited state of half-life 1·9 hours; another gamma-ray of 46 kev with a similar half-life has been reported by Helmholz (1941) but has not been found by Bergström, Thulin and Andersson (1950) who made spectrometer measurements with ^{83}Kr separated from fission products.

The tracks of the fast electrons in the magnetic field applied to the chamber show a spread of initial curvatures too wide to be explained as scattering of high-energy conversion-electrons, and they must therefore be due to β-particles. Since the resolving time of the chamber is about $\frac{1}{100}$ sec, one particle must follow the other within this time if they are to be observed as a pair of tracks of similar width. No β-transition of about

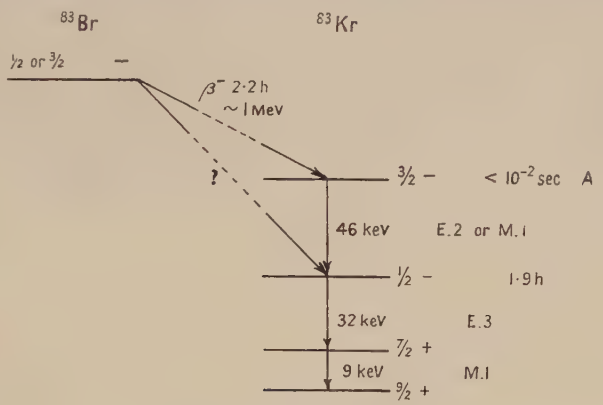

Possible decay scheme for ^{83}Kr.

1 MeV energy (known for ^{83}Br) can have so short a half-life, and hence the low-energy member of the pair must be the later one and is most probably the conversion electron produced in the decay of a short-lived excited state in ^{83}Kr. Liberation of an atomic electron by the β-particle (Bruner 1951) seems too unlikely to explain the number of pairs which form a substantial part of all fast electron events observed with ^{83}Br. Of the possible positions of the short-lived level, that shown in the decay scheme at A (see figure) seems most consistent with the allowed β-transition, and the proposed spins and parities of the other states as taken from Goldhaber and Sunyar (1951) and from Feenberg and Hammack (1949).

The γ-ray from state A has been given the definite energy of 46 kev because of Helmholz's spectrometer measurements, and it is consistent with rough measurements of curvature which have been made on the slow electrons in the cloud-chamber photographs. This decay scheme seems to explain the results of Helmholz and of Bergström *et al.* The failure of the latter to detect the 46 kev gamma-ray would be expected owing to the rapid decay of state A during the transference of the source from the separator to the spectrometer. The long half-life reported by Helmholz could be due to the parent β-decay from ^{83}Br (2·2 hours) because the source used was a film of selenium which had been bombarded with deuterons and then placed directly into the spectrometer. In this source ^{83}Br can

be produced directly or indirectly as shown, and the indirect production by the decay of ^{83}Se could explain also the initial constancy of activity observed by Helmholz.

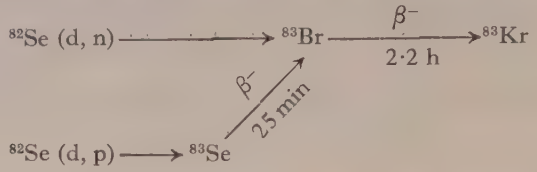

In the present experiments deuteron-bombardment of selenium was again used to produce ^{83}Br, but the bromine was separated chemically before insertion into the cloud-chamber in the form of ethyl bromide.

On the scheme given the 46 kev transition could be of either electric quadrupole or magnetic dipole type, for which respectively a half-life of 10^{-5} sec or 10^{-8} sec is expected if the transition probabilities of Weisskopf (1951) are corrected for internal conversion by means of the data of Hebb and Nelson (1940). The longer half-life makes the electric transition particularly interesting and it is compatible with the K/L conversion ratio reported by Helmholz, whereas the magnetic transition is not. In view of this it seems valuable to get more accurate information on the K/L ratio, and experiments have been started in conjunction with Dr. P. T. Barrett, who is also searching for short half-lives in the krypton transitions.

I am grateful to Dr. W. I. B. Smith and the cyclotron team for their help with the bombardments, and to Professors P. B. Moon and W. E. Burcham for valuable discussions.

Department of Physics, J. Walker.
University of Birmingham.
1st April 1952.

Bergström, I., Thulin, S., and Andersson, G., 1950, *Phys. Rev.*, **77**, 851.
Bruner, J. A., 1951, *Phys. Rev.*, **84**, 282.
Feenberg, E., and Hammack, K. C., 1949, *Phys. Rev.*, **75**, 1877.
Goldhaber, M., and Sunyar, A. W., 1951, *Phys. Rev.*, **83**, 906.
Hebb, M. H., and Nelson, E., 1940, *Phys. Rev.*, **58**, 486.
Helmholz, A. C., 1941, *Phys. Rev.*, **60**, 415.
Weisskopf, V. F., 1951, *Phys. Rev.*, **83**, 1073.

---

^{83}Kr—An Investigation of the Radiations succeeding the Metastable State

Measurements by Bergström (1951) with a beta-ray spectrometer upon electromagnetically separated $^{83}Kr^{m}$ have shown that the radiations from the 114 min metastable state consist of two highly converted gamma-rays of energies 32·2 kev and 9·3 kev. Proportional counter examination of these radiations shows that the transitions are in cascade and that the lifetime of the 9 kev level is less than 10^{-7} sec.

The $^{83}Kr^{m}$ was formed as the decay product of ^{83}Se and ^{83}Br produced by bombardment of metallic selenium with 7 Mev deuterons; the krypton was separated by melting the selenium in a side-tube to the counter, whilst free bromine was retainedin a liquid-air trap using $SeBr_4$ to provide the carrier.

The pulse-size distribution was recorded on moving film and analysed by projection in a micro-film reader. The peaks of the spectrum occurred in the following manner: at 9 kev when the 32 kev gamma-ray escaped detection, at 41 kev when both transitions were detected in coincidence (9+32=41), and at 28 kev when K-conversion of the 32 kev transition was followed by a krypton K x-ray of 13 kev energy having an escape probability of approximately 99% (9+32−13=28).

From the asymmetry of the peak at 28 kev it is possible to infer the existence of an unresolved 32 kev line which would occur when the 9 kev gamma-ray escaped from the counter. It is conceivable that the small prominence at 19 kev was, in fact, the corresponding escape peak (32−13=19).

Two additional pulse-size distributions of the higher energy peaks recorded with resolving times of approximately 10^{-4} and 10^{-7} sec showed little or no difference when normalized at an energy of 41·5 kev. On this evidence it seems probable that the half-life of the intermediate state is less than 10^{-7} sec.

The ratio of the K to L conversion coefficients of an isomeric transition can be calculated from a proportional counter spectrum, providing the fluorescent yield of the isotope and the escape probability of the K and L x-rays are known. In this instance, the L and M x-rays of krypton were detected with 100% efficiency, whilst the escape probability of the K x-rays was very nearly 100%. The fluorescent yield for krypton is 58% for the K shell; hence, the total area under the peaks at 19 and 28 kev corresponds to $0{\cdot}58\,N_K$, where N_K represents the number of K conversion electrons emitted in the 32 kev transition. Similarly, the 32 and 41 kev peaks correspond to $0{\cdot}42\,N_K+N_{L+M}$. This reasoning leads to a value for the K/L+M conversion ratio of 0·32, which is in good agreement with that found by Bergström.

Goldhaber and Sunyar (1951) propose that the 32 kev transition of ^{83}Kr is an electric octopole leading to a low lying state of spin 7/2 and even parity. The 9 kev transition to

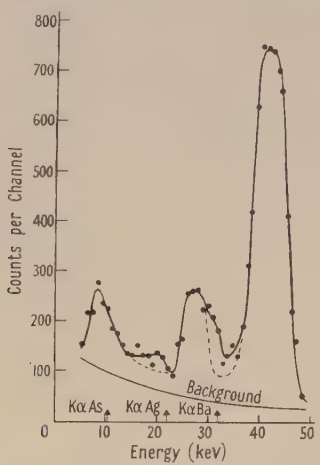

Pulse-size distribution of the radiations from ^{83}Kr^{m}.

the ground state with spin 9/2 involves a spin change of unity; if the parity changes, it is likely to be an electric dipole; if not, a magnetic dipole with a possible admixture of electric quadrupole. The values for the corresponding total internal conversion coefficients shown in the table were derived from the non-relativistic formulae of Hebb and Nelson (1940). These figures were used to correct for internal conversion in Weisskopf's relationship for the expected half-life T.

	Elec. Dipole	Mag. Dipole	Elec. Quadrupole
N_e/N_γ	17	8	2×10^4
T (sec)	10^{-11}	5×10^{-8}	10^{-5}

Since the 32 kev transition in ^{83}Kr is not totally internally converted, it is impossible to calculate an accurate value for the conversion coefficient of the 9 kev transition from the proportional counter spectrum; an estimate of this may be obtained as follows:

$$N_e/N_\gamma = \frac{\text{No. of converted 9 kev transitions}}{\text{No. of unconverted 9 kev transitions}}.$$

Therefore,
$$N_e/N_\gamma \simeq \frac{I_9+I_{28}+I_{41}}{I_{19}+I_{32}} = 10\pm5$$

where I corresponds to the area under the ' line '.

On the calculated conversion coefficient of 10 ± 5, and until a more accurate measurement of N_e/N_γ can be made, the nature of the 9 kev transition can be tentatively

identified as magnetic dipole; the isomeric levels of ^{83}Kr would therefore have the spins and parities shown by Walker (1952).

The author is grateful to the Department of Scientific and Industrial Research for a maintenance grant and to Professor P. B. Moon for many stimulating discussions.

Department of Physics, P. T. Barrett.
University of Birmingham.
1st April 1952.

Bergström, I., 1951, *Phys. Rev.*, **81**, 638.
Goldhaber, M., and Sunyar, A. W., 1951, *Phys. Rev.*, **83**, 906.
Hebb, M. H., and Nelson, E., 1940, *Phys. Rev.*, **58**, 406.
Walker, J., 1952, *Proc. Phys. Soc.* A, **65**, 449.

A Note on Time Reversal in Polarized Nuclear Processes

It has been demonstrated by various authors (e.g. Wolfenstein 1949, Blin-Stoyle 1951) that in a nuclear process in which the bombarding particles (spin $\frac{1}{2}$) are polarized, the angular distribution of the outgoing particles in the centre of mass coordinate system has the form

$$\mathfrak{I}(\theta)=I(\theta)[1+\mathbf{n}\,.\,\mathbf{P}_{\mathrm{i}}f(\theta)], \qquad \ldots\ldots (1)$$

where $\mathbf{n}$ is a unit vector normal to the plane of the process and $I(\theta)$ is the angular distribution obtained when the polarization $\mathbf{P}_{\mathrm{i}}$ is zero.

Conversely, if a nuclear process in which the initial particles are unpolarized results in outgoing polarized particles of spin $\frac{1}{2}$, their polarization $\mathbf{P}_0$ has the form $\mathbf{P}_0=\mathbf{n}g(\theta)$.

In a recent paper (Dalitz 1952) the particular case of elastic nucleon–nucleon scattering is considered and it is shown that provided the Hamiltonian is invariant under rotation and reflection of the coordinate system and time reversal, then $f(\theta)=g(\theta)$.

It is the object of the present note to show that this result is a particular case of a more general theorem. We shall, in fact, prove for the inverse nuclear processes

$$\mathrm{A}+\mathrm{P}\rightarrow\mathrm{B}+\mathrm{Q}\text{ (denoted by I) and }\mathrm{B}+\mathrm{Q}\rightarrow\mathrm{A}+\mathrm{P}\text{ (denoted by II)}$$

in which the particles P have spin $\frac{1}{2}$ and are polarized, that

$$f_{\mathrm{I}}(\theta)=g_{\mathrm{II}}(\theta). \qquad \ldots\ldots (2)$$

(Elastic scattering is implied, of course, when A and P are identical with B and Q respectively.)

Referring to a previous paper (Blin-Stoyle 1951) it can be seen by slight rearrangement of the results given there, that $f_{\mathrm{I}}(\theta)$ and $g_{\mathrm{II}}(\theta)$ are given by the expressions

$$\sum_{abpq}\Big|\sum_{Ll}(-1)^L S^{apLM}_{bql0}(\mathrm{I})\,Y^M_L(\theta)\Big|^2 f_{\mathrm{I}}(\theta)=2i\sum_{abq}\Big\{\sum_{Ll}(-1)^L S^{a\frac{1}{2}LM}_{bql0}(\mathrm{I})\,Y^M_L(\theta)\Big\}^*\times\Big\{\sum_{Ll}(-1)^L S^{a-\frac{1}{2}LM'}_{bql0}(\mathrm{I})\,Y^{M'}_L(\theta)\Big\} \qquad \ldots\ldots (3)$$

and

$$\sum_{abpq}\Big|\sum_{Ll}(-1)^l S^{bql0}_{apLM}(\mathrm{II})\,Y^M_L(\theta)\Big|^2 g_{\mathrm{II}}(\theta)=2i\sum_{abq}\Big\{\sum_{Ll}(-1)^l S^{bql0}_{a\frac{1}{2}LM}(\mathrm{II})\,Y^M_L(\theta)\Big\}^*\times\Big\{\sum_{Ll}(-1)^l S^{bql0}_{a-\frac{1}{2}LM'}(\mathrm{II})\,Y^{M'}_L(\theta)\Big\}, \qquad \ldots\ldots (4)$$

where the scattering matrix $S^{apLM}_{bqlm}(\mathrm{I})$ (cf. Wigner and Eisenbud 1947) is related to the function $F^{apLM}_{bqlm}(\mathrm{I})$ defined in the above paper by

$$S^{apLM}_{bqlm}(\mathrm{I})=i^{-L}(2l+1)^{1/2}F^{apLM}_{bqlm}(\mathrm{I})\delta_{a+p+M,\,b+q+m} \qquad \ldots\ldots (5)$$

with an analogous relation for $S^{bqlm}_{apLM}(\mathrm{II})$.

a, p, b and q refer to the z-components of the spins of A, P, B and Q, and L. M and l, m are the orbital angular momentum quantum numbers representing the relative motions of A, P and B, Q respectively. The factor $\delta_{a+p+M,\,b+q+m}$ implies the conservation of the z-component of angular momentum and removes the necessity of summing over M and M' in (3) and (4).

It is also demonstrated in an appendix to the above paper that

$$F^{ap\,LM}_{bq\,lm}(\mathrm{I}) = \pm F^{-a-p\,L-M}_{-b-q\,l-m}(\mathrm{I}) \qquad \ldots\ldots (6)$$

only one of the signs holding for a given process.

Now, if the Hamiltonian is invariant under reflection of coordinate axes and time reversal, it can be shown (e.g. Coester 1951) that

$$S^{bqlm}_{apLM}(\mathrm{II}) = \pm S^{-a-p\,L-M}_{-b-q\,l-m}(\mathrm{I}) = \pm S^{apLM}_{bqlm}(\mathrm{I})$$

by (5) and (6), the relevant sign being determined by the process under consideration.

It therefore follows at once from (3) and (4) and the fact that $L+l$ is always even or always odd for a given process, that the equality (2) is true provided the Hamiltonian possesses the invariance properties listed.

I am indebted to Professor Pryce for informing me that the foregoing theorem is an example of a more general relation which can be shown to hold between inverse physical processes.

The Clarendon Laboratory,
Oxford.
19th March 1952.

R. J. Blin-Stoyle.

Blin-Stoyle, R. J., 1951, *Proc. Phys. Soc.* A, **64**, 700.
Coester, F., 1951, *Phys. Rev.*, **84**, 1259.
Dalitz, R. H., 1952, *Proc. Phys. Soc.* A, **65**, 175.
Wigner, E. P., and Eisenbud, L., 1947, *Phys. Rev.*, **72**, 29.
Wolfenstein, L., 1949, *Phys. Rev.*, **75**, 1664.

Neutron Flux and Spectrum Measurement

The measurement of a neutron spectrum by observing the recoil protons produced in a hydrogenous medium is usually subject to two difficulties. If the energy spectrum of all the protons produced in an ion chamber containing hydrogen is to be measured, the dimensions of the chamber must be large compared to the range of a recoil proton. For protons of more than a few hundred kilovolts energy this requires either a very high pressure filling or a very large chamber. If, alternatively, the proton recoils from a thin hydrogen-containing film are observed, then, although the chamber dimensions may be reduced to one proton range, the number of recoils from a thin film is inconveniently small.

An attempt to overcome the first difficulty is described here, in which a scintillating anthracene crystal is used instead of an ion chamber. A crystal of quite small size (~ 5 mm side) will fulfil the condition as to proton range, and, provided the relation between light output and proton energy is known, it should be possible to determine the energy spectrum of proton recoils in such a crystal. Scintillations from the recoiling carbon atoms are negligibly small since not only is their energy lower, but also the light output per Mev dissipated in the crystal is much less. The relation between light output and proton energy has been calculated by Birks (1951) in terms of the energy–range relation for protons, and is given as

$$\frac{dS}{dE} = \frac{A}{1+B\,dE/dx}, \qquad \ldots\ldots (1)$$

where S represents light output, A and B are constants, and dE/dx is the rate of energy loss of a proton in anthracene.

Anthracene was chosen for this work because of its high luminous efficiency, which is important since the statistical spread in the number of electrons released at the photocathode must be kept as low as possible to give the best energy resolution. Unfortunately, the use of an organic scintillator gives the counter a disproportionately high sensitivity to γ-radiation, and its use is limited to measurements in the absence of γ-radiation, or where the γ-radiation effect may be subtracted by means of a 'background' run.

A counter consisting of a clear piece of anthracene, weighing 0·433 g, cemented to the window of an E.M.I. photomultiplier type VX 5045 was exposed to 2·54 Mev neutrons

emitted from the D–D reaction at 90° to the beam, and a pulse height distribution was taken with a 30-channel pulse analyser (fig. 1). Using eqn. (1), this distribution was transformed to the energy spectrum of the recoil protons to give fig. 2. On the same figure is plotted the neutron spectrum $N(E)$ derived from

$$N(E) \propto \frac{E}{\sigma(E)} \frac{d}{dE} \{N'(E)\}. \qquad \ldots\ldots (2)$$

$N'(E)$ is the distribution of proton energies, and $\gamma(E)$ is the n–p scattering cross section.

To test the counter further it was used for an absolute measurement of the flux from the D–D source, under conditions for which this flux was known. To this end the counter

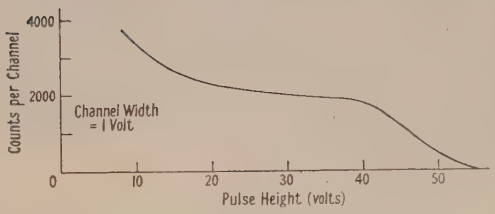

Fig. 1.

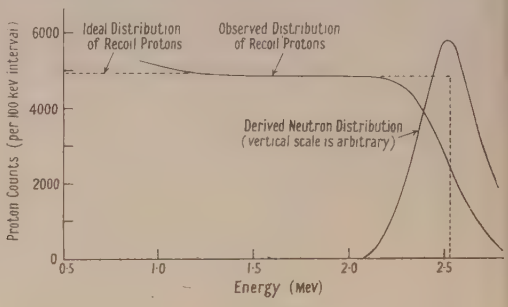

Fig. 2.

and an Ilford type C2 nuclear plate were simultaneously exposed at equal distances from the source, and the number of pulses above 27·5 volts amplitude was counted. From this, and from eqn. (1), the total number of proton recoils was calculated, and so the number of neutrons falling on the crystal. This figure was compared with that obtained from examination of the plate, and the results are: crystal $8{\cdot}7(\pm 0{\cdot}2)\times 10^7$ neutrons/cm², plate $8{\cdot}0(\pm 0{\cdot}5)\times 10^7$ neutrons/cm².

Atomic Energy Research Establishment, M. J. Poole.
Harwell, Berks.
7th March 1952.

Birks, J. B., 1951, *Proc. Phys. Soc.* A, **64**, 10.

The Range–Energy Relation for Protons in Aluminium

No experimental determinations of the stopping power of aluminium for protons in the energy range from 5 to 10 Mev appear to have been reported. To fill this gap, Ilford C2 nuclear emulsions have been used to measure the energy loss of initially 10 Mev protons in traversing a thickness of aluminium which reduces their energy to about 3 Mev.

The source of protons was the extracted beam of the Birmingham 60 in. cyclotron, operated with no ion-source arc to give a suitably low intensity. The plates were tilted slightly from the horizontal so that the protons entered the emulsion at a small glancing angle. Part of the beam struck the plate after passing through a sheet of aluminium mounted just before the plate with its plane vertical: part of the beam passed below the aluminium and struck the plate directly. The difference in height of the two beams is only about a millimetre, and is in the vertical direction in which the beam energy is known not to vary greatly.

The table shows the results of six determinations, including measurements made with four different plates and three different absorbers. 20 to 30 tracks were measured at each range, the mean range being thus determined within $2\,\mu$. In this table, U refers to the unstopped beam, S to the beam which has traversed the aluminium absorber. Columns 4 and 5 are obtained by converting ranges in the emulsion into proton energies by means of the range–energy relation for C2 emulsions given by Rotblat (1951), and then converting these energies into ranges in aluminium by means of the range–energy relation calculated by Smith

(1947). Column 6, which is the difference between columns 4 and 5, is the thickness of aluminium which the beam would have traversed if Smith's range–energy relation had been accurate. Column 7 gives the actual thickness of aluminium traversed.

Column 8 lists, as a percentage of the absorber thickness, the difference between the known thickness of aluminium and that predicted from Smith's range–energy relation. The errors quoted are probable errors calculated from the spread of the measured track lengths in the emulsion, and do not include the uncertainty in the range–energy relation for the emulsion.

In all cases, Smith's figures predict too low a value for the thickness of aluminium. In column 8, the agreement between the average for plate 1, $(1{\cdot}0\pm0{\cdot}2)\%$, and the average for the other three plates, $(0{\cdot}6\pm0{\cdot}2)\%$, suggests that there is no serious systematic difference between plates. The final average of column 8 suggests that Smith's range figures are too low by $(0{\cdot}8\pm0{\cdot}14)\%$; when the $\frac{1}{2}\%$ uncertainty in Rotblat's range–energy relation is included, the error in Smith's ranges becomes $(0{\cdot}8\pm0{\cdot}5)\%$. This correction applies essentially to the range at 10 MeV, since the range of the stopped beam is so much smaller than that of the unstopped beam.

The stopping power of a substance for heavy particles may be written (Smith 1947)

$$-\frac{dE}{dx}=\frac{4\pi e^4z^2}{Mv^2}NZ\log\frac{2mv^2}{I}, \qquad \ldots\ldots (1)$$

where $-dE/dx$ is the rate of energy loss of the particle, ez the charge of the particle, v the velocity of the particle, Z the atomic number of the stopping substance, N the number of

1	2	3	4	5	6	7	8
Plate	Range in Emulsion (μ)		Range in Al (mg/cm^2)		Thickness of Al traversed (mg/cm^2)		$\frac{\text{Measured}-\text{Smith}}{\text{Measured}}$ (%)
	U	S	U	S	Smith	Measured	
1	498·9	41·6	151·2	11·4	139·8	141·2	$1{\cdot}0\pm0{\cdot}4$
1	492·6	38·2	149·4	10·5	138·9	141·2	$1{\cdot}6\pm0{\cdot}4$
1	490·8	30·0	148·6	8·0	140·6	141·2	$0{\cdot}4\pm0{\cdot}2$
2	512·9	55·0	155·6	15·2	140·4	140·6	$0{\cdot}2\pm0{\cdot}4$
3	513·2	91·4	155·7	25·8	129·9	131·3	$1{\cdot}1\pm0{\cdot}4$
4	524·2	70·1	159·4	19·6	139·8	140·6	$0{\cdot}6\pm0{\cdot}2$

stopping atoms per unit volume, I the average excitation potential of the electrons of the stopping substance; e, m are the charge and mass of the electron. Ranges are obtained from (1) by numerical integration of the expression

$$R=\int_0^E\frac{dE}{-dE/dx}. \qquad \ldots\ldots (2)$$

The parameter I cannot be calculated accurately and the value of 150 ev used by Smith is an empirical one (Wilson 1941) on which the probable error is more than large enough to account for a 1% range error at 10 MeV. If the error in Smith's ranges is assumed to be due entirely to an error in I, then it may be shown that the percentage range error should vary little over the range of proton energies from 10 to 80 MeV.

Bloembergen and van Heerden (1951) have measured the ranges of fast protons in aluminium, and have found, also, that Smith's ranges are too low. The corrections they find are $(0{\cdot}9\pm0{\cdot}4)\%$ between 56 and 76 MeV, $(1{\cdot}4\pm0{\cdot}9)\%$ between 35 and 52 MeV. These results, and that quoted above for 10 MeV protons, are consistent with the assumption that the error in Smith's ranges is due entirely to an error in his value of I.

From eqns. (1) and (2) it may be shown that

$$\frac{\Delta R}{R}=\left(2+\frac{E}{R\,dE/dx}\right)\frac{\Delta I}{I}, \qquad \ldots\ldots (3)$$

where ΔR is the error in range caused by an error ΔI in I. The present experiment implies a value $I=155\pm3$ ev, and is to be compared with 159 ± 5 ev found by Bloembergen and van Heerden at energies between 35 and 76 MeV, and with 156 ± 3 ev deduced from Sachs and Richardson's (1951) direct measurement of the stopping power of aluminium for 18 MeV protons. The three experimental values are in good agreement, and yield a mean value

$I = 156 \pm 2$ ev. This figure has been used in conjunction with eqn. (3) to prepare the curve, which gives the percentage correction which should be added to Smith's tabulated ranges from 2 to 80 MEV. The range–energy relation corrected in this way is unlikely to be in error by more than $\frac{1}{2}\%$.

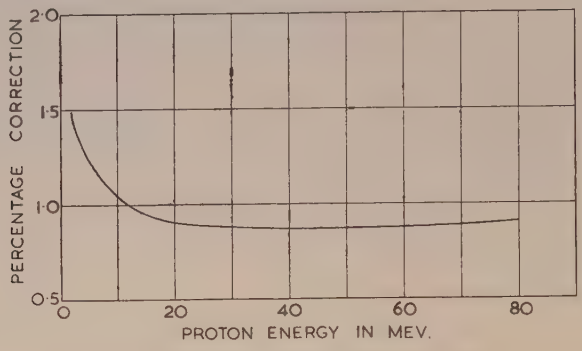

Percentage correction to be added to the proton ranges in aluminium tabulated by Smith (1947).

The author's thanks are gratefully offered to Dr. J. Fremlin for helpful discussion, to Mrs. E. Munday for her aid in processing plates and measuring track lengths, to Mr. W. Hardy who operated the cyclotron, and to the University of South Africa for the award of a scholarship.

Department of Physics,
University of Birmingham.
18th January 1952.

D. H. SIMMONS.

BLOEMBERGEN, N., and VAN HEERDEN, P. J., 1951, *Phys. Rev.*, **83**, 561.
ROTBLAT, J., 1951, *Nature, Lond.*, **167**, 550.
SACHS, D. C., and RICHARDSON, J. R., 1951, *Phys. Rev.*, **83**, 834.
SMITH, J., 1947, *Phys. Rev.*, **71**, 32.
WILSON, R. R., 1941, *Phys. Rev.*, **60**, 749.

The Response of a NaI Scintillation Counter to Slow and Fast Neutrons

The fluorescence of NaI(Tl) crystals under charged particle and γ-ray excitation has been described by Hofstadter (1950) and others. We have used a neutron source, free from γ-ray background, to determine its response to slow and fast neutrons with a view to using it to investigate the inelastic scattering of fast neutrons.

An E.M.I. photomultiplier fitted with a crystal of NaI(Tl) ($13 \times 10 \times 8$ mm) was mounted close to the target of a D+D neutron source operated with a 40 μA resolved beam of 190 kev deuterons; the target was formed by the occlusion of deuterium in an aluminium sheet 0·3 mm thick which gives rise to a negligible γ-ray background (Beghian *et al.* 1950). Slow neutrons were produced in a tank of water surrounding the target, whereas for measurements with fast neutrons the crystal was placed in contact with the target.

The γ-rays produced by the capture of slow neutrons in iodine gave a continuous pulse height distribution extending up to about 6·2 MEV. This limit probably corresponds to a γ-ray of 7·2 MEV detected by pair production in the crystal (cf. 7·0 MEV, Kubitschek and Dancoff 1949). No distinctive peaks can be identified in the spectrum although a steep rise in the vicinity of 2·2 MEV can probably be attributed to neutron capture radiation by the hydrogenous moderator. Intense 478 kev γ-radiation arising from $^{10}B(n, \alpha)^{7}Li^{*}$ in the glass of the phototube was minimized by mounting the scintillation crystal on a ' Perspex ' pillar. The efficiency of the crystal for the detection of γ-rays arising within it was estimated from the photoelectric, Compton and pair production cross sections, and this was used to assess the number of quanta originating in the capture process; the number

of capture processes was determined from the β radioactivity (^{128}I) in the crystal. In this way the number of γ-rays with energy greater than 3 MeV was found to be of the order of 1 quantum per neutron captured.

The pulse height distribution due to fast neutrons cuts off at about 2·5 MeV. We attribute it to γ-rays due to inelastic scattering. At 450 kev there is indication of a complex photoelectric line which must be attributed to a number of γ-rays of closely similar energy : although recoiling sodium nuclei resulting from direct collisions with neutrons have a continuous spectrum with a maximum energy of 450 kev, it does not seem possible that they could account for a peak.

A chromium disc (2 cm diameter $\times$ 0·4 cm thick) was then mounted in contact with the target and the pulse height spectrum due to γ-rays from inelastic scattering of the neutrons in the chromium was obtained : the difference counting rate with and without the scatterer is shown in the figure. Although the background due to primary fast neutrons is large, there is a good indication of a γ-ray at 1·4 MeV in agreement with earlier measurements (Grace *et al.* 1951). No lower energy γ-ray is detectable above 250 kev. A rise in the Compton distribution at low energies is seen which is probably due to degradation of radiation in the chromium and to the detection of neutrons which have suffered inelastic scattering. The geometrical arrangement was such that the presence of the chromium scatterer did not interfere with the direct neutron beam from the target to the crystal.

The cross section for this process was estimated to be $1{\cdot}5 \times 10^{-24}$ cm^2, in fair agreement with an earlier figure (Grace *et al.* 1951) of $1{\cdot}2 \pm 0{\cdot}4 \times 10^{-24}$ cm^2.

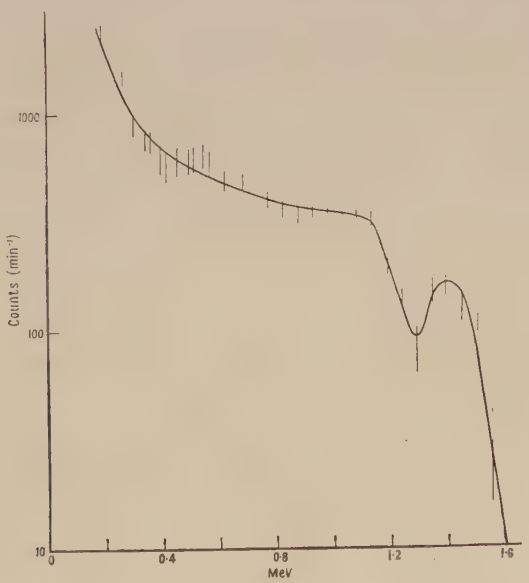

Pulse height distribution due to γ-rays from chromium excited by fast neutrons.

This method of investigating inelastic scattering seems to be limited to nuclei with well-spaced levels and large cross sections. It is hoped that with the use of a collimated fast neutron beam the method may be made more sensitive.

We are greatly indebted to Dr. F. V. Price for putting the facilities of the high voltage set at our disposal.

The Clarendon Laboratory,
Oxford.
26th March 1952.

M. A. Grace.
H. R. Lemmer.
H. Halban.

Beghian, L. E., Grace, M. A., Preston, G., and Halban, H., 1950, *Phys. Rev.*, **77**, 286.
Grace, M. A., Beghian, L. E., Preston, G., and Halban, H., 1951, *Phys. Rev.*, **82**, 969.
Hofstadter, R., 1950, *Phys. Rev.*, **80**, 631.
Kubitschek, H. E., and Dancoff, S. M., 1949, *Phys. Rev.*, **76**, 531.

The Kinetic Formulation of Conduction Problems

Problems in electrical conduction are usually formulated by means of the Boltzmann equation. An alternative formulation, using an integrated form of the Boltzmann equation derived by simple kinetic theory arguments, has proved useful in solving certain 'thin-conductor' problems (Chambers 1950, 1951). Recently Huxley (1951) has given a lengthy 'free path' formulation, in which the current density is found by first finding the position of the centroid of a group of electrons and then taking its time derivative. His final equations are exceedingly complicated. It seems worth while to point out, therefore, that a much simpler and more general formulation may be obtained by calculating the current density $\mathbf{I}$ directly on a kinetic theory basis.

Consider a volume element $d\mathbf{r}=dx\,dy\,dz$ at point $\mathbf{r}_0$ in the conductor, and electrons passing through it with energy E and velocities in the range $d\mathbf{v}=dv_x\,dv_y\,dv_z$ about $\mathbf{v}_0$, or with wave numbers in the range $d\mathbf{k}$ about $\mathbf{k}_0$. For free electrons, $\hbar\mathbf{k}=m\mathbf{v}$; for electrons in an ionic lattice $\mathbf{v}=(1/\hbar)\,\mathrm{grad}_{\mathbf{k}}\,E$. Let f_0 be the unperturbed electron distribution function (so that $f_0\,d\mathbf{r}\,d\mathbf{k}/4\pi^3$ is the number of electrons in $d\mathbf{r}$, $d\mathbf{k}$), f the perturbed value in the presence of applied fields, and $\delta f=f-f_0$. Let the relaxation time for electron collisions be τ, and assume that the distribution function of electrons immediately after collision corresponds to $\delta f=0$. Now electrons passing through $\mathbf{r}_0$ with velocity $\mathbf{v}_0$ and energy E at time t_0 will have followed a certain trajectory since their last collision; the value of $f(\mathbf{r}_0,\,\mathbf{v}_0,\,t_0)$ is found simply by integrating the number scattered into the trajectory at previous points along it with energy $E-\Delta E$ (where ΔE is the energy then acquired from the applied fields before reaching $\mathbf{r}_0$), weighted by their probability of reaching $\mathbf{r}_0$:

$$f(\mathbf{r}_0,\,\mathbf{v}_0,\,t_0)=\int_{-\infty}^{t_0}(dt/\tau)f_0(E-\Delta E)\exp\{-(t_0-t)/\tau\}\,.$$

Hence, on writing $f_0(E-\Delta E)=f_0(E)-\Delta E\,df_0/dE$ and integrating by parts, we obtain

$$\begin{aligned}\delta f(\mathbf{r}_0,\mathbf{v}_0,t_0)&=-(df_0/dE)\int_{-\infty}^{t_0}(dt/\tau)\,\Delta E\exp\{-(t_0-t)/\tau\}\\&=(df_0/dE)\int_{-\infty}^{t_0}dt\,(d\,\Delta E/dt)\exp\{-(t_0-t)/\tau\}.\end{aligned}$$

Now $\Delta E(t)=-e\int_t^{t_0}\mathbf{E}(\mathbf{r},s)\,.\,\mathbf{v}(s)\,ds$ where $\mathbf{E}\,(\mathbf{r},\,t)$ is the applied electric field (magnetic fields, if present, have no direct effect on ΔE, but alter $\mathbf{v}(t)$) and $d\,\Delta E/dt=e\mathbf{E}(\mathbf{r},\,t)\,.\,\mathbf{v}(t)$; further,

$$\mathbf{I}=-\frac{e}{4\pi^3}\int_{\text{all }\mathbf{k}}\mathbf{v}\,\delta f\,d\mathbf{k}\,,$$

and lastly, if $\tau=\tau(\mathbf{v})=\tau(t)$, $\exp\{-(t_0-t)/\tau\}$ must be replaced by $\exp\{-\int_t^{t_0}ds/\tau(s)\}$, so that finally we obtain

$$\mathbf{I}(\mathbf{r}_0,\,t_0)=-\frac{e^2}{4\pi^3}\int_{\text{all }\mathbf{k}}\mathbf{v}\frac{df_0}{dE}d\mathbf{k}\int_{-\infty}^{t_0}dt\;\mathbf{E}(\mathbf{r},\,t)\,.\,\mathbf{v}(t)\exp\{-\int_t^{t_0}ds/\tau(s)\},\qquad\ldots\ldots(1)$$

which is the general solution of the Boltzmann equation for any isothermal conductor in stationary or varying, uniform or non-uniform fields $\mathbf{E}$ and $\mathbf{H}$, provided that the conductor is of dimensions large compared with the mean free path $l=\tau|\mathbf{v}|=\tau v$, and that the charge distribution is uniform, i.e. that $\int\delta f\,d\mathbf{k}=0$. If $\int\delta f\,d\mathbf{k}\neq0$, a simple 'diffusion' term appears; and for a general formulation of 'thin conductor' problems the equation needs only slight modification (cf. Chambers 1950, 1951). More important, since eqn. (1) can be applied to electrons in an ionic lattice, where $\mathbf{v}=(1/\hbar)\,\mathrm{grad}_{\mathbf{k}}\,E$, it can be used (Shockley 1950) to elucidate the difficult problem of magneto-resistance effects in metals.

For free electrons, assuming $\tau=\tau(v)$ only (whether in a metal, semiconductor, or ionized gas), eqn. (1) gives, for $\mathbf{H}=0$ and $\mathbf{E}$ uniform,

$$\mathbf{I}(t_0)=-\frac{8\pi e^2m^2}{3h^3}\int_0^\infty v^3\frac{df_0}{dv}\,dv\int_{-\infty}^{t_0}dt\;\mathbf{E}(t)\exp\{-(t_0-t)/\tau\}.\qquad\ldots\ldots(2)$$

Huxley's equations (1), (38), and (41), for the special case $l=\tau v=$constant, yield (2) after sufficient integration and rearrangement. For $\mathbf{H}=H_z$ (uniform and constant) (1) becomes

$$(I_x+iI_y),\ I_z=$$
$$-\frac{8\pi e^2m^2}{3h^3}\int_0^\infty v^3\frac{df_0}{dv}dv\int_{-\infty}^{t_0}dt[(E_x(t)+iE_y(t))\exp i\omega(t_0-t),\ E_z(t)]\exp\{-(t_0-t)/\tau\} \quad \ldots\ldots (3)$$

where $\omega=-eH_z/mc$. This relatively simple expression replaces and generalizes Huxley's equations (1) to (5) and (38).

Royal Society Mond Laboratory,
Cambridge.
20th March 1952.

R. G. Chambers.

Chambers, R. G., 1950, *Proc. Roy. Soc.* A, **202**, 378; 1951, *Thesis*, University of Cambridge.
Huxley, L. G. H., 1951, *Proc. Phys. Soc.* B, **64**, 844.
Shockley, W., 1950, *Phys. Rev.*, **79**, 191.

A Combinatorial Problem in Electron–Photon Cascade Theory

In electron–photon cascade theory in approximation A the following problem arises: to find the number of different cascades in which one primary electron or photon gives rise to given numbers of electrons and photons, the cascades being distinguished only by the order in which the bremsstrahlungs and pair productions occur. A somewhat similar combinatorial problem in counting cosmic rays has been considered by Schrödinger (1951).

Suppose that a primary j gives rise to $2n+j$ electrons and m photons; for a primary electron ($j=1$) the number of electrons must be odd and for a primary photon ($j=2$) the number even. The numbers of electrons and photons before the last collision are $2n+j$ and $m-1$ if this collision is a bremsstrahlung and $2(n-1)+j$ and $m+1$ if the collision is a pair production. Hence, if $N(n, m)$ is the number of possible cascades,

$$N(n, m)=N(n, m-1)+N(n-1, m+1). \quad \ldots\ldots (1)$$

The solution of this difference equation is

$$N(n, m)=\frac{m+1}{n+m+1}\cdot\frac{(2n+m)!}{n!\,(n+m)!}, \quad \ldots\ldots (2)$$

satisfying the obvious initial condition $N(0,0)=1$. The values of $N(n, m)$ for small values of n, m are given in the table. Each entry in the table is found by adding to the number on the left the number on the right of the one above. The value of N increases rapidly with increasing n and m; the number of different possible cascades in which a primary photon gives rise to 20 electrons and 20 photons exceeds 10^8.

n \ m	0	1	2	3	4
0	1	1	1	1	1
1	1	2	3	4	5
2	2	5	9	14	20
3	5	14	28	48	75
4	14	42	90	165	275

The cascades may be represented by the different ways of ordering $m+n$ 1's and n 2's such that from the left there are never more 2's than 1's. A 1 stands for a bremsstrahlung, a 2 for a pair production, and the orderings represent all collisions if the primary is an electron and all except the first (which must be a pair production) if the primary is a photon.

For example, if a primary electron gives rise to five electrons and one photon, $n=2$, $m=1$, and the different possible cascades (five in number) are represented by

11122, 11212, 11221, 12112, 12121. These orderings also represent the cascades in which a primary photon gives rise to six electrons and one photon. The ordering 12121, for example, represents the cascades given in the figure.

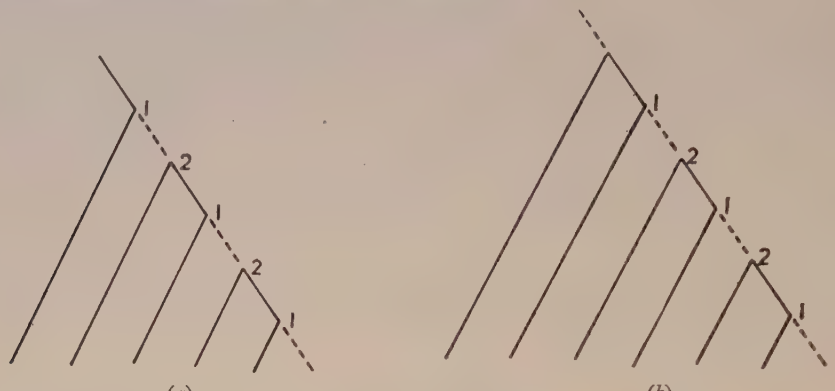

The cascade 12121.
(*a*) Primary electron giving five electrons, one photon.
(*b*) Primary photon giving six electrons, one photon.

The author wishes to thank Dr. H. Messel and Mr. G. Szekeres for helpful discussions.

Department of Mathematics,
The University of Adelaide,
South Australia.
13th February 1952.

R. B. Potts.

Schrödinger, E., 1951, *Proc. Phys. Soc.* A, **64**, 1040.

The Parameters of Partially Degenerate Semiconductors

In semiconductor problems, the concept of the Fermi level is of considerable importance, and some interest attaches to methods for its evaluation. For this purpose, consider a simple n-type semiconductor, with an impurity concentration of N_d donor centres per unit volume, each having an energy $-\epsilon_d$ with respect to the bottom of the conduction band. Then the free electron concentration n_e and the Fermi level ϵ^* can be determined from

$$n_e = n_0(m_e/m)^{3/2} F_{1/2}(\eta^*) \quad \ldots\ldots (1)$$

and

$$n_e = N_d[(1+\exp(\eta^*+\eta_d)]^{-1}, \quad \ldots\ldots (2)$$

where

$$\eta^* = \epsilon^*/kT, \quad \eta_d = \epsilon_d/kT, \quad n_0 = 4\pi(2mkT/h^2)^{3/2}$$

and

$$F_{1/2}(\eta^*) = \int_0^\infty \frac{\eta^{1/2}\, d\eta}{1+\exp(\eta-\eta^*)}. \quad \ldots\ldots (3)$$

Methods of solving these equations have been developed by Shifrin (1944) and Putley (1949) amongst others and are discussed in detail elsewhere by the present author (Blakemore 1952).

The Fermi–Dirac integral $F_{1/2}(\eta^*)$, which enters into the calculation has been accurately tabulated for $\eta^* = -4(0{\cdot}1)20$ by McDougall and Stoner (1938). For the evaluation of semiconductor parameters, however, it is often useful to have simple analytical expressions for this integral.

In cases of strong degeneracy, a good approximation is

$$F_{1/2}(\eta^*) \simeq \tfrac{2}{3}\,\eta^{*3/2}\,[1+\pi^2/8\eta^{*2}] \quad \ldots\ldots (4)$$

which is satisfactory to within a few per cent for η^* greater than $1{\cdot}5$. The range of application can be extended downwards by observing that (4) is identical with the first two terms of the expansion

$$F_{1/2}(\eta^*) \simeq \tfrac{2}{3}\,[\eta^{*2}+\pi^2/6]^{3/4} \quad \ldots\ldots (5)$$

which has an error of less than 3% for η^* greater than 0·8, as shown by curve *b* in figs. 1 and 2.

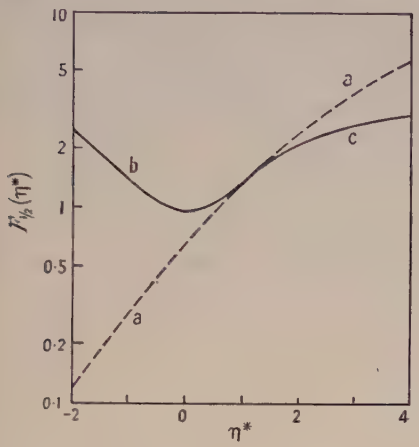

Fig. 1. The Fermi–Dirac integral, $F_{1/2}(\eta^*)$, [curve *a*], together with the approximations *b* of eqn. (5), and *c* of eqn. (6).

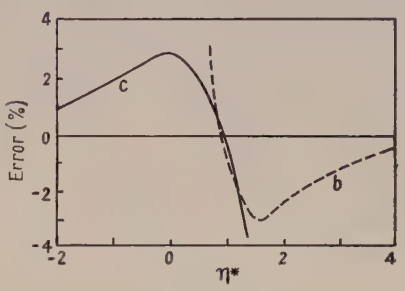

Fig. 2. Errors introduced by the approximations given in the curves *b* and *c* of fig. 1.

For semiconductors which are slightly degenerate, modifications of the classical approximation $F_{1/2}(\eta^*) \simeq \frac{1}{2}\pi^{1/2} \exp(\eta^*)$ which applies for large negative values of η^*, have been proposed by Ehrenberg (1950), and by Landsberg, Mackay and McRonald (1951). Both of the suggested modifications are of the form

$$F_{1/2}(\eta^*) \simeq \tfrac{1}{2}\pi^{1/2}[\phi + \exp(-\eta^*)]^{-1},$$

where Ehrenberg suggests $\phi = 0{\cdot}25$, and Landsberg *et al.*, $\phi = 2^{-3/2}$. The latter authors point out that different values of ϕ are useful for various small ranges of η^*. By the substitution $\phi = 0{\cdot}27$, it can be seen from curve *c* in figs. 1 and 2 that the function can be represented for all negative values of η^*, and for positive values up to 1·25, with an error of less than 3%,

The use of $F_{1/2}(\eta^*) \simeq \frac{1}{2}\pi^{1/2}[0{\cdot}27 + \exp(-\eta^*)]^{-1}$ in conjunction with (5), enables $F_{1/2}(\eta^*)$ to be covered over the complete range of η^*. A convenient point at which to change over from one expression to the other is at $\eta^* = +1$.

Standard Telecommunication Laboratories Ltd.,
Enfield, Middlesex.
27th March 1952.

J. S. Blakemore.

Blakemore, J. S., 1952, *Electrical Communication*, in the press.
Ehrenberg, W., 1950, *Proc. Phys. Soc.* A, **63**, 75.
Landsberg, P. T., Mackay, R., and McRonald, A., 1951, *Proc. Phys. Soc.* A, **64**, 476.
McDougall, J., and Stoner, E. C., 1938, *Phil. Trans. Roy. Soc.* A, **237**, 67.
Putley, E. H., 1949, *Proc. Phys. Soc.* A, **62**, 284.
Shifrin, K., 1944, *J. Phys. U.S.S.R.*, **8**, 242.

Schumann Region Absorption Spectrum of Copper Vapour

Amongst atomic spectra, that of Cu I has occupied a special place in presenting an abundance of peculiarities arising from series perturbation and auto-ionization. The spectrum has been extensively studied, notably by Shenstone, who has summarized existing knowledge of it (1948). Included in Shenstone's term lists are a number of tentative assignments to the configuration $3d^9 4s5p$. These assignments were made from measurements of a number of emission lines lying in the 1570–1750 Å range, classified as combinations with the $3d^9 4s^2\ ^2D$ metastable term. The only other allowed combinations of the $3d^9 4s5p$ levels are with the ground state, and are thus expected to lie in the short wavelength part of the Schumann region.

Partly in view of the tentative nature of Shenstone's assignments, partly in the hope of observing combinations of the ground term with levels of $3d^9 4s6p$, the absorption spectrum of copper vapour has been photographed over the range 1060–2500 Å. The copper vapour was produced in the usual way in a King furnace (Garton 1952), and the hydrogen spectrum and the Lyman continuum were used as backgrounds. The plates reveal a set of fifteen new lines in the range 1200–1430 Å, of which the strongest are a group of six between 1370 and 1420 Å, and six between 1220 and 1300 Å.

Initial studies of these plates indicate that the following of Shenstone's levels are real and combine with the ground state: $x^4P_{3/2}$, $x^4P_{1/2}$, $w^2P_{3/2}$. Three of the new absorption lines are thus accounted for by upper levels already known. The shorter wavelength lines no doubt involve upper levels arising from $3d^9 4s6p$ and $3d^9 4s4f$.

Full details of the spectra, measurements and classifications will be given later.

Department of Physics,
Imperial College, London.
17th April 1952.

W. R. S. Garton.

Garton, W. R. S., 1952, *Proc. Phys. Soc.* A, **65**, 268.
Shenstone, A. G., 1948, *Phil. Trans. Roy. Soc.* A, **241**, 297.

CONTENTS FOR SECTION B

ABSTRACTS FOR SECTION B

Further Results in the General Theory of Barrier Layer Rectifiers, by P. T. LANDSBERG.

ABSTRACT. It is pointed out that the temperature variation $V_D = a - bT$ of the diffusion potential, as deduced from the forward characteristic of rectifiers, is in broad agreement with theory. Hence formulae are derived for the temperature variation of the zero resistance of a rectifier having an arbitrary distribution of impurity centres, and subject to either diode or diffusion theory. Interpretation of experiments with the aid of these formulae leads to the temperature dependence of (*a*) the effective mass of current carriers in germanium rectifiers, and (*b*) of the mobility of current carriers in selenium rectifiers. The latter curve has the same form as that obtained from Hall effect measurement, and it is pointed out that it is of broadly the same shape as the corresponding curves for high resistivity samples of silicon and germanium. It is shown that two d.c. characteristics of the same rectifier, but corresponding to different temperatures, can intersect. Formulae for the applied voltage and the temperature rise which lead to the onset of thermal instability are deduced for all impurity centre distributions, and for diode and diffusion theory. A general theory of current creep in rectifiers is outlined, and good agreement obtained with experiments on selenium rectifiers.

Breakdown in Selenium Rectifiers, by R. COOPER.

ABSTRACT. The paper describes an experimental investigation of breakdown in selenium rectifiers. Cooling from about 110°C to −74°C caused the breakdown voltage to decrease continuously, and at the same time anomalous behaviour was observed in the current–voltage characteristics. When high voltages were applied, the current decreased as the temperature increased, but at low voltages rise in temperature caused the current to increase.

The effect of changing the thermal dissipation constant was similar to that caused by a change in ambient temperature. Reduction in the dissipation constant, effected by placing the rectifier in a vacuum, was observed to *increase* the breakdown voltage, but the leakage current at low voltages also increased.

None of the available theories appears to account satisfactorily for the observations.

Characteristics of Scintillation Counters, by G. F. J. GARLICK and G. T. WRIGHT.

ABSTRACT. Experimental studies have been made of the distribution in size of output pulses from a scintillation counter detecting monoenergetic alpha-particles. Separate investigations have been made of contributions to the pulse size spread by the photomultiplier and by the scintillating crystal. It is shown that the main effect is due to statistical fluctuations in the number of photoelectrons produced at the photomultiplier cathode. The effect of the multiplying stages on these fluctuations is investigated and also the effect of flaws in the detecting crystal. The frequency distribution of the pulses is usually found to follow the gaussian form.

The Current in the Electron Immersion Objective, by L. JACOB.

ABSTRACT. It is shown that for an electron immersion objective under the condition of constant cut-off voltage the emission current is uniquely defined by the cross-over potential. There is thus some theoretical foundation for the empirically observed law, that the current at zero modulation voltage depends only on the three-halves power of the cut-off voltage.

An Improved Method for Measurements of Optical Constants by Reflection, by D. G. AVERY.

ABSTRACT. At wavelengths outside the photographic range the determination of the optical constants of absorbing media involves the measurement of intensity changes on reflection at the surface of the medium. A review of previous methods for their determination is made and the experimental difficulties are indicated. A method is described which surmounts some of these difficulties by avoiding the direct measurement of reflection coefficients. The accuracy to be expected from the method and an example of its use are briefly discussed.

Primary Aberrations and Conjugate Change, by C. G. WYNNE.

ABSTRACT. Expressions are derived, in terms of the functions normally used in optical designing, for the variation with conjugates of the primary aberrations of any symmetrical system with isotropic object and image spaces. The possibilities of invariance of the aberrations, or their simultaneous correction for more than one magnification, are discussed.

Propagation of Ultrasonic Waves in Vapours near the Critical Point, by H. D. PARBROOK and E. G. RICHARDSON.

ABSTRACT. An experimental study is made of the velocity and absorption of ultrasonic waves in carbon dioxide and ethylene at frequencies between $\frac{1}{2}$ and 2 Mc/s and at pressures up to 100 atmospheres in a variable-path acoustic interferometer. At pressures above 10 atmospheres the results are independent of frequency (in this range) in the gaseous phase. The velocity and absorption coefficient reach a minimum near the condensation point, but especially at the critical point itself have high and indeterminate values when the change of phase takes place. The ultrasonic viscosities calculated from these measurements are of the order of 1 000 times those derived from transpiration or low-frequency oscillation experiments.

The Influence of Electrolytes on the Mechanical Properties of Certain Metal Single Crystals, by E. N. DA C. ANDRADE and R. F. Y. RANDALL.

ABSTRACT. The contact of electrolytes has a marked effect on the mechanical behaviour of single crystals of cadmium and zinc which have been exposed to the air. This is due to the disruption, or formation, of a thin surface film, probably of oxide or hydroxide. If ordinary single crystal cadmium wires are loaded so as to flow very slowly, the contact of solutions containing free cadmium ions increases the rate of flow : a similar effect exists in the case of zinc treated with solutions of zinc salts. If the surface of the wire is cleaned by preliminary thermal evaporation there is no such effect, establishing that it is due to a surface film normally present. Solutions of cadmium or zinc nitrate stop the flow and raise the critical shear stress appreciably, which is attributed to the formation of a surface film, probably of hydroxide. With the cadmium nitrate there is a temporary increase of flow before the cessation, which is attributed to the cadmium ion, for there is no such effect with the zinc nitrate. With polycrystalline wires there is no electrolyte effect. The work described supports the view that a thin oxide or hydroxide film increases the mechanical resistance of single crystal wires, and that with cadmium and zinc wires such a film is normally present.

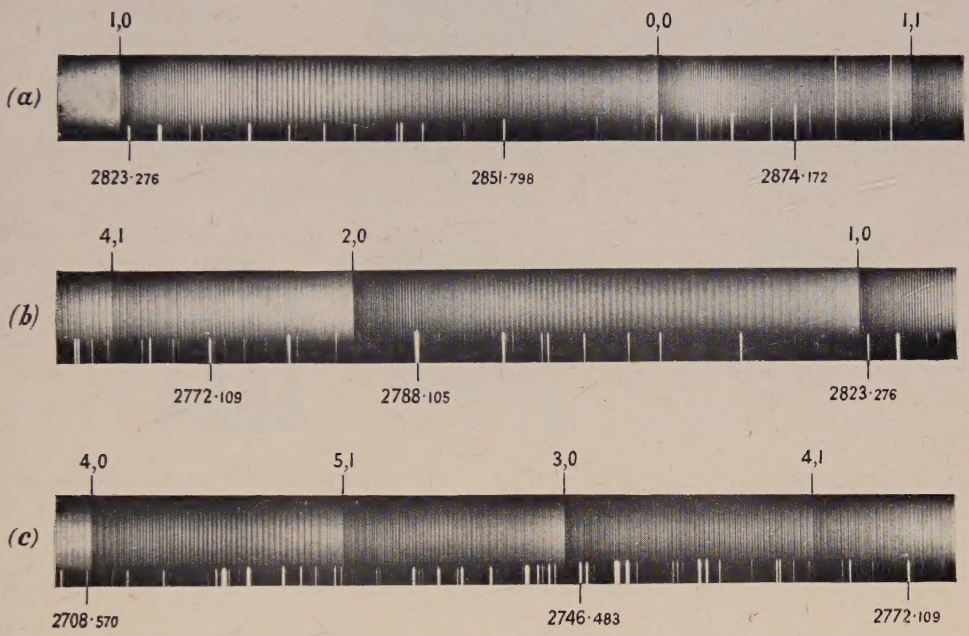

Fig. 1 (*a*), (*b*) and (*c*). Bands of the D–X system of SiS in absorption.

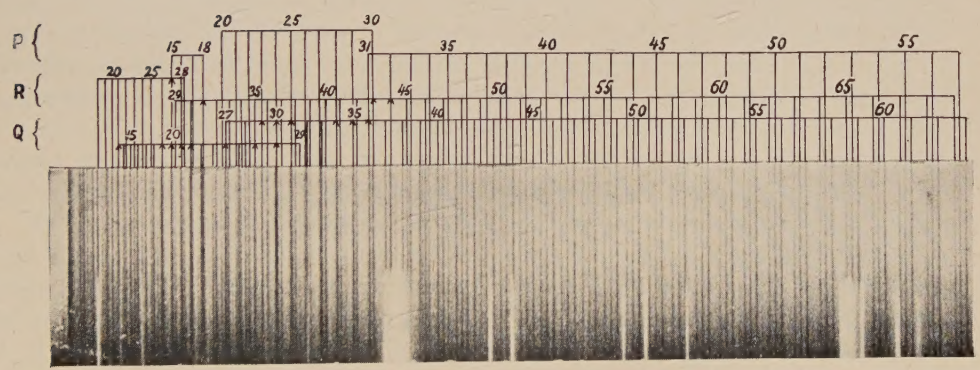

Fig. 1 (*d*). The 2,0 band. Magnification 11×.